VIABILITY OF DEPTH CAMERAS AND LIDAR AS PHENOTYPING PLATFORMS FOR BIOMASS IN CASSAVA (*MANIHOT ESCUELENTA*) AND NAPIER GRASS (*PENNISETUM PURPUREUM*)

A Dissertation

by

TYLER MORGAN ADAMS

Submitted to the Office of Graduate and Professional Studies of
Texas A&M University
in partial fulfillment of the requirements for the degree of

DOCTOR OF PHILOSOPHY

Chair of Committee,	Dirk B. Hays
Committee Members,	Russell W. Jessup
	Sorin Popescu
	Nithya Rajan
Intercollegiate Faculty Chair,	Dirk B. Hays

December 2020

Major Subject: Molecular and Environmental Plant Sciences

ABSTRACT

Changing demands for sustainable food and fuel sources will be the major driver of agriculture in the 21st Century, especially as the world population reaches its estimated carrying capacity. Efficient plant breeding methods to keep up with these demands will require innovative solutions to keep the process fast, accurate, and inexpensive. While terrestrial laser scanning and other forms of LiDAR have shown promise in making this need a reality, the cost of adopting this technology is too high for breeders who are not working with large budgets. This dissertation seeks to determine the viability of several phenotyping methods for improving two crops that will continue to be of critical importance in the developing world: Cassava and Napier grass. Through laboratory and field trials we will test the ability of multiple sensors to create 3D models of plant structure that can then be correlated to biomass in these crops. Additionally, we will test these methods using a custom-made phenotyping platform that can be easily reconstructed for use in a variety of breeding programs.

DEDICATION

I want to dedicate this dissertation to my family, especially my grandparents, my parents, and my siblings. All have been so supportive throughout this process of furthering my education, and for that I will always be grateful.

Also, above all, I dedicate my work to הַקָּדוֹשׁ בָּרוּךְ הוּא

ACKNOWLEDGEMENTS

I would like to thank my graduate committee, chaired by Dr. Dirk Hays, and supported by doctors Russell W. Jessup, Sorin Popescu, and Nithya Rajan. All have provided great help and support in assembling this collection of studies. Dr. Bruce Gooch was also instrumental in the beginning stages of this work.

My lab mates are also to thank, especially Richard Bruton and Henry Ruiz, without whom this project would not have been nearly as successful. I wish to acknowledge Ilse Barrios Perez, Matt Wolfe, Iliyana Dobreva, and Brody Teare for the time they have given of their own projects to help me with my work. And also Sheryl Strauch, for literally pulling me out of the mud when I needed it.

I would also like to thank Daniel Hathcoat for his expertise in the field and the lab, both of which contributed to the project's success. Additionally, many thanks to the faculty and support staff within MEPS and Soil & Crop Sciences, especially Dr. Amir Ibrahim and Taylor Atkinson, for their help and guidance throughout the program.

The staff at the International Center for Tropical Agriculture in Palmira, Colombia are also to be commended for their tireless efforts in helping us to obtain the necessary data to carry out this research.

Finally, I wish to thank Rabbi Dr. Peter Tarlow and his wife, Dr. Sara Alpern Tarlow, for their guidance and encouragement during the program's most difficult times. And of course, I am forever appreciative to my friends, family, and community for all of their support.

CONTRIBUTORS AND FUNDING SOURCES

The work within this dissertation was supervised by a graduate committee consisting of chair Dr. Dirk Hays and committee members Dr. Russell W. Jessup and Dr. Nithya Rajan of the Department of Soil and Crop Sciences, as well as Dr. Sorin Popescu of Ecosystem Science and Management.

Data for Chapter 3 was collected with assistance and input from Richard Bruton, Henry Ruiz, and Iliyana Dobreva. Field data from Chapter 4 was harvested by employees of the International Center for Tropical Agriculture in Palmira, Colombia, with electronic data collected with assistance from Richard Bruton and Henry Ruiz. Ilse Barrios Perez contributed ideas to statistical analysis for Chapters 3 and 4, while further analysis for Chapters 4 and 5 were based on methods developed by Richard Bruton. Field and electronic data collected for Chapter 5 was completed with help from Henry Ruiz and Sheryl Strauch. Daniel Hathcoat also assisted with field calculations for Chapter 5.

All other work related to this research was conducted by the author independently.

This research was made possible by The National Science Foundation, Award Abstract number 1543957, as part of the project BREAD PHENO: High-Throughput Phenotyping Early Stage Root Bulking in Cassava using Ground Penetrating Radar. The contents within this dissertation are the sole responsibility of the author and do not necessarily represent the official views of the NSF or other associated parties.

TABLE OF CONTENTS

Page

LIST OF FIGURES

Page

LIST OF TABLES

Page

CHAPTER I

INTRODUCTION

As the population of Earth continues quickly toward the 10 billion mark, a variety of new challenges have appeared that will test the ability of the planet's resources to meet the needs of its human population. Adding to the challenge of resource availability is the rising level of atmospheric CO_2, which requires innovative solutions to food and fuel requirements that are not only economically productive, but also environmentally sound. For this reason, crop varieties must be developed that can meet growing demand while also keeping their carbon footprints in balance. Likewise, new methods of plant breeding will need to be established that can quickly and efficiently process and develop these new varieties with a high degree of accuracy.

Two crops that may serve as potential frontrunners in this new frontier are cassava (*Manihot esculenta*) and Napier grass (*Pennisetum purpureum*). Ranking in the top ten of important global crops, cassava is currently produced in mass throughout Africa, Asia and South America for domestic use as well as export (Hillocks and Thresh, 1982). Essential to its use for farmers is early root bulking, which ensures that it can be easily taken to market with minimal time investment. Napier grass is also an important crop in the developing world, especially for its use as animal feed and as a high-biomass biofuel. Its high cellulosic content makes it a desirable source of biofuel (Tsai et al., 2018), and its nutritional content with high biomass potential keep it in high demand as food for cattle (Farrell, Simons, and Hillocks, 2010). Additionally, Napier's excellent CO_2 fixation may make it a good candidate for contributing to soil organic carbon stocks in regions where it is grown (Abud and Farias Silva, 2019).

It is currently unknown the extent to which aboveground biomass correlates to root structure or root biomass in either cassava or Napier grass. Equally unknown is the ability of remote sensing technologies, especially LiDAR, to accurately predict aboveground biomass in these crops. The first step to determining if aboveground biomass corresponds positively to root structure is to properly map the physical structure of this aboveground material within a 3D plane. To do this in a way that is fast, financially accessible, and available for field trials would allow plant breeders to make selections for crops that can be more efficiently moved from the field to the marketplace. Furthermore, to be able to make such selections nondestructively would ensure that these crop developments could be made in a way that is neither wasteful nor environmentally disruptive.

This ***project's long-term goal*** is to develop a phenotyping platform that can give breeders valuable information regarding aboveground and belowground traits of specific crop plants. The aim of this dissertation is to is to develop a platform that will allow breeders to determine, *in situ*, which cassava and Napier grass plants have sufficient biomass characteristics without the need to destroy the plant. The central hypothesis of the studies presented here is that if a depth camera or terrestrial laser scanner (TLS) can capture an accurate reflection of a plant's physical structure, then a subsample of the point cloud will positively correlate to biomass in these crops. If successful, this technology will allow plant breeders to gather large amounts of biomass information on their crops of interest with minimal manpower and cost.

Objectives

The objectives of this study are as follows:

1**. Determine the effectiveness of mapping cassava (*Manihot esculenta*) physical structure using terrestrial LiDAR and an RGB-D camera.**

While depth cameras have found homes in a variety of scientific applications, their use as crop phenotyping tools is still in its infancy. One of the major concerns that plant breeders have in adopting such tools is that their resolution is not as high as that of many laser scanners. In this experiment the ability of one such camera, the Microsoft Kinect V2, to create serviceable 3D models of cassava plants will be tested and contrasted with a standard TLS model (FARO Focus 120) under lab conditions.

2. **Define a non-destructive field technique for determining aboveground biomass in cassava (*Manihot esculenta*) based on point clouds and dry weight.**

Due to increasing demand for food in developing nations, as well as cassava's status as a staple crop in such regions, there is a need to develop new varieties with early bulking times and large root sizes in order to feed these growing populations. The industry standard for aboveground, high-throughput phenotyping is the TLS, which is capable of producing 3D images in a matter of minutes. In this experiment a custom-made, low-cost phenotyping platform will be tested against a popular TLS model (Trimble TX5) under field conditions to determine the extent to which each produce models that correlate well to dry weight biomass of cassava.

3. **Define a non-destructive field technique for correlating point clouds to dry weight in Napier grass (*Pernisetum purpureum*).**

Reductions in arable cropland are pushing more and more farmers to supplement their incomes and offset crop losses with livestock. Among the more desirable feed plants in the developing world is Napier grass, which also serves a function in deterring pests from valuable crops

providing sources of alternative fuel. This experiment seeks to determine the ability of remote sensing technology to accurately predict aboveground biomass by comparing plant dry weight to 3D point clouds. Ideally, good correlations between point clouds and biomass will open the door to using the same technology to make similar determinations in other perennial grasses.

CHAPTER II

BACKGROUND

Agricultural Challenges of the 21st Century

Between the year 1960 and 2010, the world's population was estimated to have grown from 3 to 7 billion. Likewise, agricultural production grew during this time to meet changing demands for food, due in no small part to boosts made possible through the Green Revolution. It is currently projected that the Earth's population will reach 10 billion by the year 2060 (Lanz, Dietz, and Swanson, 2018), with numerous studies suggesting that humanity is pushing the limits of the planet's carrying capacity and extracting earth's resources beyond its ability to replenish (Cohen, 1995) (Kin et al., 2019).

A sense of global responsibility for worldwide food security and adequate nutrition is a relatively recent concept, being taken seriously only in the immediate aftermath of the First World War (Zhou, 2019). According to the 1996 World Food Summit, "food security" is defined as, "all people, at all times, have physical and economic access to sufficient, safe, and nutritious food that meets their dietary needs and food preferences for an active and healthy life" (Gibson, 2012). Since the early 1970s, the number of people worldwide who lack proper access to adequately nutritious food has been estimated to be between 800 million and 1.2 billion, with at least 10 million currently dying of hunger every year (Gibson, 2012).

Outside of rapid population growth, perhaps the most significant challenge facing farmers and scientists alike is the gradual changing of the Earth's climate through greenhouse gas emissions and poor environmental practices. The effects of climate change are expected to be most severe in subtropical regions, thus affecting countries in the developing world – many of which lie in

the tropics – more so than in the developed world. This is compounded by the expectation that much of the population growth between now and the year 2030 will be in the developing world, and the fact that more than half of the workforce in such areas is dedicated to agriculture (Reynolds, 2010). Farmers will be faced with a variety of new or exacerbated stresses, such as high temperatures, salinity, and lack of rainfall. This will be of particular concern to the African continent, where irrigation is not as widely available and dependence on rainfall is high (Reynolds, 2010).

Although food crops for human consumption are of primary concern, the role that animal protein plays in both sustenance and consumer demand should not be underestimated. Livestock currently makes up 40% of global agricultural gross domestic product and contributes to 30% of the protein in human diets (with the diets of developed nations consisting of more than 50% animal protein) (Malik et al., 2015). Currently, 30% of the world's land is used for livestock operations, but this amount is expected to grow as global warming changes the arability of land worldwide, as livestock are often depended upon to diversify farm operations and offset losses in years of crop failure (Malik et al., 2015). At the beginning of the 20th Century, crops harvested for animal feed were estimated to be 4.6–5.3 billion tonnes of dry matter per year (Bouwman et al., 2005). Current projections show that in order to adequately feed livestock by the year 2030, this amount will have to increase to 6.5 to 8 billion tonnes of dry matter per year, especially in the realm of grasses (Havlik, et al., 2014). In order to meet these needs, production of high-biomass grasses will be essential.

Concern for natural resources in the face of population growth and changing climate is also driving the need for alterative, cleaner sources of energy and decreased reliance upon fossil fuels. At the current rate of consumption, it is expected that petroleum reserves will only last another

40 to 50 years, making the development of alternative fuel sources an issue of the utmost concern (Gupta and Demirbas, 2010). Current sources of alternative fuel, such as ethanol and biodiesel, are based around sugars, vegetable oil, grains, and lignocellulose. Grasses are exceptionally helpful in this respect because of their high oxygen content and their ability to be bred for high biomass. *Pernisetum purpureum*, in particular, is also useful in the development of biochar, which can not only be useful as a fuel source, but also as a soil conditioner (Adeniyi, Ighalo, and Onifade, 2019). In the interest of food security, it is also preferable to create biofuels out of crops and plant parts that are not normally consumed (Gupta and Demirbas, 2010).

Environmental health is important to the sustainment of agricultural operations. Without sound ecological practices governing agriculture, farmers run the risk of repeating past mistakes, such as the Dust Bowl of the 1930s, that may affect land productivity for years to come (Cordova and Porter, 2015). Likewise, crop production, even in research settings, cannot be taken for granted when the demand for food is so high (Martin, 2019). Thus, new non-destructive methods of plant breeding are necessary.

The goal of current agriculture is to supply *more* than enough food and to provide alternative sources of biofuels and petroleum-based refinery products. This not only ensures that there is a plentiful supply of sustenance even during difficult times, but it is what allows society to grow beyond one that is purely agrarian, where other technologies and fields of study can be developed to maintain a higher quality of life (Martin, 2019). With the current projected increase in population, more land conversion to agricultural operations may be needed, as well as in increase in productivity (Cameira and Pereira, 2019). Complicating matters is the annual 5-10 million hectare reduction in agricultural land due to degradation (GEF/UNCCD, 2011). As such, breeding for specific traits that promote sustainable intensification, such as high yield or

physiological structure that allows more crops to be planted in a limited area, has become a priority for scientists (Lanz, Dietz, and Swanson, 2018).

Cassava

Cassava (*Manihot esculenta*) is a dicotyledon of the family Euphorbiaceae. A perennial shrub, there are approximately 100 species of cassava currently known, although the only one that is commercially available is *Manihot esculenta* Crantz, of which there are at least three subspecies (Hillocks and Thresh, 1982). It is currently the sixth most important source of calories in the world and is popular as a food source in low income areas due to its relative ease, expense, and flexibility in growth and preparation. Cassava's resistance to drought and pests, as well as its tolerance of soil acidity, make it an ideal crop for farmers in areas that suffer from these challenges. Often planted from stem cuttings, the average *Manihot esculenta* plant grows to a height between 1 and 4 meters (depending on genotype) and can be harvested 6 to 24 months after planting (although most are harvested after 18 months) (Hillocks and Thresh, 1982).

Manihot esculenta is native to South America, and although it has been a cultivated crop for almost 9,000 years (Hillocks and Thresh, 1982), it is still known to grow in the wild in certain areas of the continent (Allem, 1987). It is thought to have originated in the savannas of the Goiás region of Central Brazil before spreading along the Amazon River, and was already an important crop to natives by the time Europeans arrived in the Americas, probably beginning with the Carib and Arawak Indians (Hillocks and Thresh, 1982).

The most intensively cultivated areas for cassava production in Latina America are Brazil, Paraguay, Colombia, Cuba, Haiti, and the Dominican Republic; however, production in Latin America is relatively small compared to the total amount produced worldwide, constituting less

than 1/5 of overall production (Hillocks and Thresh, 1982). Nevertheless, cassava has continued to be an important food component in Latin America, not only consumed by humans fresh or in flour form, but also using the leaves as animal feed. The Latin American market for the crop has remained stable over the years, with the ecological diversity, including that of pests and diseases, making Colombia an ideal spot for experimentation. This is evidenced by the International Center for Tropical Agriculture (CIAT) becoming one of the top research centers in both the country and the world for cassava study (Hillocks and Thresh, 1982).

Cassava was initially introduced to the African continent by way of the Portuguese in the 1500s. While adoption of the crop was initially slow, it later spread throughout Sub-Saharan Africa as a means of combating famine, especially during the 20th Century (Hillocks and Thresh, 1982). Cultivation of cassava has grown in Africa since the 1990s, particularly due to its tolerance of poor soils, and Africa is now the largest producer of the crop in the word. In fact, Africa produces more than all of the other cassava-growing regions combined, making up a larger total caloric intake of African diets than either sorghum or maize. In addition, the International Institute of Tropical Agriculture (IITA) in Nigeria is now one of the major cassava research centers, along with CIAT (Hillocks and Thresh, 1982).

Asia was a much later entry to the cassava industry, having not received it from European traders until the late 1700s to early 1800s. India, Java and the Philippines were the first nations to receive the crop, and it had become solidly established in the region by the end of the 19th Century, continuing to grow at a competitive rate in the 20th Century. Being a tropical plant, the primary Asian producers are southern China, India, Thailand, Philippines, Indonesia, and Vietnam. Part of cassava's appeal in these regions is that it does not compete with rice production, as it can be grown in drier conditions and on far less fertile soils than rice. While not

being the largest producer, Asia is nonetheless the leading *exporter* of cassava, being the only region that focuses more on exports than on using the crop to feed its own populations (Hillocks and Thresh, 1982).

Napier Grass

Pennisetum purpureum, also known as "elephant grass" or "Napier grass," is a monocotyledon C4 grass native to Eastern Africa (Langeland and Cherry, 2008). Known for its quick growth and resistance to drought and pests (Tsai et al., 2018), Napier grass is currently the most important fodder crop for dairy cattle is East Africa (Farrell, Simons, and Hillocks, 2010). While its consumption is largely limited to animals, it can be consumed by humans (especially in its earlier stages) and is sometimes used as a food source by people in African countries (Burkill, 1985).

Growing easily from its rhizomes (Langeland and Cherry, 2008), the average height of a Napier plant stand is between 2 and 5 meters, with a blade width of roughly 3.5 centimeters. It is a versatile plant, being able to grow successfully in tropical, subtropical, or temperate environments and across a variety of altitudes and geographic planes (Tsai et al., 2018). However, it tends to thrive in moist soil (Langeland and Cherry, 2008). Due to its high biomass and exceptional nutritional content, it is highly valued as a forage crop for cattle in tropical areas (Mapato and Wanapat, 2018), with particularly strong demand for its use in dairy heifers (Loresco et al., 2019).

While typically considered to be a pest-resistant plant, Napier grass has, since the mid-2000s, been investigated for use as a "trap plant" for certain sub-Saharan insects, particularly the African maize stalkborer (*Busseola fusca*) and the spotted stalk borer (*Chilo partellus*). It is most commonly used as part of a "push-pull" system, where a desirable crop is surrounded by

repellent plants, and then further outside by an attractant plant (in this case, the Napier), in order to drive insects away from the desired crop. While not as desirable as other grasses in terms of being a food source, research has shown that Napier is preferred over crops of interest by these insects for oviposition (Khan et al., 2007).

Napier grass was first introduced to the U.S. in 1913 for use as a forage crop, a use that has continued into the 21st Century. It is also treated as an invasive weed in some areas of its introduction– most notably, Florida (Langeland and Cherry, 2008). Still, the crop is noted for its high biomass potential. Additionally, its cellulose content (which constitutes 40%-45% dry base weight) makes it ideal in the production of alternative fuels (Tsai et al., 2018), and it has been explored for additional use as charcoal, bio-gas, and bio-oil (Strezov, Evans, and Hayman, 2008).

Remote Sensing

Changes in climate, environment, and society pose challenges to the agricultural sector and require increasingly specific breeds of crop plants to meet the unique environmental difficulties associated with certain regions. For this reason, plant breeding and genetic engineering are at the forefront of agricultural concern. Phenotyping, naturally, is also of great importance in this capacity (Qui et al., 2018). The goal of phenotyping is to identify desirable plant traits, such as height, yield, biomass, physiology, and responses to stress so that these traits can be selected for in breeding programs (Mishra et al., 2016). This can help give further information on plant health and growth, including how well a plant utilizes water, sunlight, etc. (Li et al., 2014). In essence, this gives us an idea of how certain genotypes interact with a plant's environment (Houle et al., 2010).

Until the widespread implementation of remote sensing methods in agriculture, phenotyping of crops was almost entirely dependent upon destructive sampling; at least, as it relates to biomass. Destructive sampling methods not only cost breeders valuable crops, but are also incredibly labor intensive for researchers (Ojoatre et al., 2019). This time-consuming measure makes non-destructive solutions all the more valuable for the plant breeding field.

Plant phenomics, the study of phenotype by way of high-throughput phenotyping methods (Marko et al., 2018), is an emerging field that offers a potential solution to this need for non-destructive sampling. Current technologies allow us to capture phenotypic traits with a high degree of accuracy (Fritsche-Neto and Borém, 2015) and have already been successful in determining plant qualities, such as leaf area density (Hosoi and Omasa, 2007) and drought tolerance (Andrade-Sanchez et al., 2013), based on imaging of physiological structure.

While phenotyping indoors is possible, the need for field-ready phenotyping is of the utmost importance, requiring that breeders be able to capture large numbers of plants without removing them from their natural environment (Young et al., 2019). One of the primary ways in which LiDAR has been explored in field conditions is by attaching sensors to UAVs, which are able to quickly and easily capture information on large numbers of plants. However, UAVs are equipped to capture this information from the top down, while some breeders desire biomass information to be captured from the side or the ground up (Young et al., 2019). Researchers have tried to accommodate this need by developing “phenocarts” or “phenomobiles”– vehicles modified to include LiDAR sensors for capturing phenotypic data from the ground level. Many designs have been implemented thus far, although cost and construction of such devices have been limiting factors (Fritsche-Neto and Borém, 2015).

Terrestrial Laser Scanners

One of the most popular techniques used for remote sensing of environmental and agricultural structures is LiDAR (Light Detection and Ranging), which uses lasers to generate reflective information that can then be analyzed to determine certain characteristics of the subject, such as size or shape. Although development of the principles of LiDAR began as early as the 1930s (Weitkamp, 2005), the technology progressed at a great rate after the construction of the laser in the 1960s, and has continued to become more refined into the 21st century (McManamon, 2015). While air-mounted LiDAR is a popular option due to its lack of labor intensiveness, terrestrial laser scanners (TLS) are an alternative method that have been much explored due to their ability to capture data on the ground, thus obtaining a side view of the crops in question as opposed to simply top down. TLS has already been used as a tool for measuring plant height in several crops such as maize (Tilly et al., 2014b), rice (Tilly et al., 2014a), and perennial grasses (Zhang and Grift, 2012).

LiDAR has been used in agricultural experiments since the 1980s. While 2D LiDAR has been used for agricultural purposes, devices that produce full 3D images have been at the forefront of experimentation in the 21st Century (Qui et al., 2018). TLS is an active sensor; that is, it emits its own radiation toward the subject so that the data can be recorded, rather than measuring reflectance based on natural light, as with passive sensors (Fritsche-Neto and Borém, 2015). Also, much like other forms of LiDAR, TLS operates largely on the time-of-flight principle. Time-of-flight is a method of data capture in which a series of lasers scan the surface of an area and record the time it takes for that light to be reflected back; this is what allows the scanner to determine depth. More specifically, this is a measurement of time delay: the time it takes for a beam of light to hit its target, bounce back, and then reach a light detector on the device. This is

because light travels at a constant velocity, thus making it possible to determine range based on its travel time (Vosselman and Maas, 2010).

In the realm of plant imaging, LiDAR has some advantages over other 3D cameras (such as stereovision). Most notably, it is not as deeply affected by lighting conditions (Gene-Mola et al., 2019). However, the cost of LiDAR equipment (especially TLS) is prohibitively expensive, with many units costing between $10,000 and $70,000 based on condition. 2D LiDAR has been proposed as a method of dealing with overwhelming TLS cost (Wang et al., 2017). However, the use of cheaper depth cameras may still make 3D phenotyping an option for those on restrictive research budgets.

Microsoft Kinect

While 2D plant modelling can be a reasonable substitute for TLS in some circumstances (Qui et al., 2018), those on a tight budget can still achieve 3D imaging through RGB-D cameras. RGB-D cameras combine LiDAR technology with that of a traditional RGB camera by fusing a color image with the laser points that are captured (Gene-Mola et al., 2019). This way, one can achieve a full color image of high quality that also captures the depth of the scene, thus creating a one-sided 3D model (although multiple angles can be combined to create a full 3D model).

The Microsoft Kinect was originally developed for use with the company's X-Box 360 video game console. This first version, Kinect V1, was released in 2010 and was intended to be used predominantly as a motion tracker to enable hands-free gaming (Butkiewicz, 2014). It operated using structured light projection to determine depth; that is, it utilized preexisting lighting conditions and a dispersal of points from the sensor to map the surrounding area and determine the relative location of objects in the room, specifically the human body (Naeemabadi et al.,

2018). Despite initially selling well, the Kinect V1 ultimately proved unpopular for its intended purpose as a video game accessory, but found a home in the scientific community as a cheaper alternative to the more expensive depth cameras at the time (Tien-Long and Van-Bien, 2019).

Recognizing that there was a market for Kinect, Microsoft released a new model, the Kinect V2, in 2014. Despite the lackluster reception of the V1 for such a purpose, this new model was also aimed at the gaming community, being compatible with the X-Box One console (Tien-Long and Van-Bien, 2019). Taking into account user complaints about the V1, Microsoft aimed to correct these shortcomings and provide a sensor with greater usability for the scientific community as well as the video game market (Rahman, 2017).

The Kinect V2 is an upgrade to the V1 in virtually every way, containing a 1920 x 1080 x 16 bits per pixel color camera, a 512 x 424 x 16 bits per pixel 16-bit time-of-flight depth sensor, a 0.5 m to 8 m absolute range (with the ideal range being within 4.5 m), and a 70° Horizontal – 60° Vertical angular field of view (Rahman, 2017). As mentioned, the Kinect V2, like the TLS, functions using the time-of-flight concept. This is a step up from the first version, which utilized structured lighting and triangulation techniques to determine depth. The time-of-flight approach allows the V2 to be much more precise (within picoseconds), minimize blur, and create sharper images when tracking motion. Unlike a TLS, the Kinect functions similarly to flash LiDAR, sending simultaneous blasts of light through multiple laser diodes rather than relying on a single laser to rapidly cover an area (Butkiewicz, 2014). This allows it to capture depth images instantaneously, making it less susceptible to wind and movement distortion than a TLS (Rahman, 2017). This method of operation has also led to some confusion as to whether the Kinect V2 can technically be classified as LiDAR. LiDAR tends to operate by means of a narrow, focused beam of light, while Kinect illuminates the scene through its multiple diodes and

then captures available information (Wasenmüller and Stricker, 2016). Regardless of the remote sensing classification, the Kinect is capable of producing 3D point clouds nearly identical to that of TLS, albeit at a lower resolution.

The V2 has both a regular RGB camera as well as an HD RGB-D (depth camera) (Naeemabadi et al., 2018), so that images of both can be taken at the same time. This can only be done with the Software Development Kit (SDK) from Microsoft, however, as the cameras are separate and thus take pictures from slightly different points of view. It also contains three infrared (IR) emitters that are used for the depth perception and requires a 3.0 USB computer connection in order to function, as the sensor transfers approximately 2.1 Gbit/s of data when operating (Rahman, 2017).

Microsoft, wanting to encourage the development of the Kinect as a low-cost sensor, has released the Microsoft SDK 2.0, a software development kit, for researchers and amateurs to use in exploring different functions for the sensors. This includes drivers and code samples that can be used to tailor the Kinect to specific purposes (Tien-Long and Van-Bien, 2019). In addition, in 2019 Microsoft released a new model, the Azure Kinect, that caters specifically to research interests. Among the updated features is an advanced AI that is aimed principally at research in the medical field (Vision Systems Design, 2019).

Although the Kinect V2 is superior to its predecessor in terms of power and quality, it is not without its drawbacks. While it produces clearer 3D images than V1, its point clouds are still not as clean and dense as one that could be achieved with a TLS. Additionally, its range is far shorter than that of many TLS, the standard having a range of at least 120 m (as opposed to the Kinect's maximum of 8 m) (Lachat et al., 2015). Most frustrating to those seeking to employ the Kinect in the field is that it also has problems functioning in direct sunlight due to the infinite influx of

infrared rays from the sun into its IR receptor (Nasir, Taj, and Khan, 2016), although this can be mitigated by using the sensor indoors, at night, or on cloudy days (Marin, 2017). Researchers may also hesitate to use the V2 as production of the sensor for Windows was discontinued in 2015 (Protalinski, 2015), with the version designed specifically for the X-Box One also discontinued in 2017 (Moscaritolo, 2017). Nevertheless, the Microsoft SDK for V2 is still operable, and V2 sensors continue to be easily found for purchase, either in new or used condition. The V2 sensor also remains affordable as compared to the current Azure model, with V2 sensors costing between $50-200 depending on condition (Butkiewicz, 2014), and the Azure retailing at $399 (Vision Systems Design, 2019).

As the Kinect was designed predominantly as a motion capture device, its focus is on capturing depth in real time as opposed to still images. It does this by capturing images with a very high frequency (a maximum of 30 Hz). Although this can create noise or other problems in capturing still images, it has still been largely successful in scientific experiments (Tien-Long and Van-Bien, 2019). The Kinect has already been employed for research in the fields of medicine and hospital management (Scano, Molteni, and Tosatti, 2019) (Silverstein and Snyder, 2017), geophysics (Hämmerle et al., 2014), archaeology (Hämmerle et al., 2014), and agriculture (Nir et al, 2018) (Andújar et al., 2016). Despite its drawbacks in range and resolution, the Kinect's low cost, small size, resistance to wind distortion, and high portability (Hämmerle et al., 2014) make it a reasonable and flexible competitor to TLS and other forms of LiDAR in the agricultural field.

CHAPTER III

CREATING 3D MODELS OF CASSAVA (*MANIHOT ESCULENTA*) PLANT STRUCTURE USING A NONTRADITIONAL SENSOR

Introduction

The application of remote sensing techniques in the field of agriculture has been, historically, geared toward vegetation index extraction (Xie et al., 2018), monitoring crop stress (Leon et al., 2003) (DeGloria et al, 1986) and observing the development of disease (Bajwa et al., 2017). Recently, however, the goal of many of these applications has shifted toward the determination of plant phenotype (the physical representation of a plant's genes interacting with the environment). Advancements in gene mapping have largely been responsible for the rising interest in high-throughput phenotyping, as the genetic sequencing and annotations of many major crops have lacked phenotypic functions (Furbank, 2009). Thus, fast, cheap, and reliable determination of phenotype in the field is one of the major frontiers of plant breeding in the 21st Century.

One crop that is of considerable interest to breeders is cassava (*Manihot esculenta*). A tropical plant that is native to South America, cassava has now become an important food source in many countries. The African continent is currently the largest user of this crop, producing between 50 and 80 million tonnes annually while being used as a daily food source by more than 200 million people (Anikwe and Ikenganyia, 2018). The need for intensive planting, early root bulking, and adaptation to stress make the physiological structure of this plant a prime subject for breeding programs utilizing high-throughput phenotyping techniques.

Late storage root bulking cultivars occupy land for long periods, reducing the production potential for other crops (Suja et al., 2010). The selection of early storage root bulking (ESB) can significantly increase the efficiency of cassava production (Wholey & Cock, 1974). Early storage root bulking (ESB) in cassava has become important where increased production on available land is necessary and in semi-arid regions where ESB cultivars can be harvested within one rain cycle (Kamau et al., 2011). ESB can increase the economic returns for smallholder farmers in several ways: allowing the crop to be planted during the optimal season, providing food harvest during the lean season, allowing double and inter-cropping opportunities, extending harvest over a longer period of time, and allowing cassava's transition to more intensive commercial production systems that supply factories with raw materials during greater portions of the year (Tumuhimbise et al., 2012). To meet these demands, development of ESB varieties that can be harvested in less than 8 months is required. It is for these reasons that ESB has become a major breeding objective for the national cassava and RT (potatoes, sweet potatoes, and yams) breeding programs (NARS) worldwide and is considered key for the transition of cassava into an industrial crop. ESB is estimated to increase yields by 50% to 100% per unit of cropping time in cassava, since the 25 tons harvested per hectare in 12 to 24 months could then be harvested in 8 to 6 months.

However, at present, there are no defined morphological or visual methods available to select for the accumulation of starch in the root and tubers of cassava and other RT crops, making it difficult for breeding projects to identify ESB (Okogbenin & Fregene, 2002). As such, destructive sampling of plants to assess roots is required. This creates an enormous hurdle for identifying sources of ESB from adapted and un-adapted germplasm. It requires large nurseries of individual genotype replications for destructive sampling at progressive time intervals

throughout the growing season. The land resource and labor costs required are out-of-reach for even developed countries and especially for NARS breeding programs in Africa, Central America, and Asia. This forces breeders to conduct late season yield harvest. As such, selection of current cultivars of cassava and RT crops such as potato, sweet potato, and yams are biased against ESB and thus, water-use efficiency (WUE). Cassava breeders have hypothesized that as-yet determined above ground phenotypic markers could be indicators of ESB. However, at present, few affordable phenotyping technologies have been defined that could be deployed to address this hypothesis.

Modern methods of plant phenotyping generally include the use of 2D image-based technologies such as broadband RGB and NIR, hyperspectral, fluorescence or thermal analysis. These techniques have been adapted from traditional satellite and aerial applications for field, greenhouse or laboratory use, and have in some cases even been used to model plant responses in 3D (Santos & Ueda, 2013) (Pound et al., 2014). Analysis of plants in 3D could allow for a better understanding of certain morphological traits, which have thus far been unexplored due to the laborious nature of the data acquisition (Dhondt et al., 2013).

Even though the technology exists to quickly and easily model plants in 3D, tools such as airborne and terrestrial laser scanners (TLS) and flash LiDAR are often not practical due to their prohibitively expensive costs. Still, some research exists on the use of 3D imaging tools within the biological sciences (Popescu, 2007; Eitel et al., 2014;Ma et al., 2016). A number of studies suggest that 3D phenotyping can be successful, with many showing significant correlation to biomass (Ehlert et al., 2010), plant height (Tilly et al., 2014a), and other phenotypic traits (Hosoi & Omasa 2011). However, two issues limit the widespread adoption of 3D plant phenotyping

platforms: 1) the complexity of the data analysis process, and 2) the substantial platform acquisition costs.

Due to their low cost and wide availability, RGB-D cameras, also known generally as “depth sensors,” have seen wide experimental use in the robotics and computer vision fields (Nir et al, 2018). These sensors generally utilize one of three principles to create depth data: stereo vision, structured light, or time-of-flight (Islam et al., 2017). But with low cost comes limitations, and in depth sensors this takes the form of reduction in accuracy and precision as well as a lack of stability across operating environments.

Nevertheless, the RGB-D cameras such as the Kinect V2 may still serve as a possible solution to the burdening cost of 3D plant phenotyping. To this end, two sensors will be tested as a means for collecting structural data on cassava in a greenhouse setting. The goal of this chapter is to determine the ability of this technology to accurately capture a 3D model of plant (*Manihot esculenta*) physical structure, which can then be used for various phenotyping purposes in the field. This will be determined based on the following objectives: 1) To define the extent to which a depth sensor point cloud reflects the information captured by a TLS point cloud by comparing cloud distances, 2) to determine if the point clouds maintain the same distance when comparing vegetation only, and 3) to quantify the point density of both the depth sensor and the TLS. It is expected that while the Kinect will capture a less dense point cloud, the controlled environment of the greenhouse will render it capable of producing an accurate representation of the plant architecture.

Methods

Location

The experiment was carried out in the greenhouse facilities of the Norman Borlaug Institute for International Agriculture (Texas A&M University, College Station). An indoor location was chosen in order to eliminate plant movement due to wind for the TLS, and sunlight exposure for the Kinect. Because the TLS takes several minutes to collect data for an image, it was necessary to minimize the effect of wind on the plants, as having a constantly moving subject would have produced a distorted, largely unusable image. Previous research has shown that the Kinect works poorly in direct sunlight (Lachat et al., 2015) (Marin, 2017), therefore attempt to completely remove this hurdle were made by capturing the images indoors. More information about the sensors' limitations is included in the following sections.

Kinect V2

Beginning in the early 2010s, video game developers began experimenting with ways to allow a hands-free gaming experience, mostly in the form of motion trackers. This led to the development of devices such as the Microsoft Kinect series of sensors (Caruso, Russo and Savino, 2017). The first incarnation (V1), released in 2010, tracked motion through structured light. The most recent version (V2), released in 2014, included several improvements over its predecessor. One such improvement was the use of an infrared (IR) time-of-flight sensor over the structured light sensor found in V1, resulting in a reduction of noise, improved depth accuracy, and a higher framerate (Zennaro et al., 2015). Additionally, the 1920 X 1080 RGB camera used in the Kinect V2 is of a higher quality than that found in the older version. However, being a low cost sensor, the Kinect V2 has some limitations related to depth image

accuracy, noise from ambient light (Lachat et al., 2015) and sensor-to-sensor interference (Kunz & Brogli, 2016). The sensor's lens, for instance, tends to be most effective in the center of the image, continually worsening the depth measurements as it radiates outward (Fig. 1). These errors can be several centimeters at the corners of the image, particularly when captured at distances over 3 m (it is not recommended that the Kinect be used for at a distance greater than 4.5 m). Still, if the far corners of the image are not the primary area of interest, users can expect an average distance error of < 1 cm (Lachat et al., 2015_b).

Sunlight, if cast directly in the subject or the sensor itself, creates noise in the image or a complete lack of data capture altogether (Lachat et al., 2015_a) (Marin, 2017). However, this can largely be overcome in field conditions by collecting data during periods of low light, cloudy days, or at night. Another issue is that resolution is lost the further away the camera is from its subject; hence, the ideal range being 0.5 to 4.5 m when the camera is technically capable of capturing data at 8 m (Fig. 1).

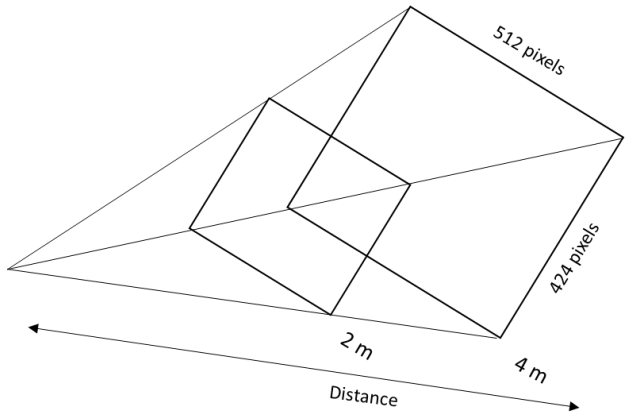

Distance (m)	Pixel Size (cm)
1	.27
2	.55
4	1.09

Figure 1. Depth point spacing in relation to distance from the Kinect sensor.

One area of difference in depth cameras, such as the Kinect, as compared to terrestrial LiDAR is in their data capture process. While traditional LiDAR uses a focused laser beam to capture data,

the Kinect uses multiple lasers to illuminate the scene, then gathering information in a manner similar to flash LiDAR. This distinguishes the Kinect and being a nontraditional sensor, especially in the realm of 3D phenotyping and plant imaging.

FARO Focus 120

The terrestrial laser scanner used in this study as the baseline for comparison against the Kinect is the FARO Focus 120 (FARO Technologies, Lake Mary, Florida) (Table 1). This particular laser scanner operates at 905 nm, which is in the near-infrared region of the spectrum. It has a range of 0.6 to 120 m and a range error of ± 2 mm at 10 m and 25 m. It can scan an area of 360° horizontally and 300° vertically and has a built-in color camera capable of capturing at 70 megapixels (this color information is then used to colorize the point cloud). While this sensor is capable of producing high resolution point clouds, it is prone to distortion if any objects in the scene move during scanning. This can be a major issue in field settings as plant leaves are known to move numerous times during the several minutes the scanner needs to capture an image, with even slight breezes causing a loss in quality.

Table 1. Key features of the Microsoft Kinect V2 and the FARO Focus 120.

Feature	**Microsoft Kinect V2**	**FARO Focus 120**
Type	RGB-D	Terrestrial Laser Scanner
Wavelength (nm)	860	905
FOV (H X V)	70° X 60°	360° X 300°
Range (m)	~0.8 – 4.5	~0.6 – 120
Depth Pixel Array (H X V)	512 X 424	
Color Camera	1920 X 1080	70 megapixel
Frames Per Second	30	

Plant Material

In September of 2016, six cassava *(Manihot esculenta)* cuttings were planted in pots in a greenhouse at Texas A&M University. The cuttings were first suspended in a water/fertilizer mixture to promote root development and were transplanted into potting soil once ample root material was established. The plants consisted of three different varieties, all of which produced a similar upright phenotype and had no distinguishable characteristics between varieties other than the color of the stem (Fig. 2). All plants received the same treatment with periodic fertilization, adequate water, and any required chemical treatments to promote growth. At the time of data collection, the plants were approximately seven months old.

Figure 2. FARO models of the six cassava plants arranged by height, with the bounding box visible.

Data Collection

Measurements were taken inside a seed preparation room at the greenhouse facility. As mentioned previously, an indoor location was chosen to minimize environmental variables, especially those related to plant movement and sunlight. These two variables were controlled to allow both scanners to produce the most accurate point clouds possible. It should be noted,

however, that there was an air conditioning unit which sometimes ran in the room where the images were captured, creating very minor plant movement on and off throughout the experiment. The effect on the data appears to be minimal, however.

Scans were taken simultaneously with the FARO Focus 120 TLS sensor and the Microsoft Kinect V2, which were placed 90° to one another surrounding the plant at a distance of 1.3 m from the edge of the turntable and a height of 0.97 m (Fig. 3). These distances were measured from the sensor location within the instrument. The FARO settings used are presented in Table 2. The resulting point density was stated to be 12.27 mm at 10 m from the sensor. These settings were applied as to maintain a good resolution that was also not time intensive (less than three minutes per scan) and would be representative of the typical amount of time permitted for a field campaign.

Figure 3. Simultaneous image capture process for the Microsoft Kinect V2 (left) and the FARO Focus 120 (right).

Table 2. FARO Focus 120 scan settings.

Setting	**Value**
Resolution	1/8
Quality	4
Vertical Scan Area	-60° to 90°
Horizontal Scan Area	0° to 90°
Color Images Captured	Yes

Kinect images were captured using a makeshift client-server program. To allow the future use of multiple Kinect sensors at one time, an adapted version of the open-source RoomAlive Toolkit was produced. These modifications were necessary as the 2017 version did not allow data streams to be collected simultaneously. In general, the Github repository (https://github.com/Microsoft/RoomAliveToolkit) was duplicated and an executable version of the software was rebuilt using Visual Studio 2007 Community Edition. The modifications included the use of the "Parallel For Each" statement in C# to allow the multiple Kinect streams to be completed.

For each plant, eight scans were taken in subsequent 45° increments (i.e. scans were taken at 0°, 45°, 90°, 135°, 180°, 225°, 270°, and 315°). The position of the Kinect sensor and its field of view (FOV) meant that the sensor needed to be faced downward at approximately 30° so that the entire turntable was visible. This resulted in some of the taller plants having their top not visible in the resulting point clouds. These parts were later removed from the corresponding FARO scans for analysis.

In order to eliminate the need to move the instruments between the different data capture angles, plants were placed on a modified turntable to facilitate their rotation (Fig. 4). The base was a

Copco 45.72 cm non-skid turntable (Lazy Susan). J-B Weld reinforced epoxy was used to attach two bamboo stakes (Miracle Grow 1.219 m) to the top of the turntable. Eastpoint 40 mm table tennis balls were attached at the end of each of the stakes to be used as targets for registration. To ensure that each of targets could be recognized as unique objects in the point clouds, the table tennis balls were placed at four different height levels: 0 cm, 5 cm, 8 cm, and 11.5 cm.

Figure 4. Modified turntable for plant rotation with table tennis ball targets for registration.

Preprocessing

For the initial processing, files from the FARO scanner where converted from their proprietary .fls format to .xyz format in order to facilitate easy transfer between software programs. This was done by exporting the data from the FARO® SCENE software. The Kinect files were already in a format that is easily accessible by a variety of software programs (.xyz). The rest of the preprocessing and analysis was done using CloudCompare version 2.10. alpha (CC), an open source 3D point cloud (and triangular mesh) editing and processing software (Fig. 5).

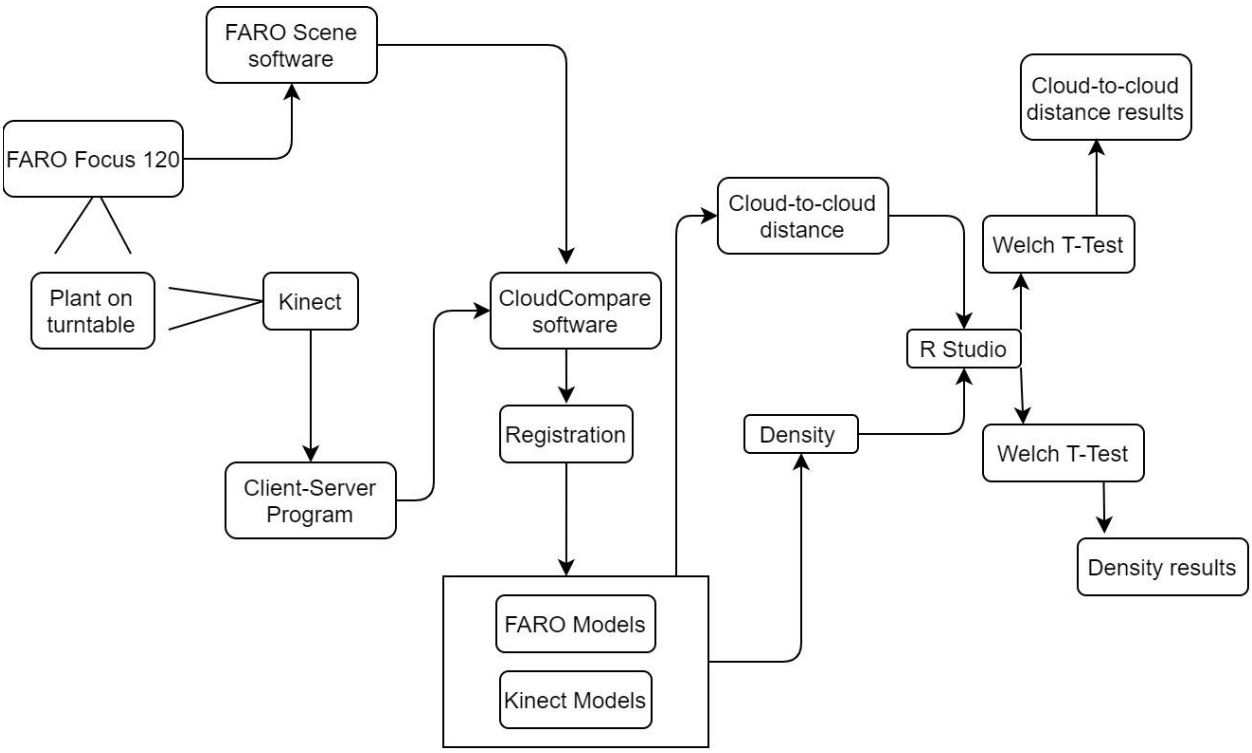

Figure 5. Outline of the data collection and analysis workflow.

Each file was manually cropped close to the plant perimeter using the Segment tool in CC to discard unnecessary background points (i.e., anything in the greenhouse that was not a part of the experiment), making sure to also leave the targets intact. This resulted in a scan with points representing the plant, pot, turntable and a small portion of the floor. After cropping, all scans were cleaned using the Statistical Outlier Removal (SOR) tool in CC. Within SOR, the number of points used for mean distance estimation was 6, while the standard deviation multiplier threshold was set to 1.00. Determination of these settings was done based on trial and error, attempting to cleanup many of the noise points, while not removing large numbers of points representing plant leaves and stems.

Registration for each plant was carried out using only four of the eight scans: those corresponding to 0°, 90°, 180°, 270°. For plant 5, the 180° scan was corrupted, therefore the

135° scan was used instead. All scans were registered with the 0° scan as the reference, using the table tennis balls that were attached to the plant turntable as targets, as well as some points on the turntable itself where necessary. After the four scans were registered together, the point clouds were merged to create a single 3D model. After all individual plants were merged into 3D models, FARO files were then registered to their corresponding Kinect images. The registration errors obtained are presented in Table 3. As mentioned previously, some of the Kinect models were lacking the top portions of the cassava plant due to the FOV of the sensor. In addition, the ground points needed to be removed from each model. To facilitate a proper cloud-to-cloud comparison between the FARO and Kinect models, the Segment tool in CC was used to manually clip the extent of the point clouds so that it would be exactly the same. This was done by loading the both the FARO and Kinect models of a given plant and visually assuring that the ground points and any points above the FOV of the Kinect were removed.

Table 3. Errors from registering FARO clouds to their corresponding Kinect clouds (m).

Plant	**Mean Error**
1	.0040
2	.0061
3	.0063
4	.0055
5	.0064
6	.0058

Analysis

The Cloud-to-Cloud distance tool within CC was used to calculate point distance between the two models. The tool achieves this by calculating distance from a reference cloud to a compared

cloud using either simply the nearest neighbor distance or one of three local modeling strategies to better incorporate surface features into the distance estimation. The analysis can be used on only two clouds at one time. The reference cloud should be the cloud which is of the greatest extent and the highest density, therefore in this analysis the FARO model was set as the reference and the Kinect as the compared cloud. The octree level was left in the default as it suggests that CC should determine the value. No max distance was set, so all points were included in the calculations. The computation did not include splitting into the x, y and z components.

The 2D 1/2 triangulation model was suggested for this analysis, as CC suggests it is the only model which can theoretically represent sharp edges. The local model requires a value to be computed upon; this can either be on a given number of neighbors or based on a spherical neighborhood. Both a spherical neighborhood of .01 m and a nearest neighbor value of 6 were attempted. In both cases, the resulting mean distance and standard deviation values were nearly identical. The use of a nearest neighbor value is suggested if the point clouds are of a constant density, and the software states that the computations are faster. Therefore, it was decided to complete the analysis using the nearest neighbor value of 6.

The output is the mean and standard deviation of the distance between the point clouds. In addition, a scaler field is created for the compared cloud, which can be visualized to display the distance for each point. A box and whisker plot was created in R (R Core Team) to display the distance values for each of the 6 plants. In order to assess the effect of the planter pot on the Cloud-to-Cloud distance determination, the pots were manually removed using the segment tool from each set of model plants. The analysis was again run using the same methodology. R was used to conduct a Welch T-Test to compare the difference between the distance values with and

without the pot in the model. A Welch T-Test was used as the number of samples varied between the variables and they did not have equal variances according to an F-Test.

The point density of each point cloud was calculated using the Density tool in CloudCompare. Two methods are available; a precise method which estimates density based on counting the number of neighbors inside a sphere radius set by the user, or an approximate method which calculates the distance to the nearest neighbor. For this analysis the precise method was chosen. This was achieved using a radius value of 0.01, and the output was expressed in the number of neighbors for each point in the model. These values are added as a scaler field into the dataset and can be visualized in CC. A statistical comparison between the density data for the two models was made in R for each plant. A Welch T-Test was used as the number of samples varied between the FARO and Kinect models and the results of the F-Test showed the variances were not equal.

Results

Cloud-to-Cloud Distance

The average distance between the point clouds, based on the means of all plants, was 0.0093 m, with a standard deviation of 0.0013 m (Fig. 6). For this study, all mean point cloud distances were less than 1 cm except for plant 3, which was 0.011 m. The spatial distribution of the variability in distance between the point clouds for all plants seems to be evenly distributed with two exceptions (Fig. 7). One, the points indicating high cloud-to-cloud distance (red in color) seem to be grouped within the vegetation, while a few also occur as individual points on the pots. Two, the pots themselves seem to produce concentrations of points which have above-average distances (0.15 and 0.04 m).

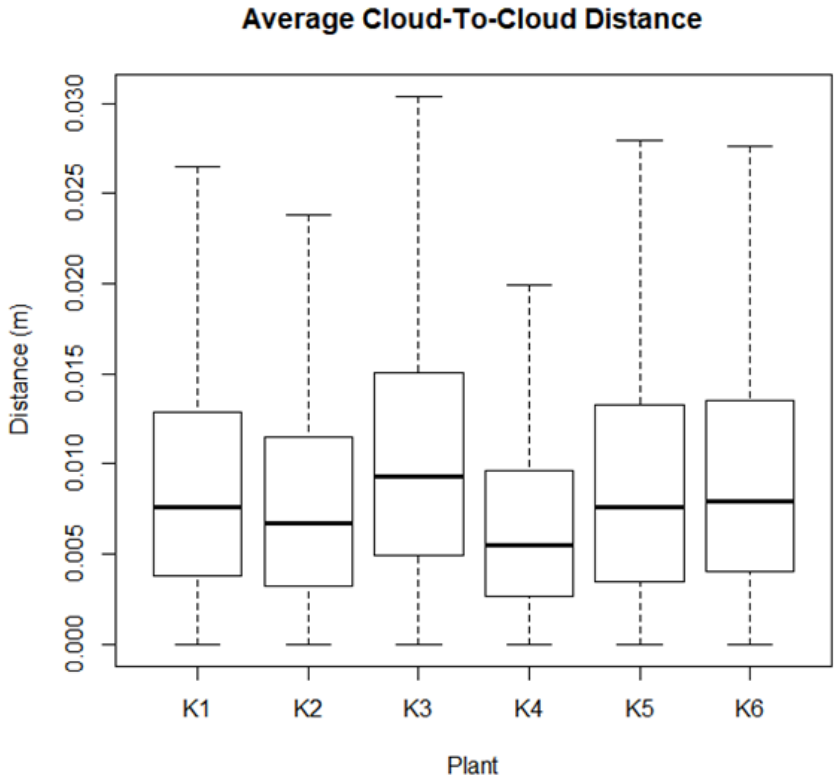

Figure 6. Distance of Kinect point cloud model from FARO model across all six plants (m), showing a relatively normal distribution across all plants. Average distance is 0.0093 m, with all distances being less than 1 cm except for one (Plant 3) at 0.011 m.

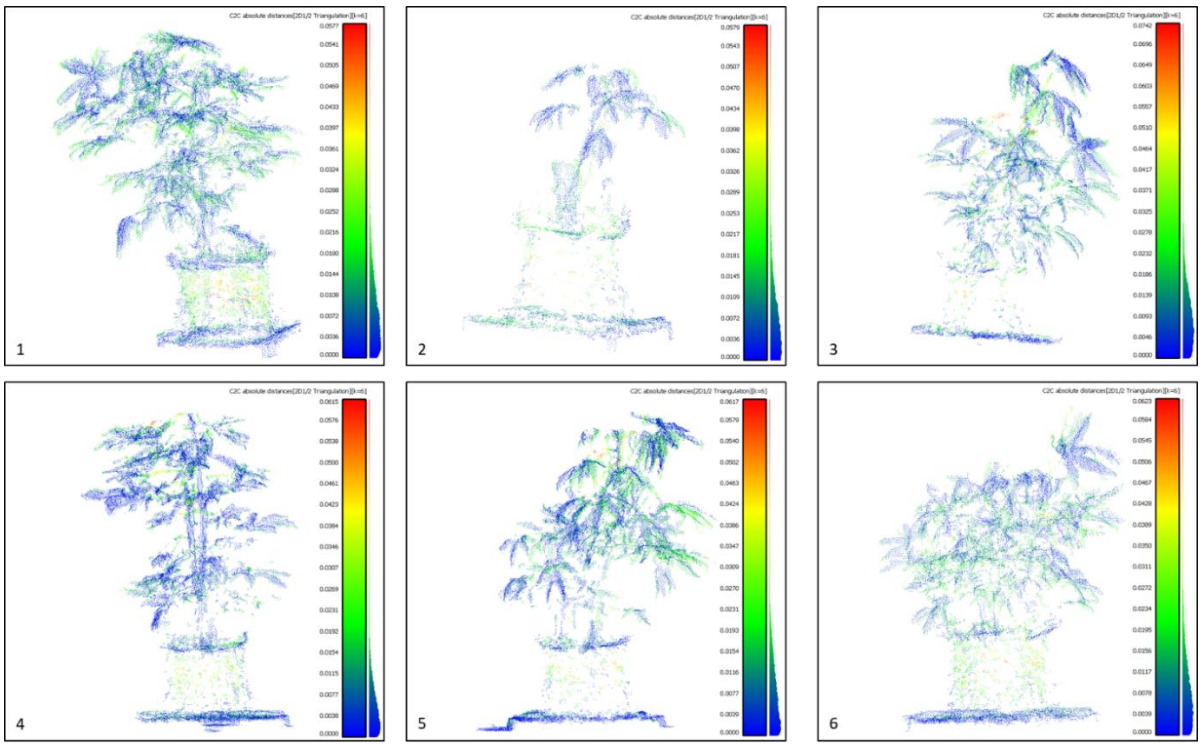

Figure 7. The Cloud-to-Cloud distance for each Kinect model visualized in CloudCompare. Points indicating high cloud-to-cloud distance (red) appear to be group primarily between vegetation and plant pots, with the pots appearing to produce points with above-average distances (0.15 and 0.04 m).

Points representing the pot, turntable and ground were removed to leave only the vegetation and a Cloud-to-Cloud distance analysis was again performed (Fig. 8). The average distance between the point clouds, based on the means of all plants, was 0.0090 m and the standard deviation was 0.0019 m. According to the Welch T-Test (Table 4), the removal of the pot made a statistically significant impact for all plants except for plant 6. However, the change in the mean distance was both positive and negative depending on the plant, and was less than 0.001 m except for plant 2, where the mean increased by 0.002 m.

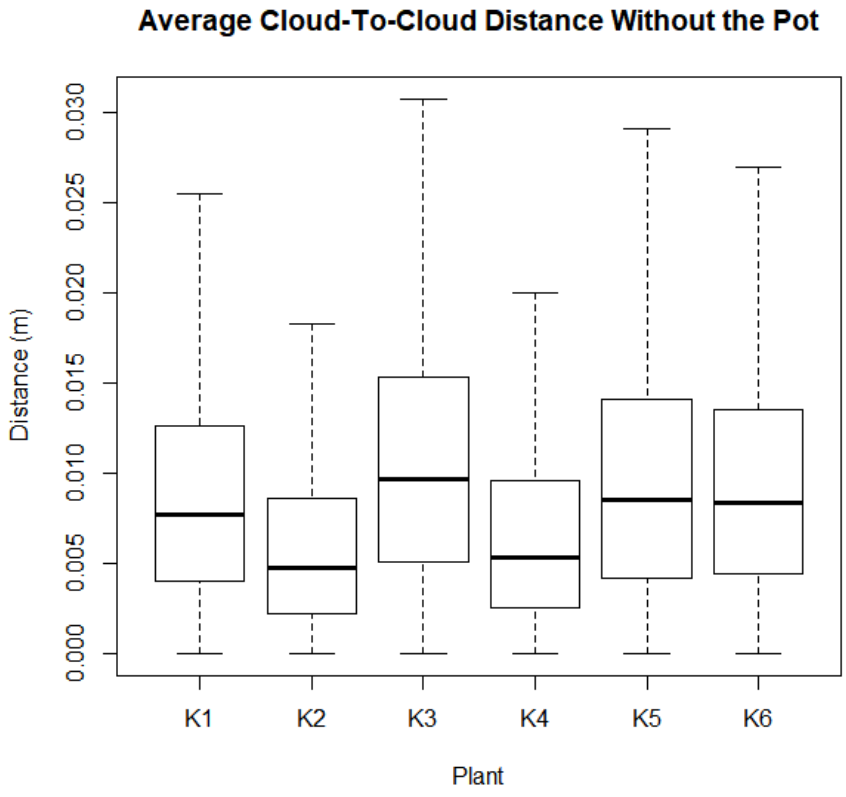

Figure 8. Distance of Kinect point cloud model from FARO model across all six plants (m) after having the planting pot and turntable removed from all images. Average distance between clouds is slightly improved at 0.0090 m.

Table 4. Welch T-Test comparing the Cloud-to-Cloud distance of the Kinect models with and without the pot. Based on p-value, impact of the removal of the pot is statistically significant in all cases except for Plant 6. All changes in mean distance were less than 0.001 m with the exception of one (Plant 2).

Plant	t-value	df	p-value	Change in Mean
1	6.5295	74476	6.641e-11	0.000335
2	18.251	11699	2.2e-16	0.002025
3	-2.6336	41714	0.008452	-0.000245
4	3.5472	58792	0.0003896	0.000204
5	-9.9175	61167	2.2e-16	-0.000628
6	1.3178	43279	0.1876	0.000094

Point Density

Point density analysis for each plant showed that the FARO scanner had a significantly greater point density than the Kinect (Table 5). The average point density for the Kinect models was 14.66 neighbors versus 74.43 neighbors for the FARO models within a radius of 0.01 m. This resulted in an average difference in the mean point density of 59.8 (Fig. 9).

Table 5. Welch T-Test comparing the point cloud density between the FARO and Kinect models, showing statistical significance between all plants.

Plant	t-value	df	p-value	Difference in Mean
1	797.85	248440	2.2e-16	55.11916
2	505.81	53850	2.2e-16	59.52009
3	573.57	164590	2.2e-16	74.3083
4	673	229100	2.2e-16	61.60727
5	694.39	206030	2.2e-16	56.74021
6	665.68	151550	2.2e-16	51.8106

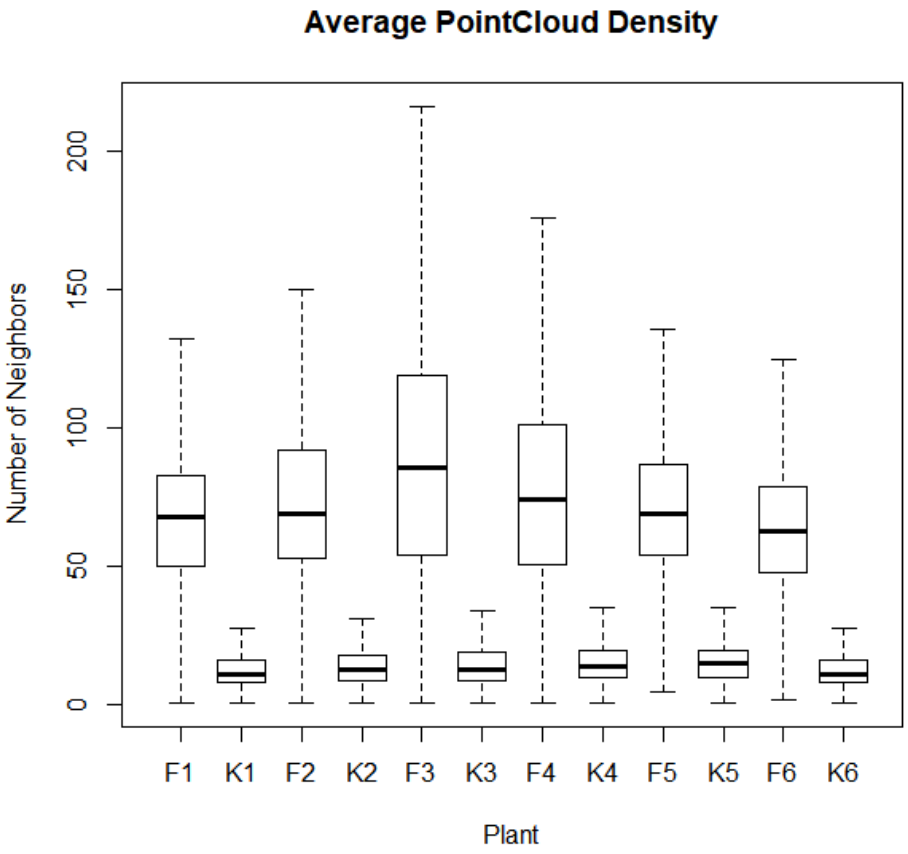

Figure 9. The average point cloud density for the FARO and Kinect models. The FARO features a much greater point density than the Kinect, showing and average of 74.43 neighbors for each point within a 1 cm radius, as opposed to the Kinect's 14.66 neighbors.

Discussion

The mean registration error of the FARO and Kinect models ranged from 0.004 to 0.0064 m and thus should have minimal effect on the point cloud comparisons. The average Cloud-to-Cloud distance was ~1 cm. This distance error is in agreement with studies showing a 1 cm error in depth estimation at distances under 4.5 m (Lachat et al., $2015_{b)}$. The mean error might be improved slightly if those points with great distances (beyond ~ 3 cm) were removed. Many of these points were concentrated around single areas in the vegetation, suggesting they might have originated from leaves moving slightly with breeze from the air conditioning. Slight

improvement in the overall Cloud-to-Cloud comparison could be achieved by using a consistent series of camera angles for each plant. In this experiment, angles were set manually by eye; a mechanical table could have eliminated much of this error. Nevertheless, an error of ~ 1 cm should have little effect on the ability to conduct many high-throughput phenotyping tasks. The ability to capture more accurate measures of phenotypic traits in a field setting by hand is questionable at best, especially at the high-throughput rates required today.

After visual assessment of the Kinect models, it was clear that the black plastic pots were not captured with much spatial accuracy or point density. For this reason, the Cloud-to-Cloud comparison was attempted with both the pot present and with only the vegetation. The removal of the non-vegetation points did not have the expected result. While a significant difference in distance existed between the models with and without the pot for all but plant 6, the difference was sometimes worse. This can be attributed to the removal of the ground and turntable points along with the pot points, which often had little variation (less than 0.01 m) in distance from the FARO model. However, the average difference of 0.009 m between the pot/pot-less models is not very meaningful, as this is well within the error of the Kinect sensor. An explanation for the lack of density, and maybe for the increased distances, within the pots is that the pot material is known to be of low reflectivity for the Kinect (Alhwarin et al., 2014). While the removal of the pot from the density analysis was statistically significant, this is of little interest to those capturing data in the field. Nevertheless, further studies should be conducted to test the Kinects' response to different colors and/or materials which would be of interest in a high-throughput phenotyping situation.

The FARO models are approximately 5 times denser than that of the Kinect. The average Kinect model had 14.66 neighbors within a radius of 0.01 m, while the FARO had 74.43. The difference

in the point density between the FARO and Kinect models for each plant was significant. However, this should have little baring on the usability of the point cloud data produced using the Kinect to conduct many phenotyping tasks. This is because the major plant parts (leaves, stems, and main stalk) are represented well, despite the lower density (Fig. 10). However, precise estimations dependent upon minute physiological features (e.g. leaf area index) might produce larger errors as compared to the FARO. In addition, the decrease in point density that occurs with increased distance from the sensor must be considered. For instance, the depth pixel size of 0.27 cm at 1 m becomes 1.09 cm at a distance of 4 m. This could have a major impact on data quality for very large plants or those captured at greater distances from the sensor.

While biomass assessments were not made for the plants used in this experiment, the results nevertheless have implications for other observable characteristics. While not as dense as the FARO point cloud, the Kinect was still capable of capturing plant structure to the degree that it could distinguish between cassava genotypes if applied in a field setting, especially if these genotypes differed significantly in areas like height. Stems were not as visible in the Kinect clouds as in the FARO, but cloud-to-cloud distances were lowest on the main stalk and leaves of each plant. This is encouraging as it shows that, at least in case of cassava, information on leaf area, leaf angle, and perhaps even leaf count can be obtained. Also unique under these circumstances was the Kinect's capability of capturing color information under indoor conditions. While this may not seem relevant to many plant breeders now due to the Kinect's inability to work in direct sunlight, this kind of information can still be obtained by using the sensor on overcast days. Likewise, new RGB-D cameras are being developed that can limit the effect of ambient light on the images captured, making usable color information from the field a possibility in the near future.

Figure 10. A side-by-side comparison of Plant 4 (Kinect on the left, FARO on the right). Note that the pot is lacking in point density for the Kinect model.

Conclusion

Plant breeders who want to incorporate high-throughput phenotyping technology into their programs face a variety of obstacles getting started. In addition to the acquisition costs and technical expertise needed to operate these systems, current technologies may be limited in areas that specific breeders find valuable. The ultimate decision of whether or not to adopt these phenotyping platforms will largely depend on application, as well as the reliability of the technology available.

One of the major advantages of depth sensors as compared to laser scanners is the ability to capture a scene rapidly. During the several minutes required to scan an outdoor scene with the FARO Focus it is almost inevitable there will be some movement in the plants, either from wind

or changes in structure. These errors will be compounded during the registration if multiple scans are used. While registration errors cannot be avoided by using a depth sensor, the issue with plant movement can be reduced. This is because the entire FOV of the Kinect sensor is captured at once. If multiple depth sensors were triggered instantaneously, the impact of motion in the scene could be generally ignored. However, the Kinect is prone to interruption from other sources of infrared light, especially from other Kinect sensors. This problem can be avoided by adjustment of the modulation frequency of the IR light used for the depth estimation. However, Microsoft does not allow adjustment of this feature at this time. The use of multiple Kinects can be accomplished by firing them sequentially; though this does negate some of the benefit, it is still much faster than a standard TLS.

The next step in this process is the creation of a field-worthy platform to test the Kinect sensors outside. One of the major limitations of the Kinect sensors is the limited FOV at close distances, which can impair the sensor's ability to capture full plants that are beyond its height or width limitations. This can be overcome by the use of multiple sensors with overlapping FOV. Such a platform would also require multiple computers with specific features in order to control the cameras, as well as a custom software package to allow maximum user interaction. The client-server program used in this study could be expanded to allow easier image capture and control of the cameras in the field, especially in the form of a smartphone app.

Despite having lower resolution, the Kinect can be a cost-effective alternative for applications that don't require sub-centimeter resolutions (e.g. height or volume approximations), as well as other types of data collection. These sensors also benefit from being highly portable and could be easily attached to many different field cart designs. Another major advantage of the depth camera is the instantaneous capture of data could provide a solution for issues of wind in the

field, although the sensor still faces challenges when being used on sunny days. But while the Kinect does seem to sufficiently capture cassava plant structure, this is not a guarantee that it will correlate positively to biomass. Additional studies will need to be conducted to determine the extent to which ground-based sensors can determine this trait, especially in cassava.

CHAPTER IV

ESTIMATING ABOVEGROUND BIOMASS OF CASSAVA (*MANIHOT ESCULENTA*) USING A NOVEL PHENOTYPING PLATFORM: A FIELD TRIAL

Introduction

Remote sensing technology offers a wide array of services in the agricultural sector, and its use continues to grow as sensor prices drop. Specifically, terrestrial laser scanners (TLS) have become more popular and increasingly available to those without large budgets. Still, in the case of plant breeding, where large-number trials are routine and cheap phenotyping methods are essential, TLS costs are still high enough to create a burden on many publicly-funded plant breeding programs. Because of this, the need for low-cost alternatives is still a worthwhile pursuit.

Cassava (*Manihot esculenta*) is a woody shrub cultivated in tropical and subtropical environments for its tuberous root, which is rich in starch and is a staple in diets throughout Latin America and Africa (Hillocks and Thresh, 1982). An important food source throughout the developing world, cassava provides more than 300 calories per day to hundreds of millions of people on the African continent alone (Anikwe and Ikenganyia, 2018). As such, it is important that the crop bulk early and provide large roots with minimal plant stress. Monitoring the aboveground growth of cassava plants through non-destructive means can allow growers to estimate bulking rates and harvest at optimal times.

Selection of early storage root bulking (ESB) is essential for maximizing efficiency in production of cassava. Being able to plant and harvest the crop within one rain cycle is particularly important for farmers in regions with limited rainfall, as well as those who

incorporate other crops into their operations (Kamau et al., 2011). This is particularly important for smaller farms, who would benefit from 50-100% increases in yields if harvest ability can be reached within 8 months (Tumuhimbise et al., 2012). It is for this reason that all methods that could contribute to ESB varieties be explored.

While remotely sensed belowground biomass information is currently being investigated as a means to accurately select for ESB in cassava, there still remains a need to have accurate biomass information for aboveground plant material. Although cassava root is valued as a food source by humans, the surface vegetative material is still an important component of animal feed in the nations in which it is cultivated (Klein, 2016). This, in addition to the possibility that aboveground biomass may correlate to early root bulking, makes the development of new phenotyping tools essential for cassava breeders wanting to select for this trait.

This study used both a ground-based LiDAR sensor and a series of RGB-D cameras as proxies for biomass sampling of cassava plants in a real agricultural field setting. The goal of this chapter is to build on previous sensor comparisons performed under controlled conditions (greenhouse settings) to predict aboveground biomass in *Manihot esculenta*. This will be achieved through several objectives: 1) To determine if an industry-standard TLS (Trimble TX5) is capable of collecting biomass data suitable for cassava phenotyping, 2) to test a custom-made, multiple-camera platform (currently known as “Scorpion”) for the improved acquisition of Microsoft Kinect V2 data, and 3) to determine if a count of points within a point cloud serves as a reliable predictor of biomass. While it is expected that the TX5 will provide a clearer, denser point cloud as compared with the Scorpion, the results of the study will determine which sensor, if either, is a viable biomass phenotyping tool that can be used in the field.

Methods

Location/Layout

The field trials used for this experiment were grown on campus at the International Center for Tropical Agriculture (CIAT) in Palmira, Colombia. The fields set up for the test were blocked horizontally based on genotype and vertically based on date planted (Fig. 11). Planting of the cassava samples began in 2016, with planting dates spaced out over a monthly basis, resulting in plants between 4 and 12 months old. Each plot contained 15 plants, consisting of 3 rows of 5 plants each. Within the plots, plants were set 1 m apart in order to prevent overlap; however, a small number of the plants did receive overlap between branches. There were no borders between plots, but there was a border surrounding the entire experiment.

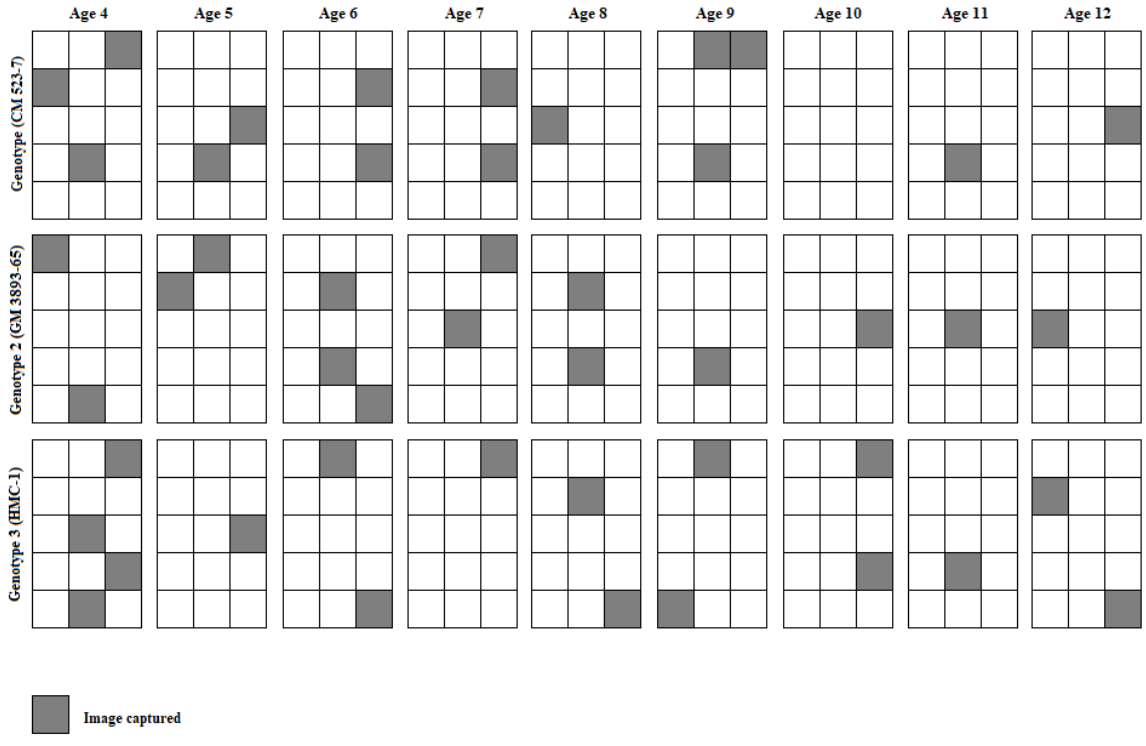

Figure 11. Field setup for plants used in experiment. Images were captured for plants across three genotypes (CM 523-7, GM 3893-65, and HMC-1) and roughly 9 age groups, the exception being Age 10 in CM 523-7.

Genotypes used in the experiment were chosen for their contrasting canopy architecture (Fig. 12). Genotype 1, CM 523-7 (also known as “standard type”), is a shrub with all branches clearly above the ground. Genotype 2, GM 3893-65-Esparrago (also known as “asparagus type), is designed to allow for greater planting density and thus grows upright with leaves protruding directly from the stalk (thus, no branches). Genotype 3, HMC-1 (also known as “low-branch type”) is another shrub type; however, it is smaller than the standard type with branches that hang low to the ground, often touching the surface.

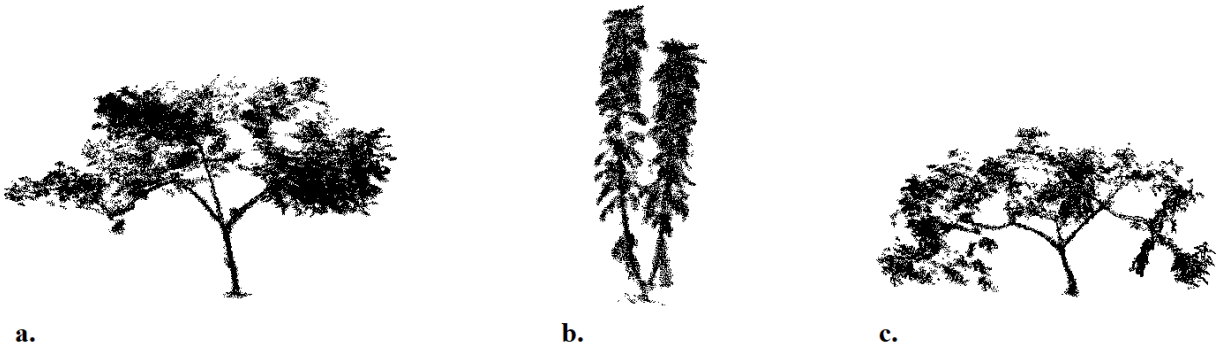

Figure 12. Cassava genotypes used in the CIAT experiment. CM 523-7 (a), GM 3893-65 (b), and HMC-1 (c).

Plant Material

Forty-seven cassava plants were chosen from the field trials for this experiment. Images were captured with both of the sensors as much as time would allow. While the intention was to get at least three images per plot, some plots were only able to have one or two images captured due to time constraints. Also, the Kinect platform occasionally encountered sensor problems; namely, one of the three cameras did not go off or produced a corrupted file. In these cases, the plant was discarded. In total, images analyzed included 15 plants from Genotype 1, 15 from Genotype 2,

and 17 from Genotype 3. This included plants from all age groups, with the exception of Genotype 1, which had no viable images collected for age 10 months.

All plants scanned were later harvested, dried, and weighed in order to provide dry weight for the leaves and stems (Fig. 13). This was completed by CIAT employees, who marked the plants in 20 cm increments from the ground level in order to provide binned biomass data. In addition, plants were harvested in a way that allowed for a distinction to be made between leaf and stem weight (essentially, the plants were harvested by collecting the leaves first and then the stems, separating them into two different bags). Harvest began the day after scanning and took roughly one week to complete. Prior to drying, the samples were places in cold storage. Commercial dryers set to 70°C were used to dry the plants before weighing.

Figure 13. Cassava fields at CIAT campus before harvest (a) and after (b).

Image Acquisition

Because wind movement of the plants would have a distorting effect on the TX5 data, in addition to the direct sunlight impairing the Kinect's ability to capture images, the scans for both sensors were taken at night when the wind was low. Because of this, no real color information was able

to be captured for any of the images. Scans of each plant were taken *in situ*, and no targets were set up for later registration of the point clouds. However, there were numerous stakes marking plots in the field, and it was decided that these would serve as suitable targets for registration.

Two scans of each plant were taken with both of the scanning platforms: on the north and the south side of the plant (Fig. 14). This was done so that there would be a fuller picture of the plant once the south side was registered to the north. There were a few circumstances when images were captured from a slightly different angle that north/south due to other plants blocking the scanner location; however, most plans conformed to the standard procedure. Each image was taken roughly 1.5 m from the center of the plant and designed so that the plant would be captured in the middle of the image.

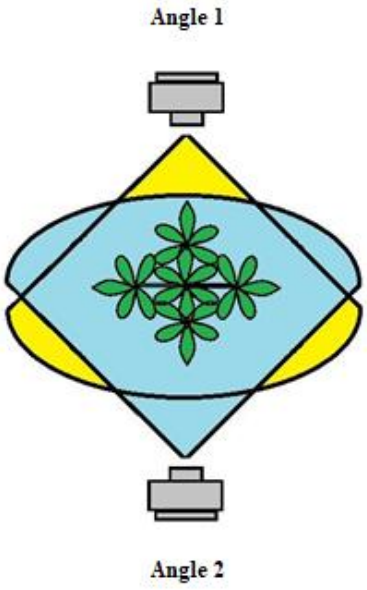

Figure 14. Scan angles for cassava plants, taken from the north and south side of each plant. Note that these same angles were used both for the TLS and the Scorpion Kinect Platform.

TX5

The LiDAR unit used for this study is the Trimble TX5, which is essentially a repackaged and rebranded FARO Focus 120 TLS. As such, it is a continuous wave terrestrial laser scanner and retains all of the same features as the Focus, including a 0.6 to 120 m meter range (with a ranging error of ± 2 mm at 10 and 25 m), and operates at a wavelength of 905 nm. These types of scanners have already been tested in the field and have proven to be both a popular and effective means of capturing phenotypic data (Omasa et al., 2007) (Friedli et al., 2016).

The settings for the TX5 were as follows: A resolution of 1/5, quality of 3x, scan size of 2959 X 3414, and a scanning window of -60° to 90° vertical and 0° to 180° horizontal. At the setting, each scan took approximately 2 minutes and 39 seconds to complete, with a point distance of 7.67 mm at 10 m. An industrial tripod was used to mount the scanner and resulted in a scanner height of approximately 1.25 meters for each scan, although this varied slightly based on the topography of the field.

Scorpion

The Microsoft Kinect V2 is an RGB-D camera that allows collection of high-resolution 3D data with a high repeat measurement frequency. Both the Kinect Version 1 (released 2010) and Version 2 (released 2014) have been previously explored as a tool for a variety of scientific fields (Wilson, 2017), including agriculture (Omasa et al., 2007) (Friedli et al., 2016), speleology, and glaciology (Hämmerle et al., 2014) (Mankoff and Russo, 2013) (Lachat et al., 2015). Although the Kinect can provide a low-cost (~$150) method of 3D imaging, it is prone to several issues that are not present with traditional terrestrial laser scanning. Two of the most obvious issues are the lower quality and shorter range. Another problem is that the Kinect seems

to perform poorly in direct sunlight (Lachat et al., 2015) (Marin, 2017), largely restricting its use outdoors.

The Microsoft Kinect V2 works utilizing a similar time-of-flight principle as the TLS. However, the Kinect functions like flash LiDAR, sending out large, multiple bursts of light at once from a 512 x 424 x 16 bits per pixel 16-bit depth sensor as opposed to creating an image from a rapidly repeating single laser point. In this way, its designation as true LiDAR is debatable. However, it is capable of producing 3D point clouds similar to that of the TX, only of a lower resolution. The Kinect is also a 1920 x 1080 x 16 bits per pixel color camera with a 70° Horizontal – 60° Vertical angular field-of-view and a 0.5 m to 8 m range. Naturally, this rage and resolution pales in comparison to the TX5, and thus a new platform needed to be developed in order to overcome this limitation.

Each image capture in this experiment utilized three Kinect sensors at once by means of a custom-built platform known as “Scorpion” (Fig. 15). The entire Scorpion system consists of three Kinect sensors, a single board computer (SBC) for each sensor, a battery with a power inverter, a metal frame to hold the sensors in place, and a plastic tote to hold the electronic components (Fig. 16).

Figure 15. The Scorpion phenotyping platform utilizing three Kinect cameras to widen the field-of-view.

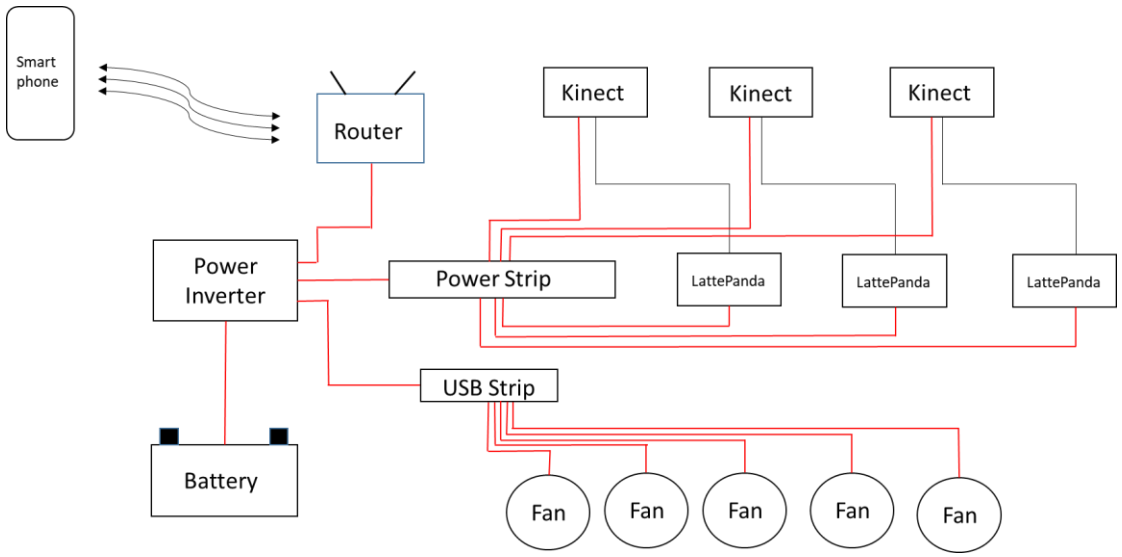

Figure 16. Scorpion platform hardware, featuring battery, power inverter, single board computers, cooling fans, and necessary USB and surge protector hookups.

The metal platform holding the Kinects consisted of a steel base and aluminum sensor frames. It was decided that three sensors would be used because it would provide good coverage of the plant while not being too heavy. The basic structure was constructed out of 3 cm steel square tubing with a 1.98 mm wall thickness and consisted of two parts: a top and a base. The base was

made into an H shape in order to allow it to remain stable on uneven terrain. The top was designed to position the sensors at slightly different distances and angles so that they could capture different parts of the plant, all while having some overlapping imagery. The two parts were connected by a single bolt to minimize tension on the structure.

The rectangular frames that hold the Kinect sensors in place were constructed out of aluminum to minimize the weight of the overall platform. The sensors are secured by bolts capped with circular 2.54 cm rubber pads to protect the sensor from damage (Fig. 17). The frames were then bolted to the steel support structure and held in place by Blue Loctite (Henkel AG & Company, KGaA), a thread locking chemical, to ensure no movement.

Figure 17. An adjustable Kinect sensor frame used to hold the camera in place with no movement.

Because a Kinect sensor requires a dedicated graphics card, Windows 8.0 or higher (for the Kinect SDK 2.0 software), and a USB 3.0 bus, it was necessary to provide an entire computer for each sensor. Issues of cost and size were mitigated by utilizing single board computers (SBCs) loaded with Windows 10 from LattePanda. Specifically, the LattePanda 4G/64GB model was chosen because it met all of these requirements. The battery and power inverter in the carrying case was used to power the sensors as well as the SBCs.

In order to capture data with the Kinect sensors, a custom-made app was developed. The Scorpion Web Controller App uses the Microsoft RoomAlive system to communicate with the sensors, SBCs, and the user to capture data. Built in C#, this app allows operators to use a smartphone to capture an image, name the image, restart the SBCs, and power the system on and off. The app allows for an easy image capture and can be used as long as the smartphone and SBCs are connected to the same Wi-Fi network (Fig. 18). This is carried out by having each SBC run, on startup:

1. The Scorpion Web Application

2. Web API Gateway (sends the order to the corresponding sensor)

3. KinectServer.exe (a program that allows capture and storage of an image)

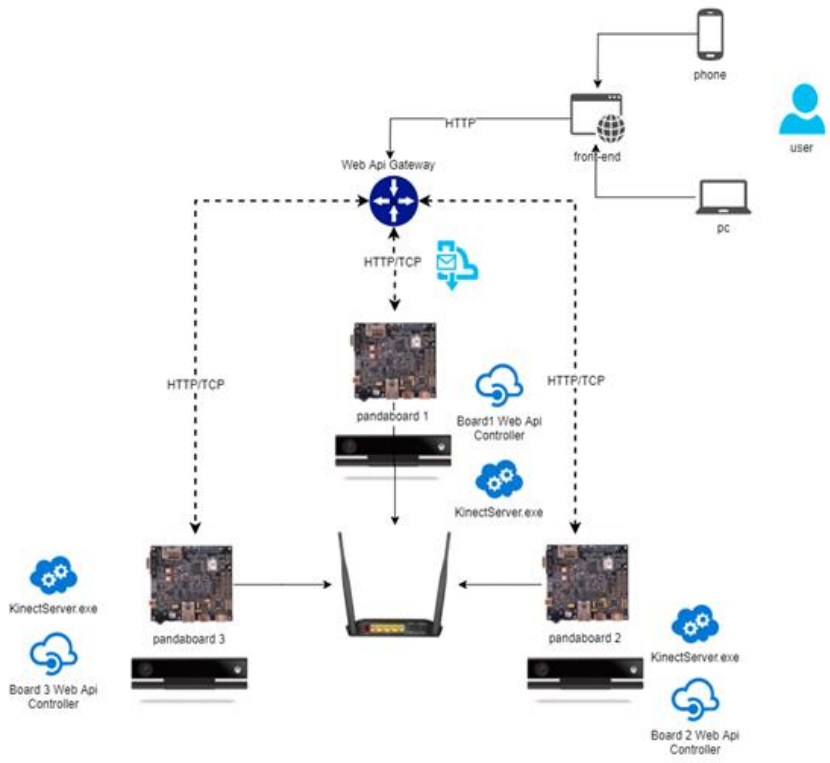

Figure 18. Overview of the Scorpion Web Controller App setup, showing single board computer and Kinect sensor operation by smartphone through wireless router.

Processing

CloudCompare version 2.10. alpha, an open source 3D point cloud (and triangular mesh) editing and processing software, was used for the preprocessing of the LiDAR files. The original TX5 files were in FARO's proprietary .fls format, which is compatible with both the FARO SCENE and Trimble RealWorks software packages. In order to view and manipulate these files in CloudCompare, the files were exported from SCENE into .xyz files. The files from Kinect were already in .csv format, which can be read my many software types, including CloudCompare.

As mentioned previously, stakes that were set up in the field were used as targets for registration (Fig. 20). For the TX5's files, each plant's north and south-angle images were registered together. After the two sides were registered together, they were merged into one cloud, creating a full 3D model for each plant (Fig. 19).

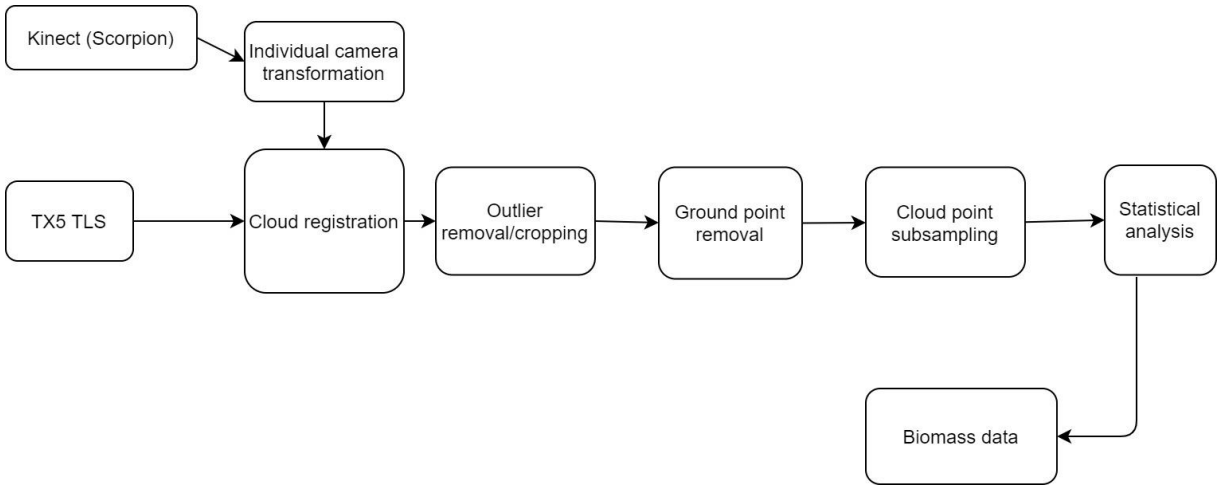

Figure 19. Data Processing flowchart.

Figure 20. Using field stakes for registration of TX5 point clouds in CloudCompare software.

For the Kinect files, before the north and south angles could be registered, the three individual cameras of the Scorpion had to be registered so that a complete shot of the angle could be created. This was achieved using the Apply Transformation tool in CloudCompare. Before the images were captured in the field, an establishing shot was taken to be used as a reference. In this case, the image was taken of a tree, which was clear enough that it could be registered based on individual characteristics (such as unique branch areas) without the need of formal targets. The cameras were numbered according to the part of the plant they represented: Camera 1 is the middle portion, Camera 2 the bottom, and Camera 3 the top. Whenever one part is registered to another (for example, registering Camera 2 to Camera 1), a series of point cloud coordinates are given that save the registration location within the workspace. When registering the same camera image from the cassava plants, these coordinates can then be plugged into the Apply Transformation tool and will automatically register based on what was given in the reference shot (Fig. 21). After these coordinates were applied to all of the Camera 2 and Camera 3 images

across the cassava plants, the north and south angles of the Kinect images were registered together.

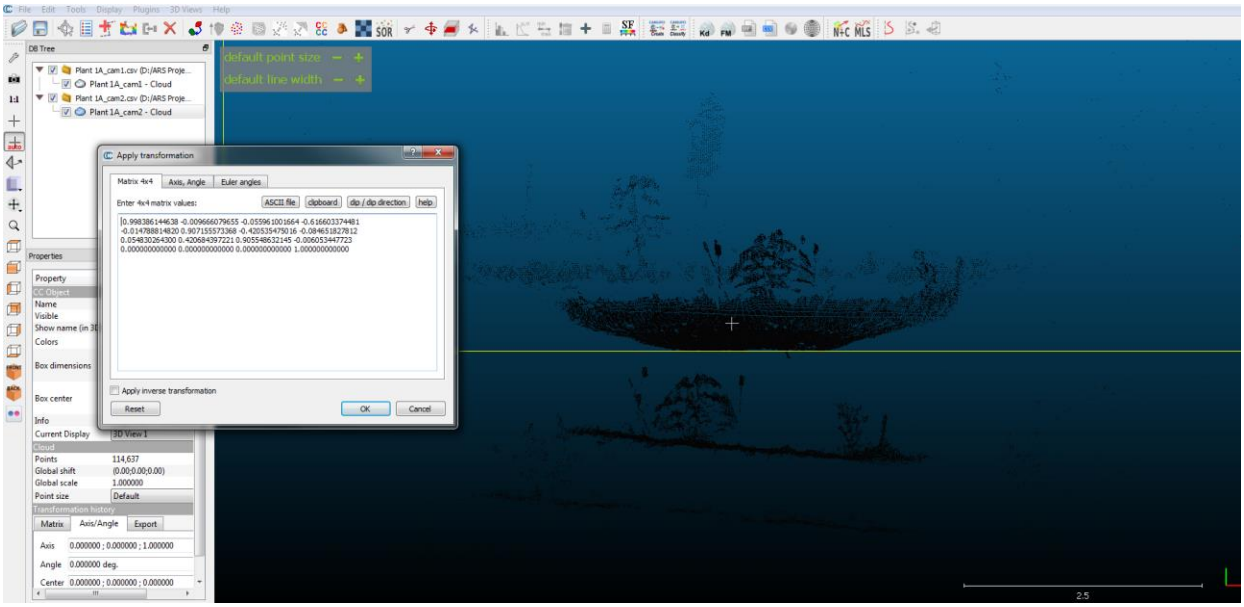

Figure 21. Applying transformation numbers derived from reference shot to a cassava plant (Kinect). This method was used to solve extensive time it would have taken to register the three Scorpion camera shots to each other for each plant.

After the point clouds were cropped to include only the plant of interest and the necessary ground points for classification, the Statistical Outlier Removal (SOR) tool was used to clean noisy points from the cloud. The mean distance estimation for the SOR was set to 6, while the standard deviation multiplier threshold was set to 1.00. These settings were determined based on previous trial and error that cleaned up the largest amount of noise points while minimizing the points that were cut out of the vegetation.

Ground Points

Before running a regression, it was first necessary to isolate only the parts of the image that would be used in the analysis. It was decided that rather than manually clipping the irrelevant

areas, and computer ground classification would be used. The statistical software R (version 3.4.2.) already featured code that would allow for such classification, called lasground_pmf (Progressive Morphological Filter). The code is able to differentiate between ground and aboveground points by using a two-variable filter: the first being the sequence of window sizes used for filtering ground returns, and the second a sequence of threshold height above the ground surface (Zhang et al., 2003). For the TLS scans, a window size of 0.2 m and a threshold height of 0.05 m sufficed.

Much trial and error were needed in determining the proper window size and threshold height for the Kinect scans. Several of the scans were properly classified using the same parameters as the TLS; however, several of the scans needed to have window sizes changed in order to carry out proper classification. In total, four plants were run with a window size of 0.2, twenty-three plants at 0.35, seventeen plants at 0.4, two plants at 0.47, and one plant at 0.50. Additionally, classification of grounds points was made more difficult as the Kinect's lower resolution produced a lower amount of ground points from which the analysis could be drawn. The problem resulting from this low point density is that some aboveground points (specifically, those that lie above the areas with a thin amount of surface points) can be incorrectly classified as ground points. This could be corrected by copying the thicker point density from other ground parts of the cloud and pasting it into the ground sections that had lower point density.

Subsampling

Before running the point cloud density against dry weight, a subsample of the point clouds was taken. This was completed through CloudCompare's subsample tool, setting the minimum space between points to 0.002 m (2 mm), as this is within the maximum range accuracy of the TX5.

This was necessary as to avoid any data degradation that may come from registering the multiple clouds together.

Analysis

Analysis was also completed using R version 3.4.2; more specifically, plotting was completed using the ggplot2 package, while bootstrap analysis was done using R's boot package. All bootstrapping was done using the bias-corrected and accelerated method (BCa) in order to offset any bias or distributional skewness in the results. Five thousand iterations were used with a confidence level of 95%.

The number of points within all of the binned levels were regressed against the entire plant's dry weight, both for the TLS files as well as the Kinect. However, because there was a separation between the leaf and stem weight in the field data, it was decided to do two analyses for each plant: regressed against the stem and leaf weight combined, and against only the leaf weight, with bootstrap analyses following both of these. The regressions were conducted in this manner because only a small amount of the stem (estimated as <5%) was captured in each image, as the plants across all genotypes are covered in leaves. Likewise, any attempt to remove the stems from the point clouds would have to have been done manually, and thus would certainly create bias.

In addition to analyzing all 47 plants by stem/leaf and leaf-only weights, regression was also run based on genotype. In all, calculations for biomass of both the TLS and the Kinect were conducted across all genotypes and individual genotypes 1 through 3.

Results

TX5 Stem and Leaf (Full Plant)

Because the terrestrial laser scanner is considered one of the industry-standard forms of LiDAR for agricultural research, the TX5's analyses were run first. In addition, it was also decided to look first at the regression of the subsampled point clouds against the entire weight of the plant, including leaf and stem. Looking at the cassava plants across all genotypes, the R^2 value was 0.73, with a P-value of 1.26e-16. The bootstrap revealed a mean R^2 of 0.74, a bias of 5.79e-4 and a standard deviation of 0.07. The 95% confidence interval was between 0.55 and 0.84 (Fig. 22).

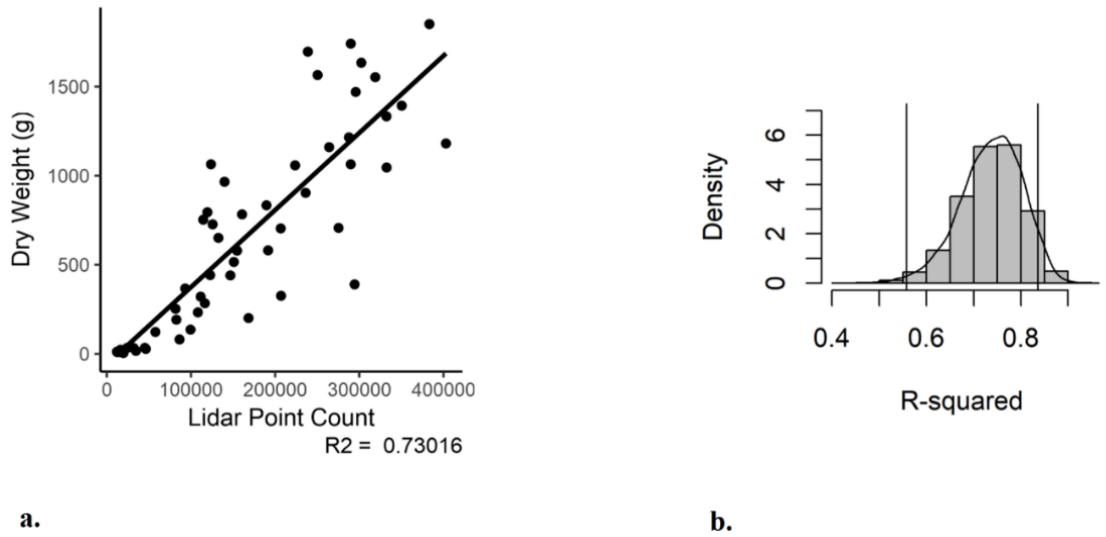

a. **b.**

Figure 22: Subsampled TX5 point cloud regressed against dry weight of stem and leaves across all genotypes. The regression R^2 value shows a correlation of 0.73 (a), while the bootstrap reveals a mean R^2 of 0.74 based on five thousand iterations, with a confidence interval between 0.55 and 0.84 (b).

After running the regression across all genotypes, the plants were then segmented by genotype and another regression analysis was run. This revealed some variation as compared with all the genotypes being considered together. Genotype 1 (CM 523-7, also known as "standard type") showed an R^2 of 0.64 with a P-value of 4.32e-5. The bootstrap revealed a mean R^2 of 0.66, a bias

of 4.84e-3 and a standard deviation of 0.1. The 95% confidence interval was between 0.36 and 0.81 (Fig. 23).

Genotype 2 (GM 3893-65, also known as “asparagus type”) showed an R^2 of 0.95 with a P-value of 1.12e-12. The bootstrap revealed a mean R^2 of 0.96, a bias of 1.37e-3 and a standard deviation of 0.01. The 95% confidence interval was between 0.92 and 0.98 (Fig. 23).

Genotype 3 (HMC-1, also known as “low-branch type”) showed an R^2 of 0.71 with a P-value of 6.45e-6. The bootstrap revealed a mean R^2 of 0.73, a bias of -7.65e-3 and a standard deviation of 0.12. The 95% confidence interval was between 0.40 and 0.88 (Fig. 23).

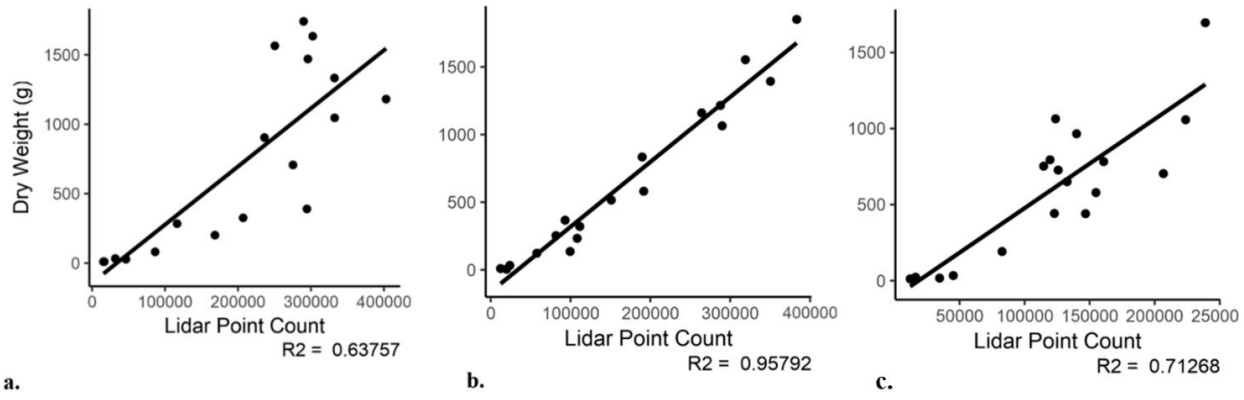

Figure 23: Subsampled TX5 point cloud regressed against dry weight of stem and leaves for standard (a), asparagus (b), and low-branch (c) genotypes. The R^2 value of the asparagus genotype was the most successful at 0.96, followed by the low-branch type at 0.71 and the standard at 0.64. Bootstrap analyses were also run on each genotype, revealing a mean R^2 of 0.66 (a), 0.96 (b), and 0.73 (c).

TX5 Leaf Only

After looking at the relationship between the subsampled point cloud and the entire dry weight of the plant, the point clouds were then regressed against only the weight of the plant leaves. It was expected that this may improve some of the correlations, as much of the visible part of the plants

consisted of leaves. Looking at this regression across all genotypes, the R^2 value was 0.80, with a P-value of 2e-16. The bootstrap 95% confidence interval was between 0.63 and 0.88 (Fig. 24).

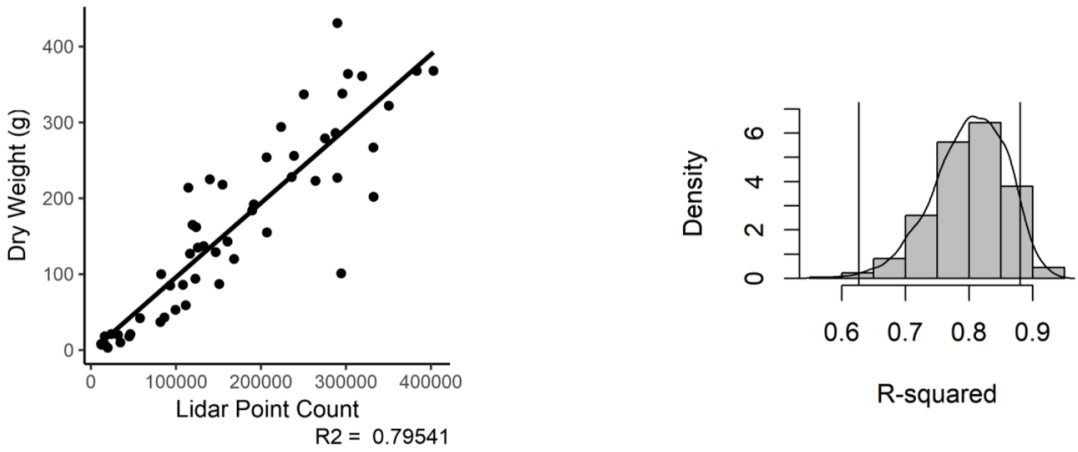

a. **b.**

Figure 24: Subsampled TX5 point cloud regressed against dry weight of leaves only across all genotypes. The regression R^2 value shows a correlation of 0.80 (a), while the bootstrap reveals a mean R^2 of 0.80 based on five thousand iterations, with a confidence interval between 0.63 and 0.88 (b).

As with the stem and leaf weight regressions, separating the plants by genotype created some variation in the correlations. Genotype 1 was somewhat improved when looking at leaf-only data, with an R^2 of 0.70 and a P-value of 8.66e-06, maintaining a bootstrap 95% confidence interval between 0.33 and 0.88 (Fig. 25).

Genotype 2 was largely unchanged, showing only a slightly lower R^2 of 0.95222 (as opposed to the 0.95792 of the stem and leaf), and a P-value of 3.35e-12. The bootstrap 95% confidence interval was 0.91 - 0.98 (Fig. 25).

Genotype 3 had the greatest improvement of the three genotypes, with an R^2 of 0.83 and a P-value of 1.13e-7, while maintaining a bootstrap 95% confidence interval of 0.58 - 0.94 (Fig. 25).

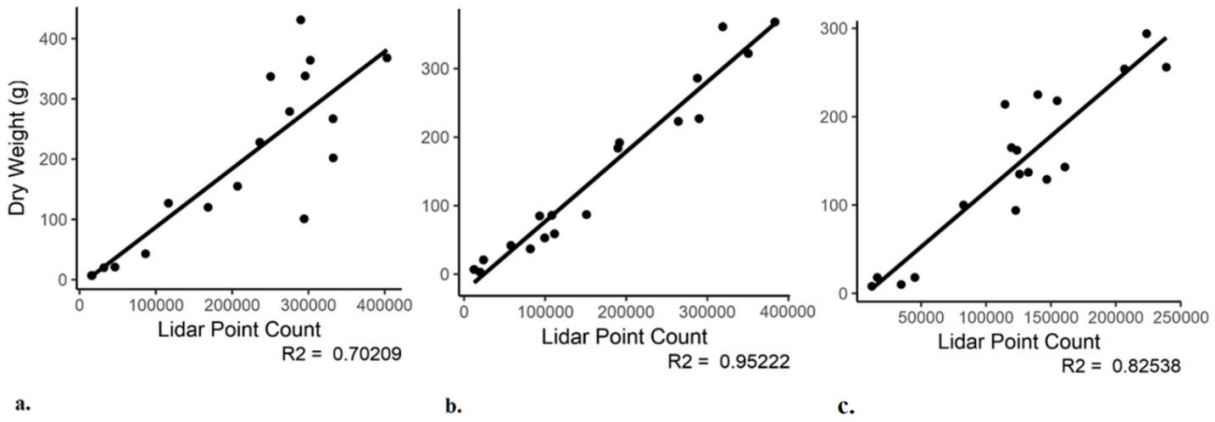

Figure 25: Subsampled TX5 point cloud regressed against dry weight of leaves only leaves for standard (a), asparagus (b), and low-branch (c) genotypes. The R^2 value of the asparagus genotype was again the most successful at 0.95, followed by the low-branch type at 0.82 and the standard at 0.70.

Kinect Stem and Leaf (Full Plant)

After the TX5 clouds were analyzed, the Kinect scans were then run through the same process, beginning with looking at the entire plant weight (steam and leaf) across all genotypes. This yielded an R^2 of 0.71, with a P-value of 1.12e-13. The bootstrap revealed a mean R^2 of 0.71, a bias of -1.39e-03 and a standard deviation of 0.09. The 95% confidence interval was between 0.47 and 0.84 (Fig. 26).

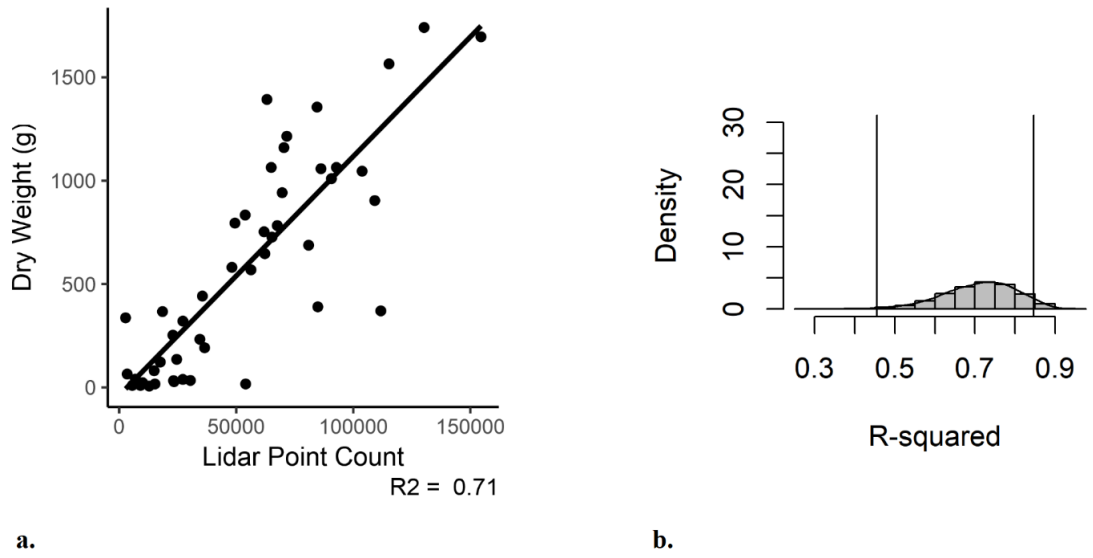

Figure 26: Subsampled Kinect point cloud regressed against dry weight of stem and leaves across all genotypes. Regression (a) and bootstrap (b). The regression R^2 value shows a correlation of 0.71 (a), while the bootstrap reveals a mean R^2 of 0.71 based on five thousand iterations, with a confidence interval between 0.47 and 0.84 (b).

As with the TX5 data, after analyzing the point cloud versus dry weight across all genotypes, same analysis was then run based on genotype. Again, this revealed variation as opposed to running all genotypes as a whole. Genotype 1 (CM 523-7, also known as "standard type") showed an R^2 of 0.81 with a P-value of 4.90e-06. The bootstrap revealed a mean R^2 of 0.81, a bias of 7.40e-04 and a standard deviation of 0.07. The 95% confidence interval was between 0.59 and 0.93 (Fig. 27).

Genotype 2 (GM 3893-65, also known as "asparagus type") showed an R^2 of 0.91 with a P-value of 2.88e-08. The bootstrap revealed a mean R^2 of 0.91, a bias of 2.36e-03 and a standard deviation of 0.04. The 95% confidence interval was between 0.78 and 0.97 (Fig. 27).

Genotype 3 (HMC-1, also known as "low-branch type") showed an R^2 of 0.67 with a P-value of 6.47e-05. The bootstrap revealed a mean R^2 of 0.67, a bias of -1.34e-02 and a standard deviation of 0.21. The 95% confidence interval was between 0.09 and 0.92 (Fig. 27).

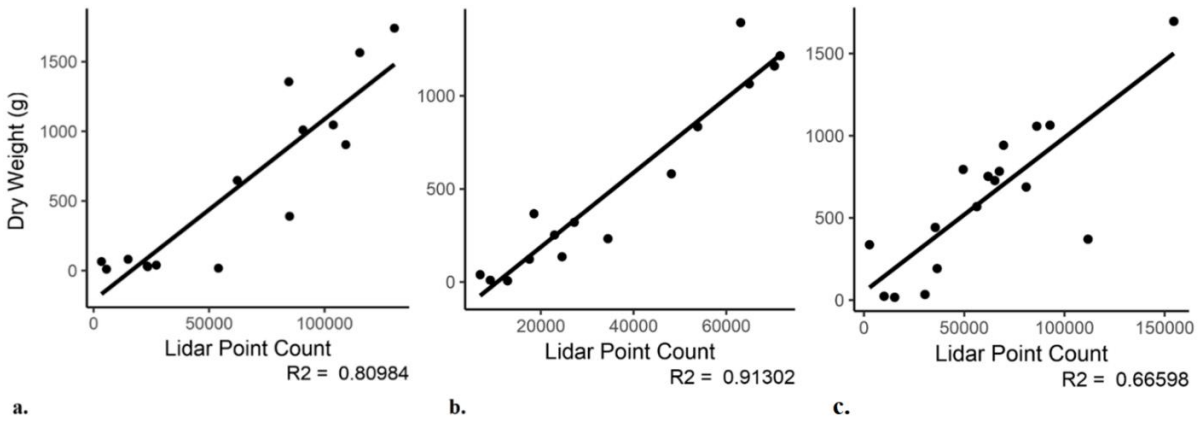

Figure 27: Subsampled Kinect point cloud regressed against dry weight of stem and leaves for standard (a), asparagus (b), and low-branch (c) genotypes. The R^2 value of the asparagus genotype was the most successful at 0.91, followed by the standard type at 0.81 and the low-branch at 0.67.

Kinect Leaf Only

Following the full plant (stem and leaf) regressions, the same procedures were carried out using the Kinect point clouds versus dry weight. It was also theorized that examining this data by leaf-only weight might improve the correlations. This was not found to be the case when looking at this regression across all genotypes, which yielded an R^2 value of 0.66, with a P-value of 5.55e-12. The bootstrap 95% confidence interval was between 0.48 and 0.79 (Fig. 28).

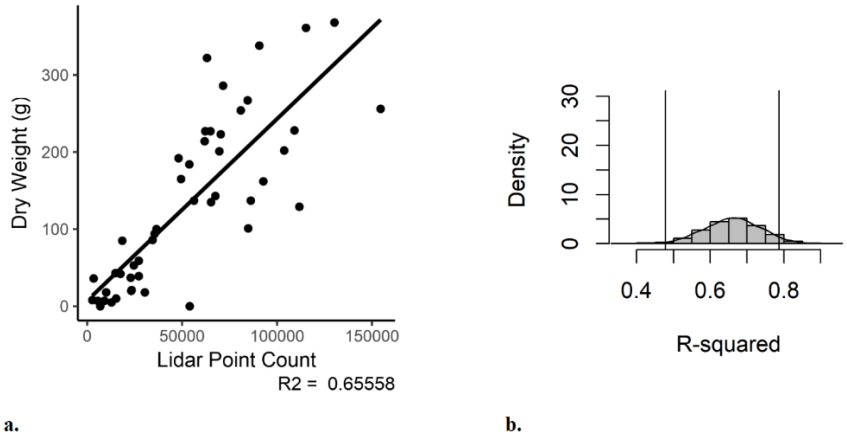

Figure 28: Subsampled Kinect point cloud regressed against dry weight of leaves only across all genotypes. The regression R^2 value shows a correlation of 0.66 (a), while the bootstrap confidence interval is between 0.48 and 0.79 (b).

Breaking the data down by genotype, Genotype 1 showed some improvement, with an R^2 of 0.76 and a P-value of 2.38e-05, maintaining a bootstrap 95% confidence interval between 0.51 and 0.90 (Fig. 29). Genotype 2, like with the TX5, showed relatively little change, with a slightly lower R^2 of 0.91202 (as opposed to the 0.91302 of the stem and leaf), and a P-value of 3.11e-08. The bootstrap 95% confidence interval was 0.80 – 0.96 (Fig. 29). Much unlike its TX5 equivalent, Genotype 3 actually had a loss of correlation when looking at leaf-only weight, and ended up being the worst in the experiment, with an R^2 of 0.62 and a P-value of 1.59e-04, The bootstrap 95% confidence interval was between 0.19 – 0.81 (Fig. 29).

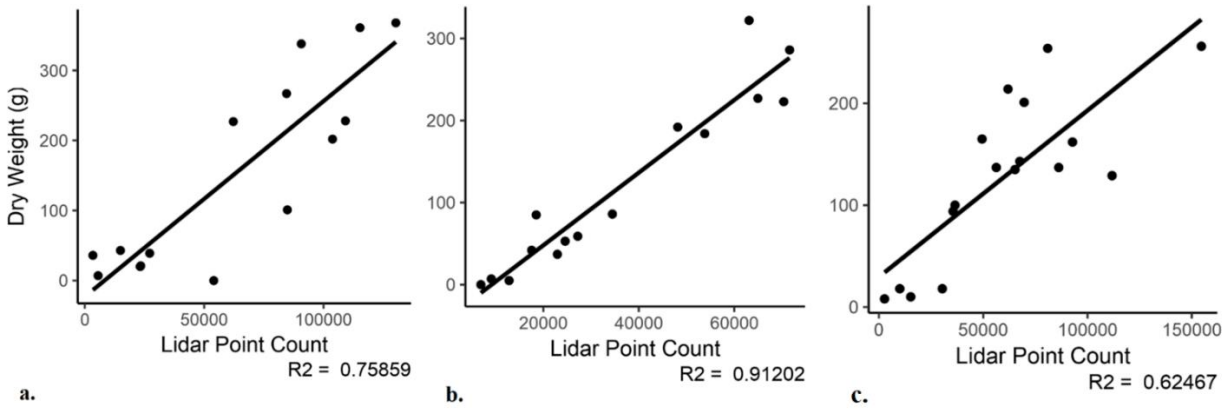

Figure 29: Subsampled Kinect point cloud regressed against dry weight of leaves only leaves for standard (a), asparagus (b), and low-branch (c) genotypes. The R^2 value of the asparagus genotype was again the most successful at 0.91, followed by the standard type at 0.76 and the low-branch at 0.62.

Discussion

The reliability of LiDAR point clouds as a representation of biomass in cassava, based on the above results, appears to be dependent largely upon genotype and, to some extent, looking at leaf only data versus stem data. When not taking into consideration individual genotypes, the TX5 terrestrial later scanner shows a clear advantage over the Scorpion Kinect platform when looking at leaf-only weight (Table 6). However, when looking at leaf and stem weight together, the

difference is not nearly as clear, with the TX5 performing better than the Kinect only by a few points in terms of R^2. This is most likely explained by the improved performance of the TX5 when considering leaf-only weight in Genotype 3. It was expected that the TX5 would outperform the Kinect in all cases, but it was not anticipated that the R^2 values would be so close, as they were in the case of the stem and leaf weight regressions.

Perhaps most surprising in all of the analyses was the performance of the Kinect in consideration of Genotype 1 (CM 523-7, standard type). This was the only case in which the Kinect outperformed the TX5 both in terms of full plant and leaf-only weights. This was particularly prevalent in looking at the stem and leaf weight, where the Kinect bested the TX5's R^2 by 17 points. This was quite unexpected, as the Kinect is known to have a much lower resolution that the TX5 or any of the industry-standard TLS models. Naturally, however, this was also based on the assumption that a denser point cloud would equal a more reliable correlation.

It is possible that the Kinect clouds turned out better in Genotype 1 because a total of six camera angles (3 on each side) were used instead of two. While each camera on the Scorpion did not necessarily capture the same parts of the plant, there did seem to be significant overlap, especially on the bottom two cameras and on plants that were shorter in stature. This could mean that the point cloud of the Kinect files was denser in the middle regions of the plant. It is also possible that because the Scorpion captures images from a lower level (that is, from the ground up), it was able to capture more information on the inner portions of the plant, which may have been blocked by leaves in the TX5 images, which were captured while being pointed directly at the surface of the plant. This analysis was made based on number of points, and the TX5's clouds were certainly denser. However, it is possible that the Scorpion's more intricate capture area, even if capturing a lower number of points, was a better reflection of the overall biomass

than simply a dense cloud. Nevertheless, it should be noted that this was only the case in this genotype, and thus was most likely dependent upon the general structure of the standard type cassava plant.

In addition, the TX5's susceptibility to wind may have influenced the outcome of the data in Genotype 1. Although care was taken to avoid the influence of wind on plant movement by performing the scans at night, it is inevitable that some leaf movement, especially considering the 2:39 scan time of the TX5, would have occurred. This could have influenced subtle, yet still important, changes in the nature of the point cloud at both the registration and analysis stages. Because the Kinect cameras could not capture images in a truly simultaneous manner (due to interference between the wavelengths of the cameras), it is possible that plant movement also affected the Kinect point clouds. However, the time taken to capture an image with the three Kinect sensors (~5 seconds) is significantly less than that of the TX5, and as such it is far less likely that plant movement affected the images in any meaningful way.

Genotype 2 (GM 3893-65, asparagus type) was overall the most successful, and conformed highest to the expectations of each sensor, with both managing R^2 values at or above 0.90 when looking at the full plant or the leaf-only weight. As expect, the TX5 performed higher, but only by 5 or less points in each analysis. Both the Kinect and the TX5 showed degradation in R^2 when being regressed from leaf-only weight as opposed to that of the full plant, although both were negligible, the TX5 having shifted from 0.9572 to 0.95222 and the Kinect from 0.91302 to 0.91202. It is likely that the structure of the asparagus-type cassava, with its leaves growing directly from the stem and covering the entire plant, was the reason why this change was so small, having very little of the stem visible in most plants. It is also likely that the structure of the

genotype led to the correlations being so high, as the lack of branches allowed a more complete image of the plants to be captured.

For the Kinect, Genotype 3 (HMC-1, low-branch type) was the least reliable in terms of R^2. It performed relatively poorly in light of both full plant and leaf-only regressions, never surpassing 0.67 in either. Like with the previous genotypes, there was correlation degradation when analyzing the leaf-only weight; however, it was less than in Genotype 1. Nevertheless, the leaf only TX5 correlation actually improved by 12 points in Genotype 3, as opposed to the 6-point improvement in Genotype 1. This made Genotype 3 the second best in terms of leaf-only regression amongst the TX5 scans. The Kinect, however, was the worst in all cases of Genotype 3.

The reason for the disappointing results for Genotype 3, as it relates to the Kinect, is likely from the structure of the plants. The branches of this genotype were designed to be lower and to reduce overall height. This meant that in many cases, the branches were so low that they were touching the ground. This made ground classification much more difficult for the computer, as the points from the surface and the leaves near the ground were often indistinguishable. Thus, it is almost certain that a number of errors occurred during this process, although they were confirmed visually as best as possible. It is feasible that this process could have been improved though confirming the ground and vegetation points by hand; however, this was difficult due to the complete lack of color information provided by either sensor (as all images were taken at night). The lower resolution of the Kinect was also most likely a contributor to the difficulty in assessing ground and aboveground points, both for the script as well as visually. Likewise, the much better performance of the TX5 in this case can most likely be attributed to the clearer point

cloud it produces, which may have made it easier for the R script to estimate ground and vegetation points in its classification.

Finally, there were several images in both Genotypes 1 and 3 that contained overlapping plants, which without doubt influenced the outcome of the regressions. Manually cropping out these images was considered; however, it would have been impossible to crop both the TX5 and the Kinect images closely enough to one another to reasonably compare the two, given the basic human error that would have occurred from cropping these manually. It is also possible that this contributed to the success across both platforms across Genotype 2, as the asparagus plants are designed for high-density planting and thus had no branches that could have contributed to overlap.

Table 6. Comparison of regression and bootstrap analysis of subsampled point clouds against dry weight, all genotypes and by genotype of Kinect and TX5. Bootstrap confidence intervals shown at 95%.

All Genotypes

Full Plant

Kinect			TX5		
R2	**P-Value**	**Boot CI (95%)**	**R2**	**P-Value**	**Boot CI (95%)**
0.71	1.12E-13	0.47-0.84	0.73	1.26E-16	0.55-0.84

Leaf Only

Kinect			TX5		
R2	**P-Value**	**Boot CI (95%)**	**R2**	**P-Value**	**Boot CI (95%)**
0.66	5.55E-12	0.48-0.79	0.80	2.00E-16	0.63-0.88

By Genotype

Full Plant

	Kinect			TX5		
	R2	**P-Value**	**Boot CI (95%)**	**R2**	**P-Value**	**Boot CI (95%)**
Genotype 1	0.81	4.90E-06	0.59-0.91	0.64	4.32E-05	0.36-0.81
Genotype 2	0.91	2.88E-08	0.79-0.97	0.95	1.12E-12	0.92-0.98
Genotype 3	0.67	6.47E-05	0.90-0.92	0.71	6.45E-06	0.40-0.88

Leaf Only

	Kinect			TX5		
	R2	**P-Value**	**Boot CI (95%)**	**R2**	**P-Value**	**Boot CI (95%)**
Genotype 1	0.76	2.38E-05	0.51-0.90	0.70	8.66E-06	0.33-0.88
Genotype 2	0.91	3.11E-08	0.80-0.96	0.95	3.35E-12	0.91-0.98
Genotype 3	0.62	1.59E-04	0.19-0.81	0.83	1.13E-07	0.58-0.94

Conclusion

The primary purpose of this study was to determine the ability of ground-based remote sensing technology to predict aboveground biomass in cassava for the purpose of eventually identifying characteristics of ESB varieties. Furthermore, the Scorpion platform was tested for its suitability as a low-cost, reliable replacement for TLS in agricultural applications; more specifically, if it could be used as a non-destructive proxy for biomass. Based on the results, it seems that it could serve as at least a comparable replacement when looking purely at aboveground vegetation. However, those wishing to utilize this technology should take into account the various performance issues the Kinect and TLS had when looking at different genotypes.

The standard type (Genotype 1) cassava plant seems to benefit more from the Kinect that any other type, having consistently higher correlations across the full plant and leaf-only dry weights than the TLS. This is even more important considering that the TLS did not break the 0.70 mark for its R^2 under either circumstance. While more testing may be needed before coming to a definitive conclusion, based on these results, it seems that breeders specializing in standard-type cassava would be more successful with their biomass assessments using the Scorpion or a similar Kinect platform as opposed to a TLS.

Asparagus type (Genotype 2) appears to be the best genotype overall for both cameras, having a consistent R^2 across both dry weight types. In fact, the Kinect more closely mirrored the TLS performance in this genotype than any other, consistently being only 4 points less than the TLS. This is likely due to the compact, uncomplicated physiological structure of the asparagus type. Because the benefits of the more expensive TLS seem to be negligible as compared to the Kinect in terms of these biomass correlations, breeders working with this genotype may find the Kinect to be a more economical choice for their high-throughput phenotyping programs.

The Low-branch type (Genotype 3) appears to be the least reliable of all the genotypes, having, in some cases, great disparity between the Kinect and TLS correlations, and getting worse for the Kinect when comparing leaf only to the full plant biomass. However, looking at leaf-only dry weight for the TLS actually improved the correlation, bringing it above an R^2 of 0.80. Improvements on the current design of the Kinect V2, or perhaps an alternative depth camera that can capture images in direct sunlight, may improve the correlations for this genotype by giving color information, which would make it easier to distinguish between the surface and the leaves of the plant that are touching the ground.

Perhaps most exciting from these results is the possibility for future phenotyping platforms involving depth cameras. While the Scorpion served as a useful tool in capturing cassava data, future designs could be tailored to suit any crop, and could incorporate many more sensors than simply the three. The low cost of these sensors would put few financial limitations on adding new layers of cameras, and point cloud resolution and camera angles would improve more and more with each added camera. Still, interference between cameras is an issue while trying to take pictures simultaneously. In order to get the most out of the fast data capturing time, further explorations of the camera's hardware and software would need to be conducted.

In all, this study provides a proof of concept for the RGB-D camera's prospects as a phenotyping tool. Cassava breeders must be careful in choosing which remote sensing platform to use based predominantly on the types of cassava with which they choose to work. Nevertheless, for those who consider an R^2 of at least 0.60 acceptable, the Scorpion system provides a good quality biomass assessment for an extremely reasonable price, especially considering the high cost of traditional LiDAR platforms.

CHAPTER V

ABOVEGROUND VEGETATION PHENOTYPING OF NAPIER GRASS (*PENNISETUM PURPUREUM*) UTILIZING INNOVATIVE REMOTE SENSING TECHNOLOGY: A MULTIPLATFORM TRIAL

Introduction

The field of plant phenomics continues to grow as more LiDAR sensors become available commercially. Studies thus far have shown remote sensing to be useful in monitoring crop stress and disease, as well as helping breeders to select for quantitative traits in various crop species (Marko et al., 2018). What appears to be lacking in the literature is the degree to which certain forms of LiDAR can accurately predict biomass in perennial grasses. The aim of this study is to assess the reliability of a low-cost depth camera to assess biomass in Napier grass (*Pennisetum purpureum*) as compared to an industry-standard terrestrial laser scanner (TLS).

A native of East Africa, Napier grass is currently an important fodder crop for cattle in the region. It also serves as a significant forage crop in the U.S. (Langeland and Cherry, 2008), and its cellulose content has made it a good contender for biofuel production (Tsai et al., 2018). Because high biomass is a valued component of this forage crop (Mapato and Wanapat, 2018), and due to the labor-intensive nature of harvest, non-destructive assessment of such a trait is an essential task for breeders.

Of the sensors available for such a task, TLS have become some of the most popular, allowing researchers to obtain high-quality 3D images of plants from a variety of angles without the need for UAVs, manned aircraft, or other vehicles. One of the more affordable of these scanners is the

Focus Series by FARO, which have since been rebranded as the Trimble TX Series. The TX5 is a continuous wave scanner that measures distances by means of phase modulation techniques, and has already been tested as a means of capturing phenotypic data (Omasa et al., 2007) (Friedli et al., 2016). However, while the cost of TLS units have come down, their costs is still prohibitively high for those on limited budgets.

The X-Box Kinect motion sensor by Microsoft is a depth sensor that may be a solution to budget constraints faced by some plant breeders who wish to utilize high-throughput phenotyping techniques in their research. The Kinect V2 sensor, released in 2014, is an RGB-D camera that allows collection of high-resolution 3D data with a high repeat measurement frequency, and was originally developed as a consumer product to allow hands-free operation of video games. Due to its commercial availability, and the fact that it was not a popular consumer item, V2 sensors can be found and purchased easily and inexpensively (~$50-150, depending on the condition), and have already been explored as a scientific tool (Wilson, 2017), including for agricultural purposes (Omasa et al., 2007) (Friedli et al., 2016).

The goal of this chapter is to determine the ability of land-based remote sensing technologies to accurately predict aboveground biomass in *Pennisetum purpureum*. The following study can be defined by the following objectives: 1) To determine the ability of a TLS (Trimble TX5) to capture an accurate 3D model of aboveground Napier grass plant structure, 2) to test the ability of a custom made, field-of-view expanded phenotyping platform (know as “scorpion”) to accurately capture aboveground Napier data, and 3) to determine if LiDAR point count regressed against estimated dry weight is an accurate predictor of aboveground biomass in this crop. While LiDAR has been researched as a method for determining crop height in perennial grasses (Zhang and Grift, 2012), this is the first time, to the author’s knowledge, that ground-based remote

sensing technology will be used to assess *Pennisetum purpureum*. It is expected that the TX5 will produce a cleaner point cloud and higher correlations to dry weight biomass than the Kinect, but that the Kinect will still retain a comparable correlation considering its lower quality. If successful, this could significantly reduce the intensive harvest methods that are currently required for biomass assessments in this crop.

Methods

Layout

The Napier grass samples used in this experiment were taken from a horticulture field owned by Texas A&M University in Bryan, Texas. The collection time of both the LiDAR data and the plant material was October 30, 2018. The field had been planted with three varieties of perennial grass: Napier (*Pennisetum purpureum*), a millet hybrid, and sorghum. For the purpose of this study, only samples of *Pennisetum purpureum* were used.

A total of 17 samples were used for this study. These samples were taken from three plots of Napier grass that were cut into segments of six by machete (Fig. 30). This was done for two reasons: 1) Napier grass is incredibly labor intensive to harvest by hand, and using smaller sample sizes made it easier to harvest the material, and 2) the sample size could be increased by scanning and harvesting subsamples of the three plots rather than using the plots themselves as the samples. While there were originally 18 samples based on the plot divisions, one (Plot 1, Segment 5) was removed because the material collected for the dry weight was lost. Flat, wooden stakes were also set up around the plots and the segmented plant parts in order to be used later in the registration process.

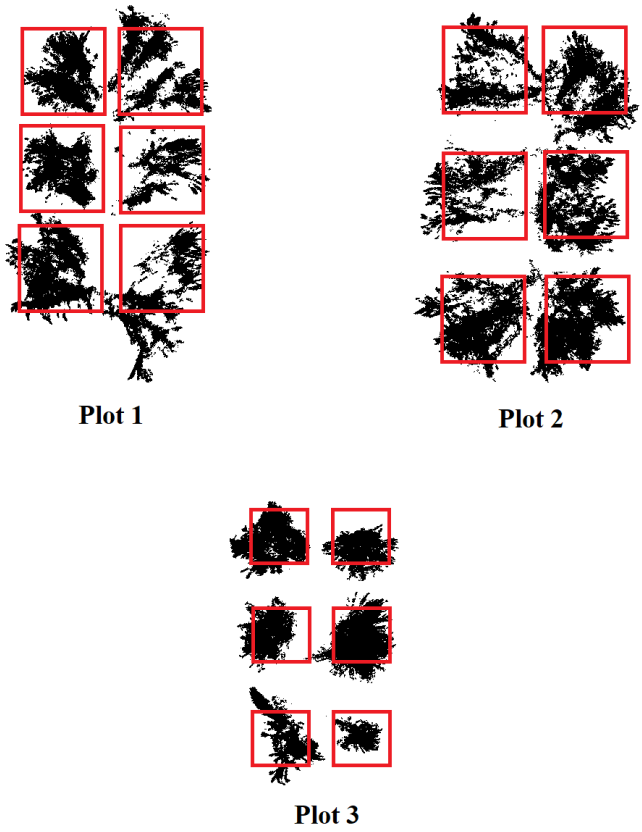

Figure 30. Napier grass plots divided into 6 segments.

In addition to having a more limited range and quality than the TLS, the Kinect also performs poorly in direct sunlight. Moreover, the TLS is susceptible to distortion caused by plant movements during its long scan time. For these reasons, all scanning was done after sunset, both to avoid direct sunlight for the Kinect and to benefit from lower wind speed for the TX5.

TX5

The Trimble TX5 (Trimble Inc., Sunnyvale, California) terrestrial laser scanner used in this experiment is a rebranded version of the FARO Focus 120 (FARO Technologies, Lake Mary, Florida). As such, it maintains the same operation at 905nm, with a range of 0.6 to 120 m and a

range error of ± 2 mm at 10 m and 25 m. It utilizes the time-of-flight principle to acquire data, thus producing high-quality point clouds immediately upon the conclusion of scanning.

Kinect

For the Kinect images, data was acquired by means of a custom-made phenotyping platform known as "Scorpion." The Scorpion is comprised of three Kinect sensors spanning a fan-shaped design and operated by three single board computers (SBC). The unit, including its power inverter and cooling fans, is powered by a single 12V 50Ah battery (Fig. 31).

Figure 31. The Scorpion phenotyping platform.

The base of the device, constructed from 3 cm steel tubing, is designed in an H shape to allow it relative stability on uneven terrain, while the arms of the device are designed to give a wider field-of-view (FOV) to the limited-range sensor, allowing for greater viewing of both horizontal and vertical space. The Kinect sensors are held in place by aluminum frames that are attached to the base. The frames, which were constructed out of aluminum in order to reduce the platform's

overall weight, are movable so as to allow each sensor to be pointing at a different angle, again increasing the overall FOV beyond that of an individual sensor. This allows each sensor to capture a different part of the plant while still having some overlapping imagery, which can then be used to register the individual images together into one large point cloud (thus capturing the whole plant when this would otherwise be impossible).

SBCs to control the Kinect cameras are necessary because each Kinect sensor requires a dedicated graphics card, Windows 8.0 or higher (to run the Kinect SDK 2.0 software), and a USB 3.0 bus. LattePanda's 4G/64GB SBC model was used as it met all of these requirements. The computers were controlled by means of a custom-made app developed by Henry Ruiz, a programmer at CIAT. Built in C#, the Scorpion Web Controller App uses the Microsoft RoomAlive system to allow users to collect data using their smartphone. The app uses a Wi-Fi network to allow the smartphone to capture images, restart the computers, and power the system on and off.

The Kinect itself is an RGB-D camera that also uses time-of-flight to capture data. However, unlike the TLS, the Kinect acquires this data by flooding the scene with infrared light from multiple laser diodes, then measuring reflectance times in a manner similar to flash LiDAR. This allows it to overcome some of the issues with wind susceptibility that often plagues TLS. Because of its use of multiple lasers, its status as a true LiDAR device is debatable. Nevertheless, it produces point clouds in a manner almost identical to TLS, taking into account a lower resolution.

Image Acquisition

The TX5 was mounted onto a standard tripod at approximately 1.25 m in height, placed approximately 2.5 m from the edge of the plant, and was set up to make a 360° scan during each image capture. The resolution was set to 1/8, with a scan quality of 4x, taking approximately 3 minutes to scan. A low resolution was chosen largely due to the time it takes to collect a scan with the TLS. The thin leaves of the Napier plants are highly susceptible to movement, even with slight breezes. Thus, the lower resolution would give a shorter scan time, and theoretically limit distortion due to this movement. Nevertheless, due to this relatively long 3-minute scan time, some movement of the plants during the scan process can be expected.

The Kinect was also placed approximately 2.5 m from the edge of the plant. This was necessary due of the size of each plant segment, which was often over 3 m tall. At the time of image capture, the distance was deemed suitable as the Kinect's ideal range is between 1.5 and 4.5 m (Rahman, 2017).

For Plots 1 and 2, six images were captured with the TX5 and 12 with the Kinect. This was done to compensate for the Kinect having a shorter range and limited FOV as compared with the TX5. For Plot 3, seven images were captured with the TX5 and twelve with the Kinect. The reason for the extra image with the TX5 is because this plot was not as clean and uniform as the others in its structure, and additional angles were needed to capture all of the segments. It should also be noted that it was not possible to take images from inside the plots, so the setup was designed to make sure that each segment had at least two camera angles, both from the Kinect as well as the TX5.

Dry Weight

After all of the images were taken, plants were not able to be harvested until November 7, due to continuous rain and flooding conditions that made the field inaccessible to vehicles and other equipment. During harvest, individual plant segments from each plot were measured for wet weight using large pieces of burlap fabric, rope, and a hanging scale (American Weigh Scales AMW-SR-20 Yellow Digital HanGinG Scale). The weight of the rope and fabric was also recorded so that it could later be removed from the final vegetative weight.

In order to avoid burdensome oven space, a sample of each plant segment was also collected and tested for wet weight. This sample was roughly equal to one or two blades of grass, from crown to top, per segment. The samples were then dried in an oven at 70°C for approximately 5 days and measured for dry weight. The total dry weight of each plant segment was then estimated based on the dry weight of its corresponding sample. This was completed by calculating the percent dry matter (dry/wet*100) and then multiplying the resulting percentage by the total sample weight.

Processing

Preprocessing of the Lidar data was completed using CloudCompare version 2.10. alpha, an open source 3D point cloud (and triangular mesh) editing and processing software. This software was chosen because of its ease of use and lack of restrictions due to its open-source nature. Before editing the TX5 files, they first had to be converted out of of their proprietary .fls format (a result of the TLS having been designed and manufactured by FARO/Trimble). These files were converted to .xyz format (which is compatible with CloudCompare) and then exported using the

Trimble RealWorks software package. The Kinect files did not need to be converted, as they were already in .csv format, which is compatible with CloudCompare (Fig. 32).

Processing

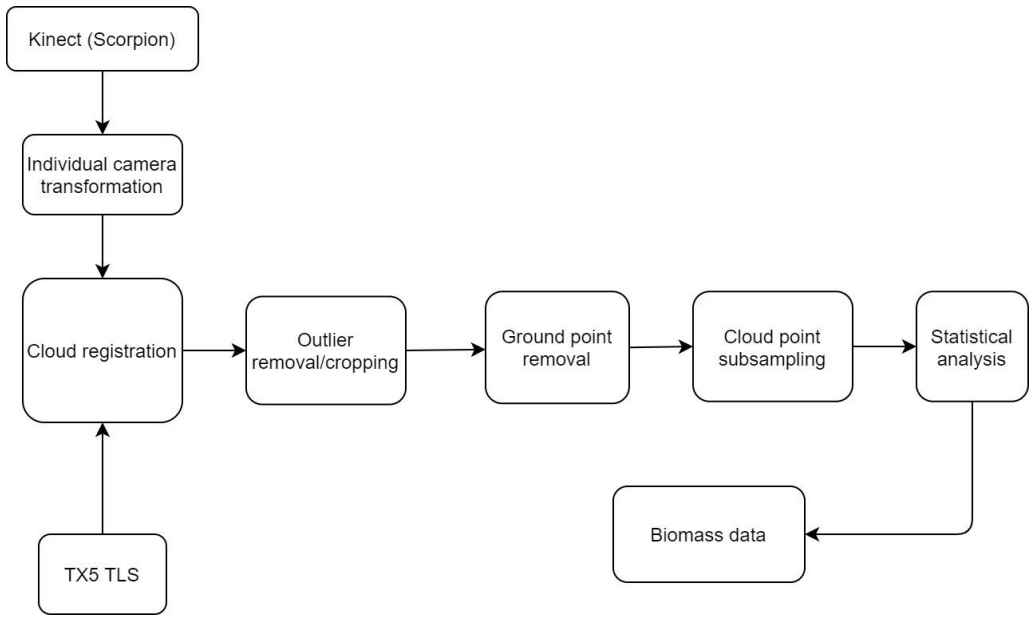

Figure 32. Data processing flowchart.

The wooden stakes that were set up around the plots in the field were used in the registration process. It was decided that because the layout included three plots that were then divided into six segments each, the registration process would focus on creating a model of each of the plots, then later remove each segment for individual analysis.

Each TX5 file was registered to the one next to it in the sequence it was taken. This was completed using CloudCompare's Align-Two-Points tool. When each of the six scans (seven, in the case of Plot 3) were registered together, the collective model was cropped to remove as much of the background as possible, leaving only the vegetative material and some ground points (Fig. 33). After cropping, the Statistical Outlier Removal (SOR) tool was used to remove noise from

the image. Keeping with previous studies, the mean distance estimation was set to 6, while the standard deviation multiplier threshold was set to 1.00. These are the default settings, and were confirmed as appropriate for these images based on trial and error, showing that it removed the largest number of noise points with minimal impact on the vegetative material.

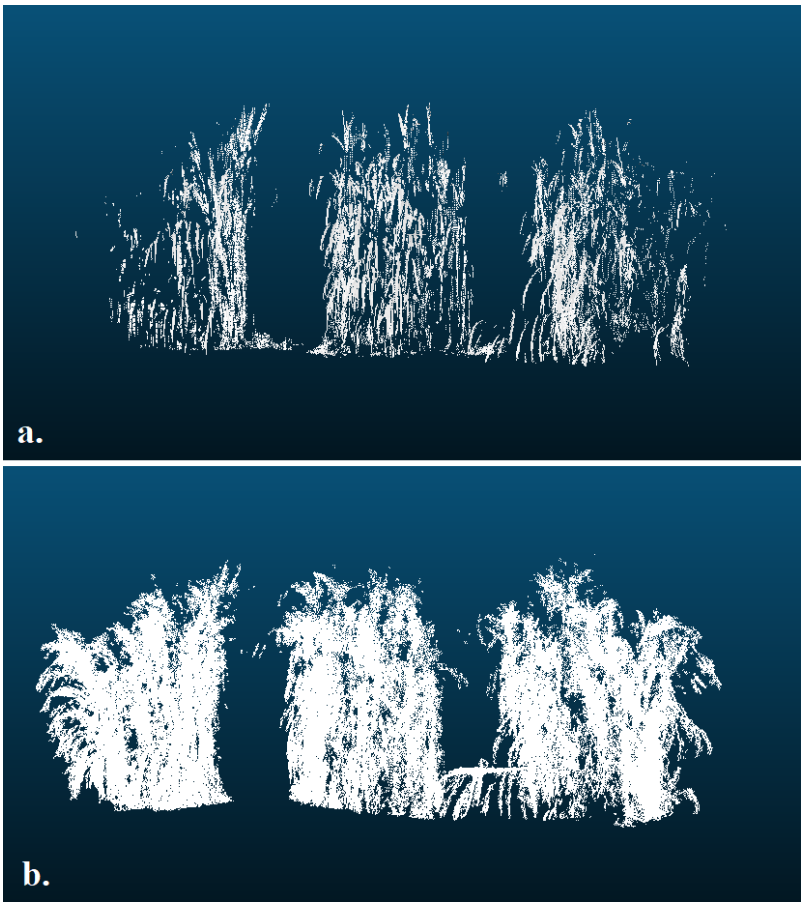

Figure 33. LiDAR image of one side of a Napier plot, representing three of the six segments, both Tx5 (a) and Kinect (b).

Due to the setup of the Scorpion platform, the Kinect files needed additional processing before the plots could be recreated through registration. Each Kinect sensor on the three arms of the platform had to first be registered together so that it could create a complete shot of the angle. This was possible through CloudCompare's Apply Transformation tool. At the beginning of the

data collection process, several establishing images of fixed subjects in the field were taken for reference (in this case, an image of the TX5 carrying case and other stable items). Each camera is assigned a number based on its position in the platform (Camera 1 being the middle portion, Camera 2 the bottom, and Camera 3 the top). When one camera image is registered to that of another (e.g., Camera 2 to Camera 1), a series of coordinates are created that save the registration location of that point cloud within the file space. This can then be applied to any image taken thereafter with that same camera by plugging the coordinates into the Apply Transformation tool. In the case of this experiment, coordinates from Camera 2 and 3 were received from the reference shot, then applied to every one of the Camera 2 and 3 shots that were taken of the Napier stands.

After all of the cameras were registered together, each of the resulting scans were registered together in the same method that was used for the TX5, resulting in large point clouds which represented each of the three plots (Fig. 4). As with the TX5, background information was cropped out of the image, leaving only vegetative matter and some ground points. The SOR tool was then used to clean up noise points in the image, using the same mean distance estimation (6) and standard deviation multiplier threshold (1.00) as before.

When the point cloud registration of both the TX5 and Kinect plots were complete, the individual segments of vegetation were cut out and made into their own files. As mentioned previously, the dry weight sample for Segment 5 of Plot 1 was lost in transportation, so no analysis was done on this segment. In total, Plot 1 had five segments, while Plots 2 and 3 each had six.

Ground Points

Before a regression could be run against the dry weight of the plant material, each of the point clouds needed to be clipped so that only vegetation would be counted in the analysis. To this end, an attempt was made to use ground classification, as this had worked well in a previous experiment. This was attempted using the lasground_pmf (Progressive Morphological Filter) code in R (version 3.4.2.), which had been used to much success in with cassava. The code operates through use of a two-variable filter composed of a sequence of window sizes for filtering ground returns and a sequence of threshold heights above the ground surface (Zhang et al., 2003).

Using this code was not quite as successful as it had been in the past; at least, in terms of the Kinect. The TLS scans were able to have ground classified easily using a window size of 0.2 m and a threshold height of 0.05. The Kinect images, however, were not easy to classify, and were thoroughly unsuccessful. This was not totally unexpected, as the loose point structure of the clouds had caused trouble with classification in the past. However, in a previous study this was able to be overcome by inserting additional points over gaps in what were obviously ground points. This procedure was not successful in this case, however, nor was changing the various window and threshold height sizes. This failure caused many aboveground points to be erroneously classified as ground points. As such, an alternative procedure was conducted with the Kinect: The correctly classified TLS point clouds were used as a guide to manually separate ground from vegetation points in the Kinect scans. This was not ideal, as it was subject to more human error. Nevertheless, given the failure of the computer to properly segment the points, this was the only option available.

Subsampling

In order to circumvent any data degradation that may have occurred from the point cloud registration, a subsample of each point cloud was taken before regression was run. This was achieved through CloudCompare's subsample tool, setting the minimum space between points to 0.002 m (2 mm). The 2 mm space was chosen because it is within the maximum range accuracy of the TX5 and has worked well in previous experiments.

Analysis

Analysis was conducted in R version 3.4.2. As a part of the process, a bootstrap analysis was conducted using R's boot package. Bootstrapping was done using the bias-corrected and accelerated method (BCa) in order to offset any bias or distributional skewness in the results. Five thousand iterations were used with a confidence level of 95%. Plotting was achieved with the ggplot2 package.

Regression was conducted by running the subsampled points of each plant segment against the segment's dry weight for both the TX5 and the Kinect point clouds. Because all of the three plots were quite different from one another in structure and biomass, regressions were run individually for each plot. The three plots were also combined for a larger sample, although this resulted in a much lower R^2 value for both the TX5 and the Kinect. A bootstrap analysis also followed each regression.

Results

TX5

The points of the registered TX5 clouds were regressed against the dry weight of each plant and broken down by plot. For Plot 1, this yielded an R^2 of 0.71, with a P-value of 7.19e-02. The bootstrap revealed a mean R^2 of 0.71, a bias of 7.19e-02 and a standard deviation of 0.19. The 95% confidence interval was between 0.31 and 0.99 (Fig. 34).

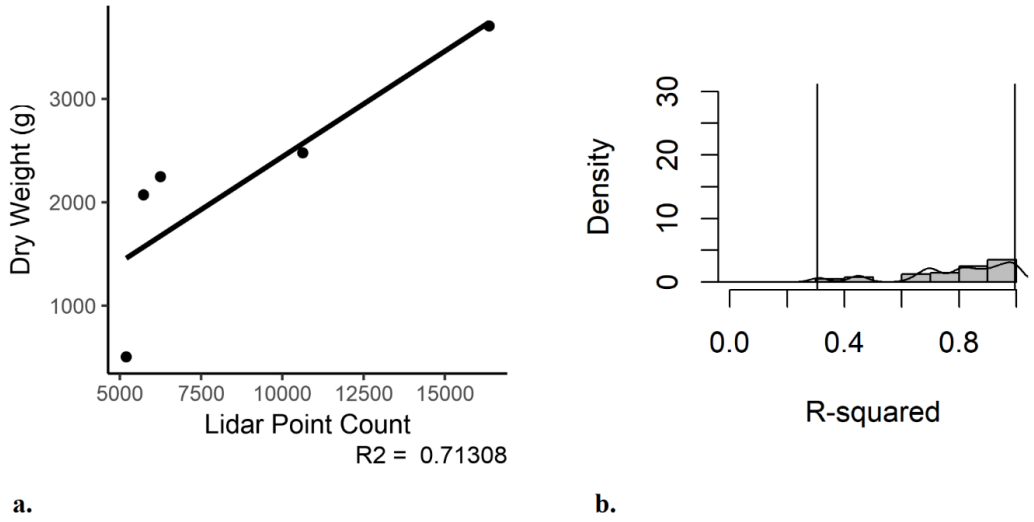

Figure 34. Subsampled TX5 point cloud regressed against dry weight of plant material in Plot 1. The regression shows an R^2 of 0.71 (a), while the bootstrap reveals a mean R^2 of the same with a 95% confidence interval between 0.31 and 0.99 (b).

Plot 2 of the TX5 test was the most successful of the experiment, with an R^2 of 0.93 and a P-value of 1.72e-03. The bootstrap revealed a mean R^2 of 0.93, a bias of -1.25e-02 and a standard deviation of 0.08. The 95% confidence interval was between 0.58 and 0.99 (Fig. 35).

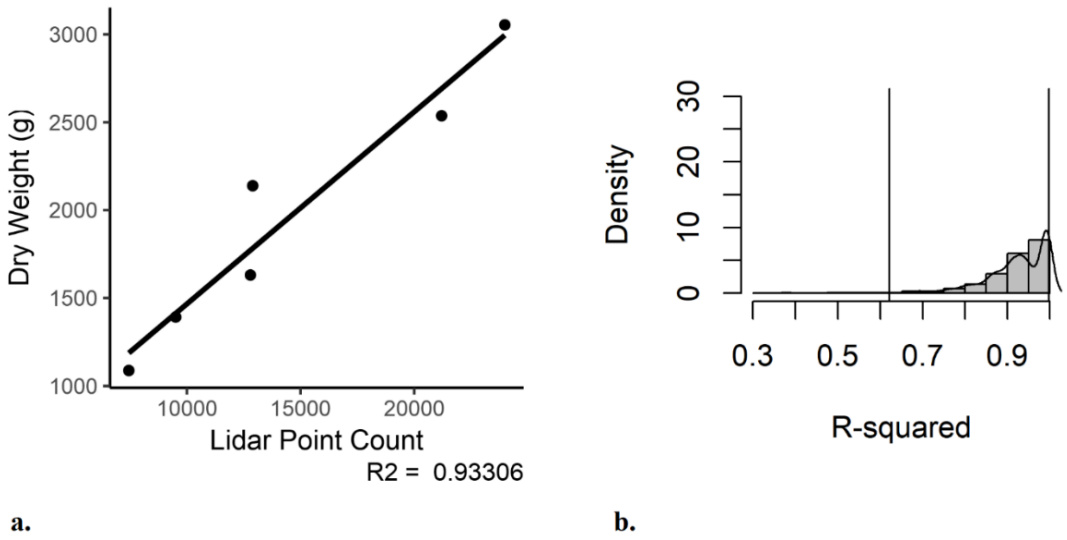

Figure 35. Subsampled TX5 point cloud regressed against dry weight of plant material in Plot 2. The regression shows an R^2 of 0.93 (a), while the bootstrap reveals a mean R^2 of the same with a 95% confidence interval between 0.58 and 0.99 (b).

Plot 3 revealed an R^2 of 0.89 and a P-value of 4.85e-03. The bootstrap revealed a mean R^2 of 0.88, a bias of 3.55e-02 and a standard deviation of 0.06. The 95% confidence interval was between 0.00 and 0.96 (note that the endpoints of the confidence interval are in the extreme) (Fig. 36).

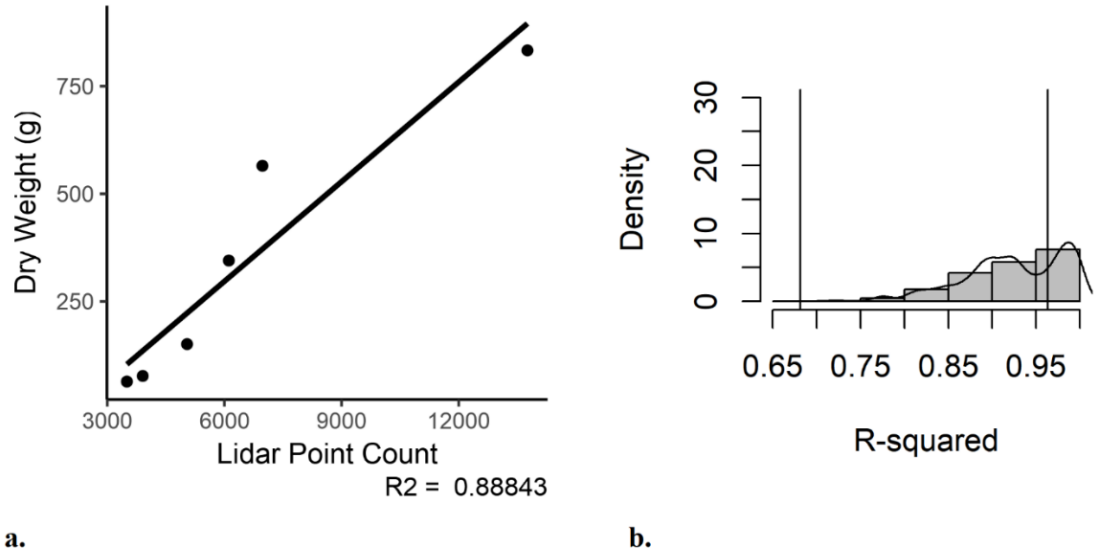

Figure 36. Subsampled TX5 point cloud regressed against dry weight of plant material in Plot 3. The regression shows an R^2 of 0.89 (a), while the bootstrap reveals a mean R^2 of the same with a 95% confidence interval between 0.00 and 0.96 (b). Note that the endpoints of the confidence interval are in the extreme.

Because the structure of the plots varied so greatly, running all of the plants together as one sample produced a much lower R^2. Nevertheless, this was completed, showing an R^2 of 0.55 and a P-value of 7.06e-04. The bootstrap revealed a mean R^2 of 0.54, a bias of 8.20e-03 and a standard deviation of 0.15. The 95% confidence interval was between 0.13 and 0.78. This correlation was improved by excluding Plot 1 from the analysis, with an R^2 of 0.87, a bootstrap bias of -1.45E-02, a standard deviation of 0.11, and a confidence interval of 0.43 and 0.96 (Fig. 37).

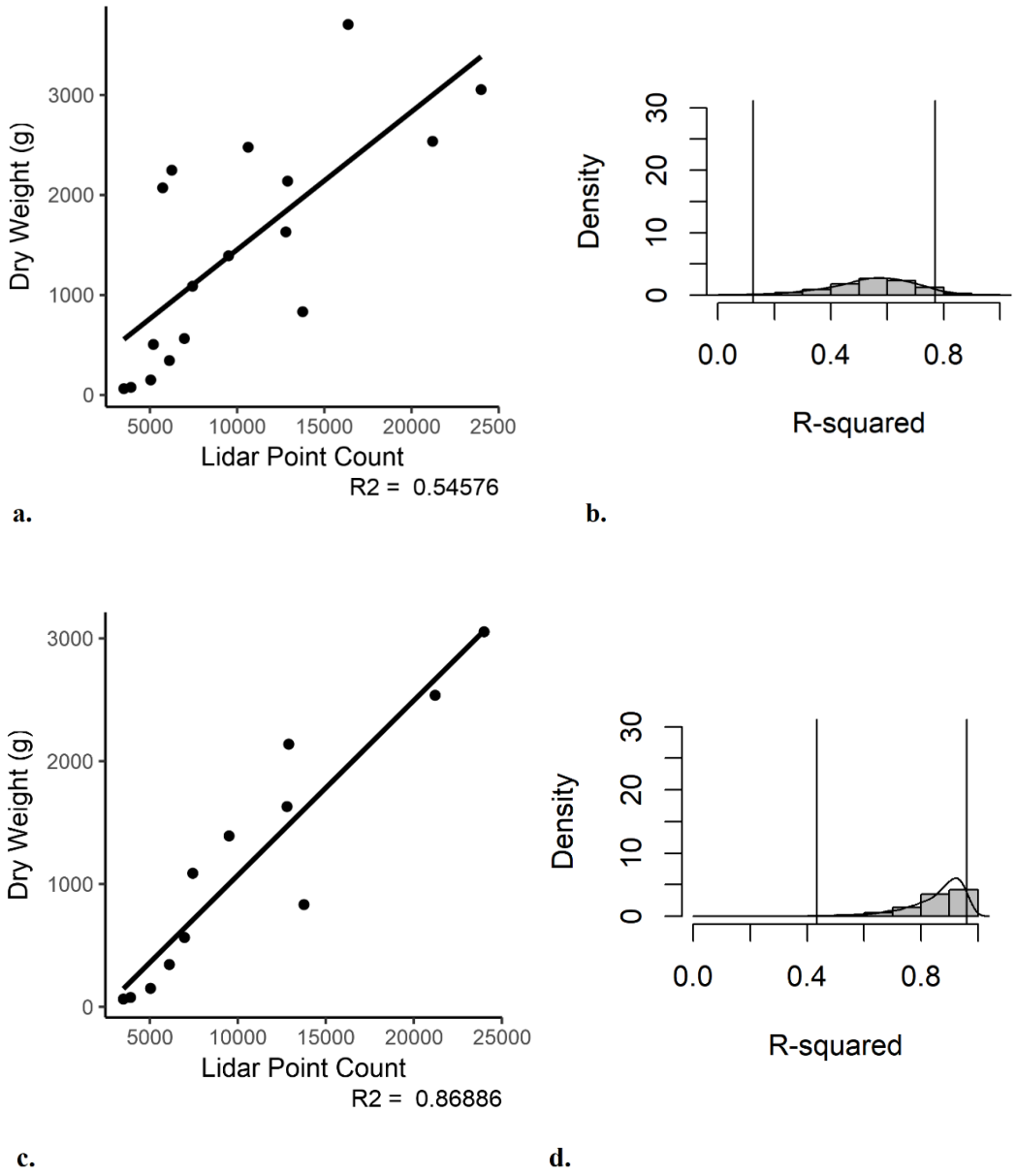

Figure 37. Subsampled TX5 point cloud regressed against dry weight of plant material across all three plots. The regression R^2 is much lower than any of the individual plots at 0.55 (a), with a bootstrap mean of 0.54 and a 95% confidence interval between 0.13 and 0.78 (b). The removal of Plot 1 from the data improved R^2 to 0.87 (c) with a confidence interval of 0.43 and 0.96 (d).

Kinect

As with the TX5, the registered point clouds of the Kinect were regressed against the dry weight of each plant and broken down by plot. For Plot 1, this yielded an R^2 of 0.82, with a P-value of

3.55e-02. The bootstrap revealed a mean R^2 of 0.81, a bias of 4.05e-02 and a standard deviation of 0.14. The 95% confidence interval was between 0.48 and 0.99 (Fig. 38).

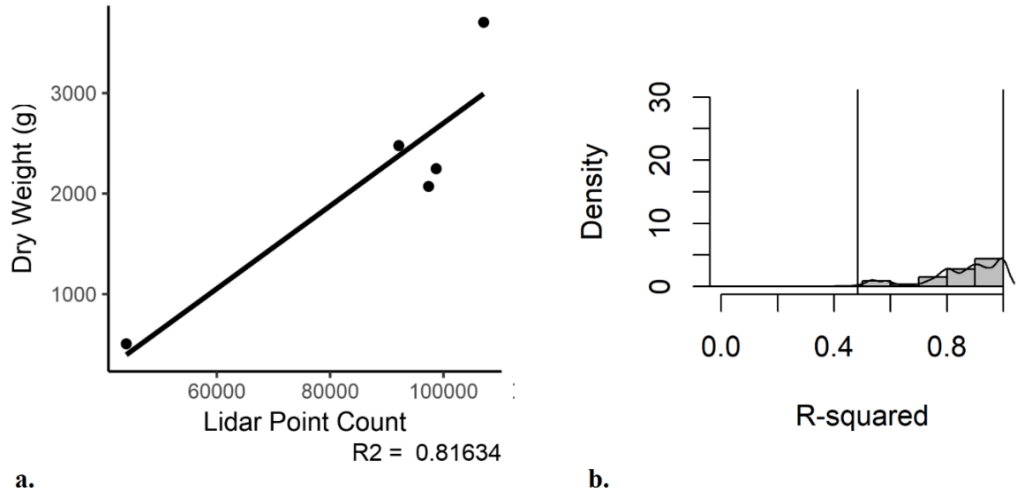

Figure 38. Subsampled Kinect point cloud regressed against dry weight of plant material in Plot 1. The regression shows an R^2 of 0.82 (a), while the bootstrap reveals a mean R^2 of 0.81 with a 95% confidence interval between 0.48 and 0.99 (b).

In contrast to the TX5 test, Plot 2 performed the poorest in the entire experiment, with an R^2 of 0.29 and a P-value of 2.70e-01. The bootstrap revealed a mean R^2 of 0.29, a bias of 8.65e-02 and a standard deviation of 0.26. The 95% confidence interval was between 0.00 and 0.89 (Fig. 39).

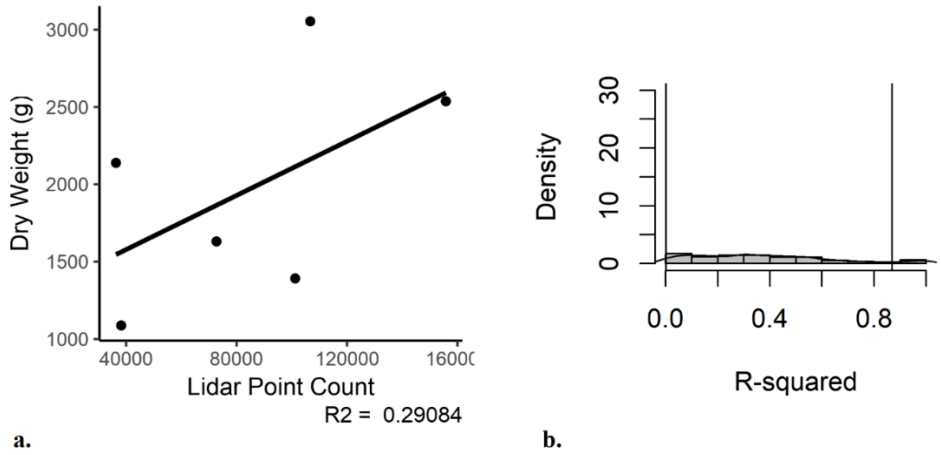

Figure 39. Subsampled Kinect point cloud regressed against dry weight of plant material in Plot 2. The regression shows an R^2 of 0.29 (a), while the bootstrap reveals a mean R^2 of 0.81 with a 95% confidence interval between 0.00 and 0.89 (b). Note that the endpoints of the confidence interval are in the extreme.

Plot 3 also performed poorer than its TX5 counterpart, with an R^2 of 0.48 and a P-value of 1.25e-01. The bootstrap revealed a mean R^2 of 0.48, a bias of 3.53e-02 and a standard deviation of 0.31. The 95% confidence interval was between 0.00 and 0.96 (Fig. 40).

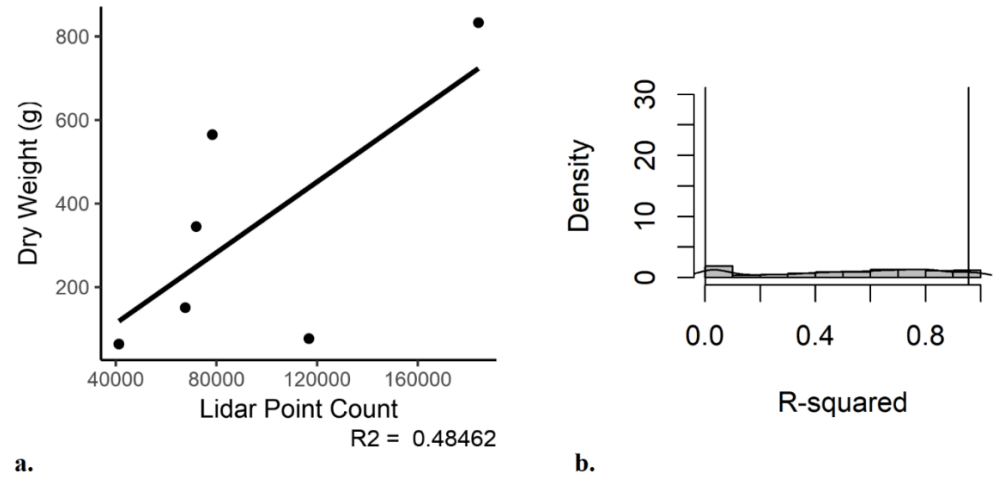

Figure 40. Subsampled Kinect point cloud regressed against dry weight of plant material in Plot 3. The regression shows an R^2 of 0.48 (a), while the bootstrap reveals a mean R^2 of the same with a 95% confidence interval between 0.00 and 0.96 (b). Note that the endpoints of the confidence interval are in the extreme.

In addition to the variety between the plots, the low correlations of Plots 2 and 3 contributed to an extremely low correlation between all of the plots run together. Nevertheless, this was completed, showing an R^2 of 0.08 and a P-value of 2.75e-01. The bootstrap revealed a mean R^2 of 0.07, a bias of 5.84e-02 and a standard deviation of 0.15. The 95% confidence interval was between 0.00 and 0.45 (Fig. 41). Removal of plots from the analysis did not improve the correlation as with the TX5.

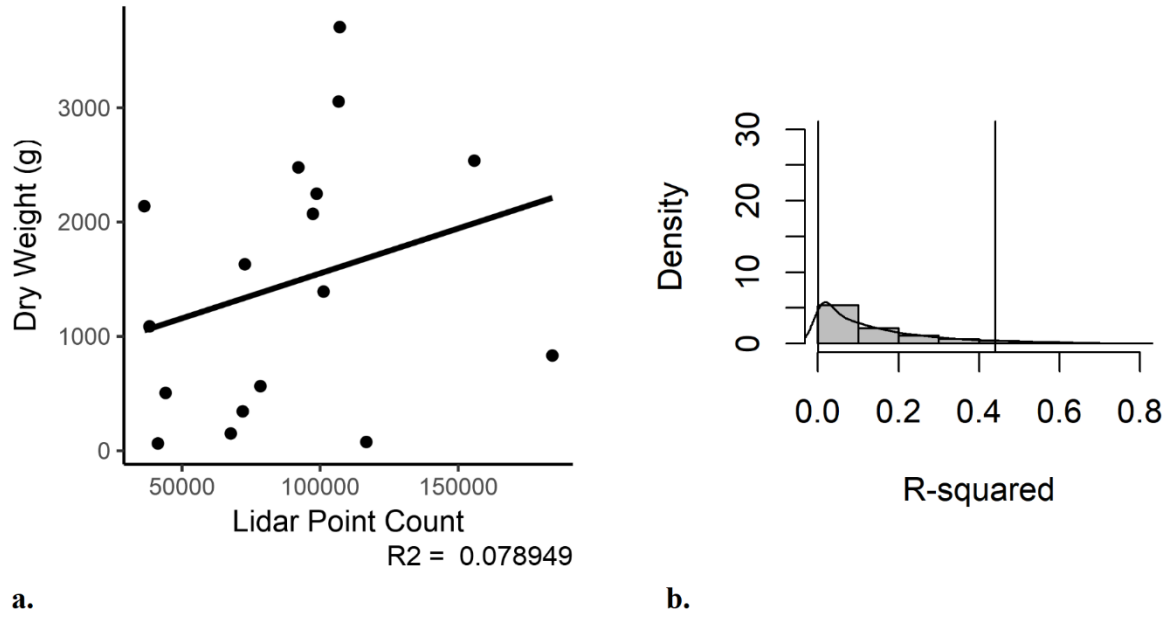

Figure 41. Subsampled Kinect point cloud regressed against dry weight of plant material across all three plots. The regression R^2 is lower than the individual plots and lowest in the experiment at 0.08 (a), with a bootstrap mean of 0.07 and a 95% confidence interval between 0.00 and 0.45 (b).

Discussion

The TLS was clearly the superior sensor as it relates to determining biomass of Napier grass. The R^2 values on the plot level remained above 0.70, with the highest correlation coming from Plot 2 at 0.93. Plot 3, which was the most unusual of the three plots, also performed well at 0.89. With the exception of Plot 1, each series of scans outperformed the Kinect substantially. While this is

within the conventional viewpoint that a higher resolution sensor will always create a better representation of a plant (or any structure, for that matter), this was somewhat unexpected for this particular experiment. Regressions were also run against the wet weights of the plants for both sensors to see if this led to any improvement, but this produced lower correlations in all cases. This, however, was deemed negligible, and the standard for biomass assessments is dry weight of the plant material.

Upon visual inspection of the point clouds, the TLS images were not nearly as thick and all-encompassing as those of the Kinect. Shadowing seemed to be an issue, and due to the lack of angles and lower number of images captured as compared to the Kinect, it was speculated that the clouds would not correlate as well to biomass. This may, however, have worked in the TLS' favor. Previous work using TLS to determine biomass in cassava has shown that using a one-sided image can produce comparable correlations to an image with two sides registered together (Bruton, 2019). This seems counterintuitive, as one would assume that a more complete model would provide a better biomass correlation. Nevertheless, the sparse point cloud of the TLS in this case, even though it did involve registering a few images, seems to have provided a better overall biomass assessment.

The Kinect had multiple issues in the experiment that may have contributed to its poor performance overall. One of the first potential issues what that the Kinect was set up 2.5 m from the edge of the plant, which made it roughly 3 to 3.5 m from the center of the plant. This was necessary in this case because the Napier plants were so tall– typically above 3 meters. If a shorter distance was used, then the top of the plant would be cut off in the picture. It is known that the Kinect's ideal range is between 1.5 and 4.5 m, but the sensor also loses resolution any time it is moved further away from the target (Rahman, 2017). Previous studies conducted by the

author have always been able to keep the Kinect sensor within 1.5 m of the center of the target plant; thus, the images in this experiment may have suffered from above-average noise, pixel size, and an overall loss of resolution. This could perhaps be remedied by use of a different platform for Napier. The Scorpion, while still boasting an impressive FOV, was designed to capture images of shorter plants from the ground up. One of the most useful features of the Kinect is that its small size and portable nature allows it to be tailor-made to suit a variety of needs in the field. A platform constructed specifically for tall perennial grasses – featuring a much larger vertical FOV and perhaps an additional camera giving a top-down perspective – would likely shorten the range needed to capture the entire plant.

Another potential problem with the Kinect was that it required, due to the limited FOV, twice as many scans as the TLS to capture the entire plot. This resulted in a much more accurate depiction of the plant, as it was able to capture multiple angles that the TLS was not. But this also required more registration to complete the overall image, resulting in extremely dense point clouds. As mentioned with previous research and the TLS in this experiment, a denser point cloud and more complete image of a plant does not necessarily equal a better correlation to biomass; in this case, the Kinect scans may have been too dense. The noise reduction and subsampling of points at 2mm was used to try to overcome this. However, the additional registration and overlapping of images almost certainly compounded the inevitable human error that comes with those techniques. This is made all the more problematic by the fact that the physiological structure of a bunched grass makes it very difficult to discern between individual blades of grass during the visible inspection of the point cloud during processing.

Two additional issues arose for the Kinect in this experiment. One was that, as mentioned in the Methods section, the ground classification did not work. All attempts that had been used to

correct the problem in previous work were unsuccessful; thus, clipping of the ground points by hand was the only option. This most certainly contributed to a point cloud structure that was not completely consistent with that of the TLS. In the same vein, the structure of the plants made it difficult to collect biomass that corresponded completely to the images. Many of the plant segments featured large portions that crawled along the ground and were nearly impossible to harvest by hand without sophisticated equipment. As such, a decision was made to take as much of the material that was harvestable by hand and leave the remainder. Because the Kinect collected the images so thoroughly due to its numerous shots and angles, it is possible that *too much* of the plant was captured to make an accurate correlation. However, it should be noted that an attempt was made to cut the Kinect point cloud to better match the TLS without any improvement. Therefore, it is likely that a variety of the issues mentioned here contributed to the poor correlations.

What is unclear at this point is why the Kinect performed so poorly in Plot 2, especially as compared with the TLS. Also unusual is that it compared so poorly when Plot 1, which was similar in structure, performed well. It is perhaps because Plot 2 was far more bunched than Plot one, with clear individual blades of grass being less apparent. In this case, the inside of the plot was less visible and more likely to be muddled due to the density of vegetation. However, the TLS performed best on this plot, and produced similar point clouds to the Kinect. It seems likely, then, that the aforementioned issues with registration, noise, resolution, and overlapping plant parts contributed more to the poor correlation. If this is the case, then a platform with a wider FOV may improve the images by reducing the need to register shots together for a full picture.

A final problem is that the regression of all the samples run together produced, in the case of both the TLS and the Kinect, far lower R^2 values. This is likely due to the fact that the three plots

were rather different in structure and biomass (although Plots 1 and 2 were far more similar). This would cause a problem if this technique were used on an entire field where the plants were not reasonable uniform. It also seems that the BCa bootstrapping method was not particularly useful, as several of the regressions featured extremes in their CI values (Table 7). This may be due to the relatively small sample size used in the plots and in the experiment overall (with five to six samples per plot, and 17 in the experiment overall), leading to a smaller number of subsample regressions that could be run during the bootstrapping process.

Table 7. Comparison of regression and bootstrap analysis of subsampled point clouds against dry weight for the Kinect and TX5. Bootstrap confidence intervals shown at 95%. Note that some CI values are in the extreme.

	Kinect			TX5		
	R2	**P-Value**	**Boot CI (95%)**	**R2**	**P-Value**	**Boot CI (95%)**
Plot 1	0.81	3.55E-02	0.48-0.99	0.71	7.19E-02	0.31-0.99
Plot 2	0.29	2.70E-01	0.00-0.89	0.93	1.72E-03	0.58-0.99
Plot 3	0.48	3.53E-02	0.00-0.96	0.89	4.85E-03	0.00-0.96
Whole Field	0.08	2.75E-01	0.00-0.45	0.55	7.06E-04	0.13-0.78

Conclusion

The goal of this study was to determine a straightforward, non-destructive technique for determining aboveground biomass of Napier grass, with hopes that this would lead to the development of new phenotyping tools to be used for other perennial grasses in the future. Furthermore, the successful acquisition of biomass data in this capacity could eventually be used to make correlations between above and belowground biomass obtained by other remote sensing methods in these types of crops.

From the results, it appears that the point cloud generated by the Kinect V2 sensor, with one exception, does not compare favorably with that of the Trimble TX5 in terms of biomass. But

perhaps the failure of the Kinect to perform comparably to the TX5 in this case is a matter of platform more than that of sensor, especially given that the Kinect has performed well with other crops. The Scorpion sensor, while suiting cassava well, was already at a disadvantage due to the sheer size of the average Napier plot. New innovations in platform, especially ones that can mitigate the need for registration, may allow the Kinect to perform better in future tests.

Most surprising in this case was the degree to which the TLS' point clouds correlated to biomass, especially given the numerous issues of shadowing that seem to occur in these types of plants. The difficulty of registration with this type of plant structure may be what made the major difference in this case. The TLS required less images to capture data, and thus less registration. Even slight movement in the blades of grass can create much distortion and overlap between points in the cloud when images are compounded together. The bunched nature of the grass and lack of a clear stem and leaves (as with the cassava) makes this kind of overlap virtually impossible to determine visually. In this case, less may have meant more in terms of viable point clouds for analysis.

Overall, the Kinect seems unlikely to replace UAVs as the tool of choice for perennial grasses. It is likely that better correlations could be achieved by a new platform and by a plot system that is more spread out and features less vegetative material in each stand. However, this may not be worth the trouble for plant breeders who need to focus on plating as much material in a limited space as possible. Nevertheless, breeders who lack the tools to make LiDAR-based biomass assessments from the air may find the TLS to be a viable ground level alternative to UAV and satellite imagery.

CHAPTER VI

CONCLUSION

Meeting the challenges of producing more food, developing alternative sources of energy, and doing so within an environmentally sound context in the next century will require new solutions that are not only reliable, but affordable for adoption on a mass scale. LiDAR has thus far proven successful in meeting this goal, but still remains a technology that is available only to those with large operating budgets. Low-cost RGB-D cameras may be a solution to improving availability of LiDAR technology to those who do not benefit from plentiful funding, at least in the case of certain crops. What this dissertation sought to complete was an assessment of how well one of these cameras, the Kinect V2, compared to terrestrial laser scanners in terms of both point cloud resolution and correlation to biomass in two important crops: cassava and Napier grass.

The laboratory experiment found that while the TLS certainly has a higher resolution and denser point cloud than the Kinect, the Kinect still has a reasonable point cloud overlap with the TLS. As would be seen later, a denser point cloud does not always mean better biomass correlations, so the ability of the Kinect to create a reasonable 3D model of a plant in this case was noteworthy. It should also be noted that the Kinect cannot be used in the same field conditions as TLS (as the Kinect cannot perform in direct sunlight), but it can capture images in a fraction of the time, making it a potentially useful tool in wind-prone areas. As long as plant breeders do not require sub-centimeter resolution, then the Kinect may be a viable alternative to TLS for their programs.

When testing the sensors for aboveground biomass determination in cassava, both the TLS and the Kinect performed fairly well to excellent in most cases. However, this was also largely

dependent upon genotype, and to some extent, making assessments based on full plant or leaf only weight. The Kinect seemed to function better than the TLS when looking at a standard cassava type, making it potentially more useful for breeders specializing in this area. Asparagus type was almost equally accurate across the two sensors, making the Kinect a suitable low-cost replacement for TLS in this case. The low branch type was not as accurate with either sensor, with the Kinect performing worse. However, it was still able to maintain an R^2 above 0.60 even in the worst case.

Napier grass proved to be the most unreliable as far as the Kinect is concerned. Surprisingly, the TLS performed well despite lots of shadowing in the images and a relatively thin point cloud, producing correlations above 0.70 in all cases. The Kinect, despite its denser point clouds due to greater angle capture, produced far less consistent results, with the highest correlation being above 0.80 and the others below 0.50. Neither sensor seemed to perform particularly well across the entire field, either, seeming to produce better results when sticking to individual plots. While improvements to the Kinect platform (Scorpion) may be able to yield better results, it is possible that the sensor's low resolution and limited field of view may make it unreliable for biomass estimation in this crop. However, it still appears to have captured plant structure fairly well and may be of some use to breeders wishing to select for other types of traits.

While the results of these tests have been largely successful, they also raise questions about the efficacy of using ground-based, 3D LiDAR to capture phenotypic data as opposed to the other methods that are currently available. Although commercial availability and ease of use add to the appeal of TLS and depth cameras, speed and minimal data complexity may be preferable to those with large field operations. Likewise, breeders interested predominantly in biomass assessment

may prefer techniques capable of strong correlations regardless of their cost or difficulty in operation.

The use of LiDAR for biomass assessments has been pioneered predominantly in the realm of ecology. Biomass, roughly defined as the dry weight of vegetation, is important in this field because it provides an assessment of carbon-based material, which is an essential component in identifying carbon sinks (Vazirabad and Karslioglu, 2011). As such, various remote sensing technologies, such as 2D and 3D LiDAR, have been conducted for forest biomass assessment (Tao et al., 2014). Nevertheless, a number of studies have used LiDAR for predicting biomass in agricultural settings. While cassava and perennial grasses are still relatively unexplored in the realm of LiDAR, consideration can still be given to the various techniques based on results from other crops.

Studies thus far have differed in their ability to predict biomass based on satellite imagery. However, in certain crops, such as oats, rye, and barley, correlations between remotely sensed data and biomass have been high (R^2 = > 0.80) (Prabhakara, Hively, and McCart, 2015). While there have not been any biomass assessments made on cassava in this case, there have been some experiments with NDVI values derived from UAV and other active sensors correlating well to yield in potatoes (MacDonald, 2018) (Zaeen et al., 2020).

UAV multispectral imaging benefits from having more extensive testing, especially in the agricultural field. Based on previous studies, this method has a record of good correlation (R^2 = > 0.75) to biomass in rice (Han et al., 2019) (Devia, 2019), corn (Jiang, 2019), and various grasses (Nasi et al., 2018). It has also proven effective in determining plant height in several types of crops. While terrestrial laser scanners are also capable of gathering information on height, it is impressive that UAV is capable of obtaining this information given its quick

collection time and utilization of top-down angles. However, UAVs are not always as readily accessible to breeders in that they require piloting skills and, in some cases, licenses to operate within certain airspace.

Two-dimensional LiDAR, which provides X and Y coordinates without a Z, remains one of the fastest ways to collect phenotypic data in the field. Also, while high-end 2D scanners are comparable in price to many 3D scanners, there are budget versions available. One study that used a 2D LiDAR on poplar trees yielded correlations of 0.79 for biomass and 0.89 for volume (Andújar et al., 2016), while another scanner (LMS-111) was used to determine biomass of vineyards in Spain, with the best correlations coming from the use of multiple scans (R^2 = > 0.62). Two-dimensional LiDAR also remains the fastest way to obtain plant structure in 3D by calculating the position of the sensor relative to the vehicle to which it is attached as it moves between rows in the field (Ramon Rosell Poloa et al., 2009).

Outside the realm of biomass, 2D has been used to determine plant height to great success in cotton, with one study based on an LMS511 PRO sensor yielding correlations of 0.98 to 1.00 as compared to field measurements (Sun, Li, and Paterson, 2017). Similarly, correlations between 0.56 and 0.94 were achieved in wheat canopy height (Walter, et al., 2019). This can be compared to height assessments that have been completed using a 3D scanner for cassava, which managed to receive results between 0.65 and 0.81 (Bruton, 2019).

One of the main advantages of 3D scanners is the ability to have a full 3D image immediately after scanning with little to no interpolation necessary, although some studies have used 3D scanners to created flattened 2D projections for biomass estimations, such as one that achieved correlations greater than 0.90 in mangrove trees (Olagoke et al., 2016). In the case of this dissertation, the results of both the cassava (especially the asparagus genotype) and the Napier

grass are comparable to results achieved with other TLS units on maize, especially when comparing those findings captured on the individual plant level (> 0.90) (Jin, et al., 2020).

Plant breeders, in many cases, will be interested in determining traits other than simply biomass, as this characteristic is only useful in some crop species. While LiDAR for biomass may be helpful, being able to capture accurate plant physical structure may be preferable those who want to breed for these alternative traits (such as certain leaf or bud angles that make the crop easier to harvest). Color information is also something that is becoming increasingly available through certain forms of LiDAR and can be of much use in a variety of phenotyping exercises. Based upon the studies conducted using 2D and 3D LiDAR, it does not appear that 3D holds significant advantages over its simpler counterparts in terms of biomass prediction. However, these alternative plant traits make 3D a more thorough and versatile solution that can provide for an assortment of needs.

The full potential of the depth camera has yet to be realized, as this dissertation presents an assessment of only two types of crop plants. But while perennial grasses may be a gamble, shrub crops seem well suited for this type of sensor. Additional tests will be required to see if grasses are still a viable option. Arguably systems such as the Scorpion are not fast enough for many breeders to collect large data sets. However, the low cost and great flexibility of the Kinect makes it a prime subject for further experimentation, and Microsoft's release of a new model (Azure) ensures that the series will continue to be explored well into the next decade.

REFERENCES

Adeniyi, A.G., Ighalo, J.O., and Onifade, D.V. 2019. Production of Biochar from Elephant Grass (Pernisetum purpureum) Using an Updraft Biomass Gasifier with Retort Heating. *Biofuels,* DOI: 10.1080/17597269.2019.1613751.

Allem, A.C. 1987. *Manihot esculenta* is a Native of the Neotropics. *Plant Genetic Resources Newsletter* Vol. 71, p.p. 22–24.

Alhwarin, Faraj et al. 2014. IR Stereo Kinect: Improving Depth Images by Combining Structured Light with IR Stereo. *Trends in Artificial Intelligence,* Vol. 8862, p.p. 409-42.

Andrade-Sanchez, P., Gore, M., Heun, J., Thorp, K., Carmo-Silva, A., French, A., Salvucci, M., and White, J. 2013. Development and Evaluation of a Field-Based High-Throughput Phenotyping Platform. *Functional Plant Biology*, Vol. 41(1), pp. 68-79.

Andújar, D., Escolà, A., Rosell-Polo, J.R., Sanz, R., Rueda-Ayala, V., Fernández-Quintanilla, C., Ribeiro, A., and Dorado, J. 2016. A LiDAR-Based System to Assess Poplar Biomass. *Gesunde Pflanzen*, Vol. 68 (3), p.p. 155-162.

Andújar, D., Dorado, J., Fernández-Quintanilla, C., and Ribeiro, A. 2016. An Approach to the Use of Depth Cameras for Weed Volume Estimation. *Sensors*, Vol. 16 (7), pp. 972-982.

Anikwe, M. and Ikenganyia, E. 2018. *Ecophysiology and Production Principles of Cassava (Manihot species) in Southeastern Nigeria*. InTech, DOI: 10.5772/intechopen.70828.

Bajwa, S.G., Rupe, J.C. and Mason, J.. 2017. Soybean Disease Monitoring with Leaf Reflectance. *Remote Sensing*, Vol. 9 (127), p.p. 1-14.

Bouwman, A.F., van der Hoek, K.W., Eickhout, B. and Soenario, I. 2005 Exploring Changes in World Ruminant Production Systems. *Agricultural Systems,* Vol. 84, p.p. 121 - 153.

Bruton, R.K. 2019. *The Terrestrial Laser Scanner for Cassava (*Manihot esculenta*) Phenotyping & the Development of a Low-Cost 3D Phenotyping Platform*. Texas A&M University, Ph.D. Dissertation.

Burkill, H. M., 1985. Entry for *Pennisetum purpureum* Schumacher [family POACEAE]. *The useful plants of West tropical Africa*, Vol. 2, Royal Botanic Gardens, Kew, UK.

Butkiewicz, T. 2014. Low-cost Coastal Mapping using Kinect v2 Time-of-Flight Cameras. *Oceans – St. John's*, p.p. 1-9, DOI: 10.1109/OCEANS.2014.7003084.

Cameira, M. and Pereira, L.S. 2019. Innovation Issues in Water, Agriculture and Food. *Water*, Vol. 11 (6), p.p. 1-7.

Caruso, L., Russo, R., and Savino, S. 2017. Microsoft Kinect V2 Vision System in a Manufacturing Application. *Robotics and Computer-Integrated Manufacturing*, Vol. 48, pp. 174-181.

Cohen, J.E. 1995. Population Growth and Earth's Human Carrying Capacity. *Science*, Vol. 269 (5222), pp. 341-346.

Cordova, C. and Porter, J.C. 2015. The 1930s Dust Bowl: Geoarchaeological Lessons from a 20th Century Environmental Crisis. *Holocene*, Vol. 25 (10), pp. 1707-1720.

DeGloria, S.D., Wall, S.L., Benson, A.S., and Whiting, M.L.. 1986. Monitoring Conservation Tillage Practices Using Landsat Multispectral Data. *Journal of Soil and Water Conservation*, Vol. 41 (3), p.p. 187-190.

Devia, C.A., Rojas, J.P., Petro, E., Martinez, C., Mondragon, I.F., Patino, D., Rebolledo, M.C. and Colorado, J. 2019. High-Throughput Biomass Estimation in Rice Crops Using UAV Multispectral Imagery. *Journal of Intelligent & Robotic Systems*, Vol. 96, p.p. 573–589.

Dhondt, S., Wuyts, N., and Inze, D. 2013. Cell to Whole-Plant Phenotyping: The Best is Yet to Come. *Trends in Plant Science*, Vol. 18 (8), p.p. 428-439.

Eitel, J. U., Vierling, L. A., Long, D. S., & Hunt, E. R. 2011. Early Season Remote Sensing of Wheat Nitrogen Status Using a Green Scanning Laser. *Agricultural and Forest Meteorology*, Vol. 151 (10), p.p. 1338-1345.

Ehlert, D., Heisig, M., & Adamek, R. 2010. Suitability of a Laser Rangefinder to Characterize Winter Wheat. *Precision Agriculture*, Vol. 11 (6), p.p. 650-663.

Farrell, G., Simons, S.A., and Hillocks, R.J. 2010. Pests, Diseases and Weeds of Napier Grass, Pennisetum purpureum: A Review. *International Journal of Pest Management*, Vol. 48 (1), p.p. 39-48.

Friedli, Michael, et al. “Terrestrial 3D Laser Scanning to Track the Increase in Canopy Height of Both Monocot and Dicot Crop Species under Field Conditions.” *Plant Methods*, Vol. 12, DOI:10.1186/s13007-016-0109-7.

Fritsche-Neto, R. and Borém, A. (eds.). 2015. *Phenomics: How Next-Generation Phenotyping is Revolutionizing Plant Breeding*. Switzerland, Springer International Publishing AG, 142 pages.

Furbank, R. T. 2009. Plant Phenomics: From Gene to Form and Function. *Functional Plant Biology*, Vol. 36 (10), p.p. 5-6.

GEF/UNCCD. 2011. *Land for Life: Securing Our Common Future*. Global Environment Facility, Washington, D.C.

Gene-Mola, J., Gregorio, E., Guevara, J., Auat, F., Sanz-Cortiella, R., Escola, A., Llorens, J., Morros, J. R., Ruiz-Hidalgo, J., Vilaplana, V., and Rosell-Polo, J. R. 2019. Fruit Detection in an Apple Orchard Using a Mobile Terrestrial Laser Scanner. *Biosystems Engineering*, Vol. 187, pp. 171–184.

Gibson, M. 2012. Food Security—A Commentary: What Is It and Why Is It So Complicated? *Foods*, Vol. 1 (1), p.p. 18–27.

Gupta, R.B. and Demirbas, A. 2010. *Gasoline, Diesel and Ethanol Biofuels from Grasses and Plants*. Cambridge, U.K., Cambridge University Press, 224 pages.

Hämmerle, M., Höfle, B., Fuchs, J., Schröder-Ritzrau, A., Vollweiler, N., and Frank, N. 2014. Comparison of Kinect and Terrestrial LiDAR Capturing Natural Karst Cave 3-D Objects. *IEEE Geoscience and Remote Sensing Letters*, Vol. 11 (11), p.p. 1896–900.

Han, L., Yang, G., Dai, H., Xu, B., Yang, H., Feng, H., Li, Z. and Yang, X. 2019. Modeling Maize Above-Ground Biomass Based on Machine Learning Approaches Using UAV Remote-Sensing Data. *Plant Methods*, Vol. 15 (10), p.p. 1-19.

Havlik, P., Valin, H., Herrero, M., Obersteiner, M., and Schmid, E. 2014. Climate Change Mitigation Through Livestock System Transitions. *Proceedings of the National Academy of Sciences of the United States of America*, Vol. 111, p.p. 3709 - 3714.

Hillocks, R. J. and Thresh, J. M. 2002. *Cassava: Biology, Production and Utilization*. Wallingford, UK ; New York: CABI Publishing, 332 pages.

Hosoi, F. and Omasa, K. 2007. Factors Contributing to Accuracy in the Estimation of the Woody Canopy Leaf Area Density Profile Using 3D Portable Lidar Imaging. *Journal of Experimental Botany*, Vol. 58 (12), p.p. 3463-3473.

Houle, D., Govindaraju, D.R., and Omholt, S. 2010. Phenomics: The Next Challenge. *Nature Reviews Genetics*, Vol. 1 (12), p.p. 855–866.

Jiang, Q., Fang, S., Peng, Y, Gong, Y., Zhu, R., Wu, X., Ma, Y., Duan, B., and Liu, J. 2019. UAV-Based Biomass Estimation for Rice-Combining Spectral, TIN-Based Structural and Meteorological Features. *Remote Sensing*, Vol. 11 (7), p.p. 1-19.

Jin, S., Su, Y., Song, S., Xu, K., Hu, T., Yang, Q., Wu, F., Xu, G., Ma, Q., Guan, H., Pang, S., Li, Y., and Guo, Q. 2020. Non-Destructive Estimation of Field Maize Biomass Using Terrestrial Lidar: An Evaluation from Plot Level to Individual Leaf Level. *Plant Methods*, Vol. 16 (1), p.p. 1-19.

Kamau, J. Melis, R., Laing, M., and Derera, J. 2011. Farmers' Participatory Selection for Early Bulking Cassava Genotypes in Semi-Arid Eastern Kenya. *Journal of Plant Breeding and Crop Science*, Vol. 3 (3), p.p. 44-52.

Khan, Z.R., Midega, C.A.O., Wadhams, L.J., Pickett, J.A., and Mumuni, A. 2007. Evaluation of Napier Grass (*Pennisetum purpureum*) Varieties for Use as Trap Plants for the Management of African Stemborer (*Busseola fusca*) in a Push–Pull Strategy. *Entomologia experimentalis et applicata*, Vol. 124 (2), p.p. 201-211.

Khoshelham, K. and Elberink, S.O. 2012. Accuracy and Resolution of Kinect Depth Data for Indoor Mapping Applications, *Sensors*, Vol. 12 (2), p.p. 1437–54.

Kin, C.S., Ut, I.M., Hang, L., Hou, U., Weng, N., Ha, U. S., Hin, L.K., Heng, C.K., Tim, T.S., Kuai, C., and Shan, L.W. 2019. *Predicting Earth's Carrying Capacity of Human Population as the Predator and the Natural Resources as the Prey in the Modified Lotka-Volterra Equations with Time-dependent Parameters*. Accessed from: arXiv:1904.05002.

Klein, C. 2016. *Handbook on Cassava: Production, Potential Uses, and Recent Advances*. Hauppauge, New York: Nova Science Publishers, Inc., 409 pages.

Kunz, A., Brogli, L. and Alavi, A. 2016. *Interference Measurement of Kinect for Xbox One*. VRST '16 Proceedings of the 22nd ACM Conference on Virtual Reality Software and Technology, Munich, Germany, Nov. 2-4, 2016, p.p. 345-346.

Lachat, E., et al. “First Experiences with Kinect V2 Sensor for Close Range 3D Modelling. *ISPRS - International Archives of the Photogrammetry, Remote Sensing and Spatial Information Sciences*, Vol. XL-5/W4, pp. 93–100. DOI:10.5194/isprsarchives-XL-5-W4-93-2015.

Lachat, E., et al 2015b. Assessment and Calibration of an RGB-D Camera (Kinect v2 Sensor) Towards a Potential Use for Close-Range 3D Modeling. *Remote Sensing*, Vol. 7, p.p. 13070-13097.

Langeland, K.A. and Cherry, H.M. 2008. *Identification and Biology of Nonnative Plants in Florida’s Natural Areas* – Second Edition. University of Florida-IFAS Publication # SP 257.

Lanz, B., Dietz, S., and Swanson, T. 2018. Global Economic Growth and Agricultural Land Conversion under Uncertain Productivity Improvements in Agriculture. *American Journal of Agricultural Economics*, Vol. 100 (2), p.p. 545-569.

Leon, C.T., Shaw, D.R., Cox, M.S., Abshire, M.J., Ward, B. Wardlaw III, M.C., and Watson, C. 2003. Utility of Remote Sensing in Predicting Crop and Soil Characteristics. *Precision Agriculture*, Vol. 4 (4), p.p. 359-384.

Li, L., Zhang, Q., and Huang, D. 2014. A Review of Imaging Techniques for Plant Phenotyping. *Sensors*, 14 (11), p.p. 20078-20111.

Loresco, M., Andal, M., Ty, K., and Angeles, A. 2019. Growth Performance of Growing Dairy Heifers Fed Fresh Mulato II (Brachiaria ruziziensis x B. decumbens x B. brizantha) and Mombasa (Panicum maximum Jacq. cv. Mombasa) Compared to Napier (Pennisetum purpureum Schum.). *Philippine Journal of Veterinary & Animal Sciences*, Vol. 45 (1), p.p. 87-90.

Ma, L., Zheng, G., Eitel, J. U., Magney, T. S., and Moskal, L. M. 2016. Determining Woody-Total Area Ratio Using Terrestrial Laser Scanning (TLS). *Agricultural and forest meteorology*, Vol. 228, p.p. 217-228.

MacDonald, E. 2018. *Are Vegetation Index Maps Derived from sUAS-Mounted Multi-Spectral Sensors an Accurate Predictor of Yield in Potatoes*? University of Prince Edward Island, Master’s Thesis.

Malik, P.K., Bhatta, R., Takahashi, J., Kohn, R.A., and Prasad, C.S. (ed.). 2015. *Livestock Production and Climate Change*. Wallingford, UK, Boston, MA, Centre for Agriculture and Bioscience International, 384 pages.

Mankoff, Kenneth David, and Tess Alethea Russo. The Kinect: A Low-Cost, High-Resolution, Short-Range 3D Camera. *Earth Surface Processes and Landforms*, Vol. 38 (9), p.p. 926-936.

Mapato, C. and Wanapat, M. 2018. Comparison of Silage and Hay of Dwarf Napier Grass (*Pennisetum purpureum*) Fed to Thai Native Beef Bulls. *Tropical Animal Health & Production*, Vol. 50 (7), p.p. 1473-1477.

Marin, G. *3D Data Fusion from Multiple Sensors and its Applications*. 2017. University of Padova, Ph.D. Dissertation. Retrieved from https://giuliomarin.github.io.

Marko, D., Briglia, N., Summerer, S., Petrozza, A., Cellini, F., and Iannacone, R. 2018. High-Throughput Phenotyping in Plant Stress Response: Methods and Potential Applications to Polyamine Field. *Polyamines. Methods in Molecular Biology*, Vol. 1694. Humana Press, New York, NY.

Martin, R.C. 2019. *Food Security: From Excess to Enough*. Toronto, Dundurn Press, 228 pages.

McFassel, G., Hsieh, S., and Peng, B. 2018. Prototyping and Evaluation of Interactive and Customized Interface and Control Algorithms for Robotic Assistive Devices Using Kinect and Infrared Sensor. *International Journal of Advanced Robotic Systems*, Vol. 15 (2), p.p. 1-9.

McManamon, P.F. 2015. *Field Guide to Lidar*. Bellingham, WA, SPIE (online publication), 171 pages.

Mishra, K.B., Mishra, A., Klem, K, and Govindjee. 2016. Plant Phenotyping: A Perspective. *Indian Journal of Plant Physiology*, Vol. 21 (4), p.p. 514–527.

Moreno, H., Valero, C., María Bengochea-Guevara, J., Ribeiro, A., Garrido-Izard, M., and Andújar, D. 2020. On-Ground Vineyard Reconstruction Using a LiDAR-Based Automated System. *Sensors*, Vol. 20 (4), p.p. 1-15.

Moscaritolo, A. October 25, 2017. Microsoft Is Ending Kinect Production. *PC Magazine*, https://www.pcmag.com/news/microsoft-is-ending-kinect-production.

Naeemabadi, M., Dinesen, B., Andersen, O.K., Hansen, J. 2018. Investigating the Impact of a Motion Capture System on Microsoft Kinect V2 Recordings: A Caution for Using the Technologies Together. *PLoS ONE*, Vol. 13 (9), p.p. 1-17.

Nasi, R., Niko, V. Kaivosoja, J., Alhonoja, K., Hakala, T., Markelin, L., and Honkavaara, E. 2018. Estimating Biomass and Nitrogen Amount of Barley and Grass Using UAV and Aircraft Based Spectral and Photogrammetric 3D Features. *Remote Sensing*, Vol. 10 (7), p.p. 1-32.

Nasir, A., Taj, M., and Khan, F. 2016. Evaluation of Microsoft Kinect Sensor for Plant Health Monitoring. *5th IFAC Conference on Sensing, Control and Automation Technologies for Agriculture AGRICONTROL 2016, IFAC PapersOnLine*, Vol 49 (16), p.p. 221-225.

Nir, O., Parmet, Y., Werner, D., Adin, G., and Halachmi, I. 2018. 3D Computer-Vision System for Automatically Estimating Heifer Height and Body Mass. *Biosystems Engineering*, Vol. 173, p.p. 4-10.

No author. April 2019. Microsoft Announces Azure Kinect Vision System. *Vision Systems Design*, Vol. 24 (4), pp. 10.

Ojoatre, S., Zhang, C., Hussin, Y.A., Kloosterman, H.E., and Ismail, M.H. 2019. Assessing the Uncertainty of Tree Height and Aboveground Biomass from Terrestrial Laser Scanner and Hypsometer Using Airborne LiDAR Data in Tropical Rainforests. *Journal of Selected Topics in Applied Earth Observations and Remote Sensing*, Vol. 12 (10), p.p. 4149-4159.

Okogbenin, E. and Fregene, M. 2002. Genetic Analysis and QTL Mapping of Early Root Bulking in an F1 Population of Non-Inbred Parents in Cassava (*Manihot esculenta* Crantz). *Theoretical and Applied Genetics*, Vol. 106 (1), p.p. 58-66.

Olagoke, A., Proisy, C., Fe´ret, J.B., Blanchard, E., Fromard, F., Mehlig, U., Machado de Menezes, M., Ferreira dos Santos, V., and Berger, U. 2016. Extended Biomass Allometric Equations for Large Mangrove Trees from Terrestrial LiDAR Data. *Trees*, Vol. 30, p.p. 935-947.

Omasa, Kenji, et al. 2007. 3D Lidar Imaging for Detecting and Understanding Plant Responses and Canopy Structure. *Journal of Experimental Botany*, Vol. 58 (4), pp. 881–98.

Popescu, S. C. 2007. Estimating Biomass of Individual Pine Trees Using Airborne Lidar. *Biomass and Bioenergy*, Vol. 31 (9), p.p. 646-655.

Pound, M. P., French, A. P., Murchie, E. H., & Pridmore, T. P. 2014. Automated Recovery of Three-Dimensional Models of Plant Shoots from Multiple Color Images. *Plant physiology*, Vol. 166 (4), p.p. 1688-1698.

Prabhakara, K., Hively, W.D., and McCart, G.W. 2015. Evaluating the Relationship Between Biomass, Percent Groundcover and Remote Sensing Indices Across Six Winter Cover Crop Fields in Maryland, United States. *International Journal of Applied Earth Observation and Geoinformation*, Vol. 39, p.p. 88-102.

Protalinski, E. April 2, 2015. Microsoft Stops Producing Kinect for Windows V2 Sensor, Will Focus on Kinect for Xbox One and Windows Apps. *Venture Beat*, Accessed from: https://venturebeat.com/2015/04/02/microsoft-stops-producing-kinect-for-windows-v2-sensor-will-focus-on-kinect-for-xbox-one-and-windows-apps/.

Qiu, R., Wei, S., Zhang, M., Li, H., Sun, H., Liu, G., and Li, M. 2018. Sensors for Measuring Plant phenotyping: A review. *International Journal of Agricultural and Biological Engineering*, Vol. 11 (2), p.p.1-17.

Rahman, M. 2017. *Beginning Microsoft Kinect for Windows SDK 2.0: Motion and Depth Sensing for Natural User Interfaces*. New York, Springer Science+Business Media, 297 pages.

Ramon Rosell Poloa, J., Sanz, R. Llorens, J., Arnóa, J., Escolà, A., Ribes-Dasi, M., Masip, J., Camp, F., Gràcia, F., Solanelles, F., Pallejà, T., Val, L., Planas, S., Gil, E., and Palacín, J. 2009. A Tractor-Mounted Scanning LIDAR for the Non-Destructive Measurement of Vegetative Volume and Surface Area of Tree-Row Plantations: A Comparison with Conventional Destructive Measurements. *Biosystems Engineering*, Vol. 102 (2), p.p. 128-134.

Reynolds, M. P. 2010. *Climate Change and Crop Production*. Wallingford, UK, Cambridge, MA, Centre for Agriculture and Bioscience International, 292 pages.

Scano, A., Molteni, F., and Tosatti, L.M. 2019. Low-Cost Tracking Systems Allow Fine Biomechanical Evaluation of Upper-Limb Daily-Life Gestures in Healthy People and Post-Stroke Patients. *Sensors*, Vol. 19 (5), p.p. 1-19.

Silverstein, E. and Snyder, M. 2017. Implementation of Facial Recognition with Microsoft Kinect V2 Sensor for Patient Verification. *Medical Physics*, Vol. 44 (6), p.p. 2391-2399.

Strezov, V., Evans, T.J., and Hayman, C. 2008. Thermal Conversion of Elephant Grass (*Pennisetum Purpureum Schum*) to Bio-gas, Bio-oil and Charcoal. *Bioresource Technology*, Vol. 99 (17), p.p. 8394-8399.

Suja, G., Susan John, K., Sreekumar, J., and Srinivas, T. 2010. Short-Duration Cassava Genotypes for Crop Diversification in the Humid Tropics: Growth Dynamics, Biomass, Yield and Quality. *Journal of the Science of Food and Agriculture*, Vol. 90 (2), p.p. 188-198.

Sun, S., Li, C., Paterson, A.H. 2017. In-Field High-Throughput Phenotyping of Cotton Plant Height Using LiDAR *Remote Sensing*, Vol. 9 (4), p.p. 1-21.

Tao, S., Guo, Q., Li, L., Xue, B., Kelly, M., Li, W., Xu, G., and Su, Y. 2014. Airborne Lidar-Derived Volume Metrics for Aboveground Biomass Estimation: A Comparative Assessment for Conifer Stands. *Agricultural and Forest Meteorology*, Vol. 198–199, p.p. 24-32.

Tien-Long, B. and Van-Bien, B. 2019. First Experiences with Microsoft Kinect V2 for 3D Modelling of Mechanical Parts. *Applied Mechanics and Materials*, Vol. 899, p.p. 329-336.

Tilly, N., Hoffmeister, D., Cao, Q., Huang, S., Lenz-Wiedemann, V., Miao, Y., Bareth, G. 2014a. Multitemporal Crop Surface Models: Accurate Plant Height Measurement and Biomass Estimation with Terrestrial Laser Scanning in Paddy Rice. *Journal of Applied Remote Sensing*, Vol. 8 (1), p.p. 1-23.

Tilly, N., Hoffmeister, D., Schiedung, H., Hütt, C., Brands, J., and Bareth, G. 2014b. Terrestrial Laser Scanning for Plant Height Measurement and Biomass Estimation of Maize. *International Archives of the Photogrammetry, Remote Sensing & Spatial Information Sciences*, Vol. 40 (7), p.p. 181-187.

Tsai, M-H, Lee, W-C, Kuan, W-C, Sirisansaneeyakul, S., and Savarajara, A. 2018. Evaluation of Different Pretreatments of Napier Grass for Enzymatic Saccharification and Ethanol Production. *Energy Science & Engineering*, Vol. 6 (6), p.p. 683-692.

Tumuhimbise, R., Melis, R., Shanahan, P., and Kawuki, R.S. 2012. Farmers' Perceptions on Early Storage Root Bulking in Cassava (*Manihot esculenta* Crantz) in East and Central Uganda and their Implication for Cassava Breeding. *World Journal of Agricultural Sciences*, Vol. 8., p.p. 403-408.

Vazirabad, Y.F. and Karslioglu, M.O. 2011. Lidar for Biomass Estimation. In Matovic, M.D. (Ed.), *Biomass: Detection, Production and Usage*. INTECH Open Access Publisher: https://www.intechopen.
com/books/biomass-detection-production-and-usage/lidar-for-biomass-estimation.

Vosselman, G. and Maas, H.G. 2010. *Airborne and Terrestrial Laser Scanning*. Dunbeath Mill, UK: Whittles Publishing, 318 pages.

Walter, J.D.C., Edwards, J., McDonald, G., and Kuchel, H. 2019. Estimating Biomass and Canopy Height With LiDAR for Field Crop Breeding. *Frontiers in Plant Science*, Vol. 10, p.p. 1-16.

Wang, H., Lin, Y., Wang, Z., Yao, Y., Zhang, Y., and Wu, L. 2017. Validation of a Low-Cost 2D Laser Scanner in Development of a More-Affordable Mobile Terrestrial Proximal Sensing System for 3D Plant Structure Phenotyping in Indoor Environment. *Computers and Electronics in Agriculture*, Vol. 140, p.p.180-189.

Wasenmüller, O. and Stricker, D. 2016. Comparison of Kinect V1 and V2 Depth Images in Terms of Accuracy and Precision. In: Chen CS., Lu J., Ma KK. (eds) Computer Vision – ACCV 2016 Workshops. ACCV 2016. *Lecture Notes in Computer Science*, Vol. 10117, Springer, Cham.

Weitkamp, C. (ed.). 2005. *Lidar: Range-Resolved Optical Remote Sensing of the Atmosphere*. New York, Springer, 455 pages.

Wholey, D.W. and Cock, J.H. 1974. Onset and Rate of Root Bulking in Cassava. *Experimental Agriculture*, Vol. 10 (3), p.p. 193-198.

Wilson, M. (2017, October 25). Exclusive: Microsoft Has Stopped Manufacturing The Kinect. *CO.DESIGN*. Accessed from: https://www.fastcodesign.com/90147868/exclusive-microsoft-has-stopped-manufacturing-the-kinect.

Xie, Q., Dash, J., Huang, W., Peng, D. , Qin, Q., Mortimer, H., Casa, R., Pignatti, S., Laneve, G. , Pascucci, S., Dong, Y., and Ye, H.. 2018. Vegetation Indices Combining the Red and Red-Edge Spectral Information for Leaf Area Index Retrieval. *IEEE Journal of Selected Topics in Applied Earth Observations and Remote Sensing*, Vol. 11 (5), p.p.1482-1493.

Young, S.N., Kayacan, E., and Peschel, J.M. 2019. Design and Field Evaluation of a Ground Robot for High‐Throughput Phenotyping of Energy Sorghum. *Precision Agriculture*, Vol. 20 (4), p.p. 697-722.

Zaeen, A.A., Sharma, L., Jasim A., Bali, S., Buzza, A., and Alyokhin, A. 2020. In-Season Potato Yield Prediction with Active Optical Sensors. *Agroecosystems, Geosciences, & Environment*, Vol. 3 (1), p.p. 1-15.

Zennaro, S., Munaro, M., Milani, S., Zanuttigh, P., Bernardi, A., Ghidoni, S., & Menegatti, E. 2015. *Performance Evaluation of the 1st and 2nd Generation Kinect for Multimedia*

Applications. 2015 IEEE International Conference on Multimedia and Expo (ICME), p.p. 1-6.

Zhang, K., Chen, S. C., Whitman, D., Shyu, M. L., Yan, J., & Zhang, C. 2003. A Progressive Morphological Filter for Removing Nonground Measurements from Airborne LIDAR Data. *IEEE Transactions on Geoscience and Remote Sensing*, Vol. 41 (4), p.p. 872-882.

Zhang, L. and Grift, T.E. 2012. A LIDAR-Based Crop Height Measurement System for *Miscanthus giganteus*. *Computers and Electronics in Agriculture*, Vol. 85, p.p. 70-76.

Zhou, Z. 2019. *Global Food Security: What Matters?* New York, Routledge, 324 pages.